PhD degree in Molecular Medicine (curriculum in Medical Nanotechnology)

European School of Molecular Medicine (SEMM),

University of Milan and University of Naples "Federico II"

Settore disciplinare: FIS/03

Novel Poly(amidoamine) Nanoparticles Designed for Drug Delivery to the Central Nervous System

Student's name Smbat Gevorgyan

Affiliation CIMAINA, Milan

Matricola n. R09883

Supervisor Prof. Paolo Milani

Affiliation CIMAINA, Milan

Anno accademico 2015-2016

Table of Contents

List of Abbreviations 6

List of Figures 9

List of Tables 11

ABSTRACT 12

1. INTRODUCTION 14

1.1 Blood Brain Barrier: Overview and challenges 14

1.2 Polymeric nanoparticles: general overview 16

1.3 Polymeric NPs targeted to the CNS 20

1.4 NPs coating by Polysorbate 80 23

1.5 Poly(amidoamine) based nanocarriers 26

1.6 Self-assembled PAAs NPs: state of the art and challenges 29

1.7 Photo-crosslinked NPs 33

1.8 Aim of the study and brief description of the results 34

2. MATERIALS and METHODS 35

2.1 Materials 35

2.2 PAA nanoparticles synthesis by UV crosslinking 36

2.2.1 Synthesis of PAA oligomers 36

2.2.2 UV-assisted crosslinking 36

2.2.3 Optimization of synthetic parameters and samples naming 38

2.2.4 Polymeric coating 39

2.2.5 Scale-up experiment 40

2.3 Nanoparticle purification 42

2.3.1 Centrifugation 42
2.3.2 Dialysis 42
2.3.3 Size exclusion chromatography 44
2.4 NPs characterization 45
2.4.1 Dynamic light scattering and zeta (ζ) potential 45
2.4.2 Confocal laser scanning microscopy 49
2.4.3 Stimulated emission depletion microscopy 50
2.4.4 Scanning Electron Microscopy 51
2.4.5 Determination of NPs composition by bicinchoninic acid assay 53
2.4.6 Spectroscopy detection techniques 53
2.5 Encapsulation of model drugs 55
2.5.1 Encapsulation of Immunoglobulin G - Cyanine® 3 55
2.5.2 Encapsulation of Streptavidin-Alexa 647 56
2.5.3 Encapusulation of β-Galactosidase 56
2.6 Stability studies 57
2.7 Assessment of PAA NPs influence on cell viability 58
2.7.1 Study of NPs behavior in the tested biological medium 58
2.7.2. MTT assay 58
2.8 Permeability studies across *in vitro* BBB model 59
3. RESULTS and DISCUSSION 61
3.1 Synthesis of PAA NPs 61
3.1.1 Development of PAA NPs synthesis method 61
3.1.2 Control experiments 63
3.1.3 Synthesis of NPs with methacrylated chitosan 65
3.2 NPs Characterization 69
3.2.1 Scanning Electron Microscopy 69
3.2.2 Confocal laser scanning microscopy 70
3.2.3 Stimulated emission depletion microscopy 71

3.3 PAA NPs synthesis optimization 73

3.3.1 Influence of PAA Oligomers molecular weight 73
3.3.2 Influence of HSA concentration 75
3.3.3 Influence of Irgacure 2959 concentration 77
3.3.4 Influence of FITC removal 80
3.3.5 Polysorbate 80 coating 82
3.3.6 Summary of PAA NPs synthesis optimization 83

3.4 Scale-up experiment 84

3.5 NPs HSA content evaluation by BCA assay 85

3.6 Encapsulation of model compounds and their release 86

3.6.1 IgG-Cy3 encapsulation 86
3.6.2 Encapsulation of Streptavidin-Alexa Fluor® 647 90
3.6.3 Encapsulation of β-Galactosidase 92

3.7 Stability studies 92

3.8 MTT assay 94

3.9 Permeability studies across *in vitro* BBB model 97

4. CONCLUSION and PERSPECTIVES 101

5. APPENDIX 103

5.1 Introduction 103

5.2 Materials and Methods 104

5.2.1 Materials 104
5.2.2 Synthesis of PLGA NPs 105
5.2.3 Characterization of nanoparticles 106
5.2.4 Lyophilization 106
5.2.5 Stability studies 106
5.2.6 RNA release 106

5.3 Results and Discussion 107

5.3.1 Synthesis of PLGA NPs 107

5.3.2 Morphological characterization of PLGA NPs 108

5.3.3 PLGA NPs stability studies 110

5.3.4 *In vitro* dsRNA release studies 114

5.4 Conclusion 115

Acknowledgements 116

REFERENCES 118

List of Abbreviations

BAC	2,2-bis(acrylamido)acetic acid
BBB	blood brain barrier
BCA	bicinchoninic acid
BSA	bovine serum albumin
CLSM	confocal laser scanning microscopy
CNS	central nervous system
CPS	counts per second
CTRL	control
DCR	derived count rate
DESE	double emulsion solvent evaporation
DLS	dynamic light scattering
DMSO	dimethyl sulfoxide
DPBS	dulbecco's phosphate buffered saline
ds	double stranded
ECGF	endothelial cell growth factor
EPR	enhanced permeability and retention
FBS	foetal bovine serum
FE-SEM	field Emission Scanning Electron Microscope
FITC	fluorescein isothiocyanate isomer I
h	hour

HEPES	4-(2-hydroxyethyl)-1-piperazineethanesulfonic acid
HSA	human serum albumin
HUVEC	human umbilical vein endothelial cells
IgG-Cy3	cyanine® 3 labeled goat anti-mouse IgG (H+L) antibody
Irgacure 2959	2-Hydroxy-4'-(2-hydroxyethoxy)-2-methylpropiophenone
kcps	kilo counts per second
kDa	kilodalton
MC	methacrylated chitosan
MPS	mononuclear phagocytic system
MTT	3-(4, 5-dimethylthiazolyl-2)-2, 5-diphenyltetrazolium bromide
MW	molecular weight
NP	nanoparticle
NPs	nanoparticles
OPAA	PAA oligomer
PAA	poly(amidoamine)
PBCA	polybutylcyanoacrylate
PBS	phosphate-buffered saline
PdI	polydispersity index
PEG	poly(ethylene glycol)
PLA	polylactic acid
PLGA	poly(lactic-co-glycolic acid)
Polysorbate 80 (P80)	polyoxyethylenesorbitan monooleate

PVA	polyvinyl alcohol
RGD	arginin–glycin–aspartic acid
RT	room temperature
SEC	size exclusion chromatography
SEM	scanning electron microscopy
SLN	solid lipid nanoparticles
STED	stimulated emission depletion
STR647	streptavidin-Alexa Fluor® 647
TEER	transendothelial electrical resistance
TEM	transmission electron microscopy
UV	ultraviolet

List of Figures

Figure 1.1	Capillary systems in the brain compared to the rest of the body	16
Figure 1.2	Different structures of polymeric NPs for drug encapsulation	17
Figure 1.3	*In vitro* blood brain barrier model based on transwell inserts	22
Figure 1.4	The chemical structure of Polysorbate 80	24
Figure 1.5	3D structure of PAA dendrimers	28
Figure 1.6	Self-assembly of a PAA NP	29
Figure 2.1	The UV lamp and reaction mixture	36
Figure 2.2	The scale-up experiment for PAA NPs synthesis	40
Figure 2.3	Dialysis purification scheme of NPs	43
Figure 2.4	Schematic representation of ionic double layers of a charged particle	47
Figure 2.5	Scheme of STED spots	50
Figure 3.1	Chemical structure of PAA oligomers	61
Figure 3.2	Synthesis procedure of PAA NPs	62
Figure 3.3	Chemical structure of methacrylated chitosan	65
Figure 3.4	Scanning Electron Microscopy (SEM) images of OHFI-8k NPs	69
Figure 3.5	CLSM images of PAA NPs encapsulated with IgG-Cy3 and FITC	70
Figure 3.6	CLSM (A) and STED (B) images of OHFI-8k formulation	71
Figure 3.7	Chemical structure of Irgacure 2959	77
Figure 3.8	Chemical structure of fluorescein isothiocyanate (FITC)	80
Figure 3.9	Standard calibration curve for BCA assay	85
Figure 3.10	The IgG-Cy3 release from PAA NPs	89
Figure 3.11	DLS data of stability studies	93

Figure 3.12 Influence of PAA NPs on HUVEC viability 95

Figure 3.13 The fluorescence level of IgG-Cy3 passed across an *in vitro* BBB model 98

Figure 3.14 Influence of PAA NPs on bEnd5 cells viability 99

Figure 5.1 Influence of ultrasound (US) power on PLGA NPs size and PdI 107

Figure 5.2 SEM images of PLGA NPs 108

Figure 5.3 CLSM (A) and bright-field (B) images of PLGA NPs 108

Figure 5.4 PLGA NPs stability studies in water and PBS media 110

Figure 5.5 PLGA NPs stability after lyophilization 112

Figure 5.6 Spectrofluorometric measurements of dsRNA release 113

List of Tables

Table 2.1	PAA NPs samples naming initials	38
Table 3.1	Control experiments of PAA NPs synthesis	64
Table 3.2	Controls experiments for NP preparation in the absence of OPAAs	66
Table 3.3	Influence of MC concentration on PAA NPs	67
Table 3.4	Influence of OPAAs MW on PAA NPs	74
Table 3.5	Influence of HSA concentration on PAA NPs	76
Table 3.6	Influence of Irgacure 2959 concentration on PAA NP	79
Table 3.7	Influence of FITC encapsulation on PAA NPs	81
Table3.8	Influence of Polysorbate 80 (P80) coating of PAA NPs	82
Table 3.9	Parameters changed for reaching the final PAAs NPs	82
Table 3.10	Real time DLS analysis of PAA NPs scale-up synthesis	84
Table 3.11	Influence of IgG-Cy3 on PAA NPs	87
Table 3.12	Influence of MC on IgG-Cy3 encapsulation in PAA NPs	88
Table 3.13	The degradation studies of OIg-2HI.2-(T8)-2k formulation	89
Table 3.14	Influence of STR647 encapsulation on PAA NPs	90
Table 3.15	Influence of β-Galactosidase encapsulation on PAA NPs	91
Table 3.16	O-2HI.2-(T8)-2k formulation's incubation	94

ABSTRACT

With the aging population, central nervous system diseases are becoming increasingly widespread. However, the treatment of such diseases represents a challenge mainly due to the presence of the blood-brain barrier, which effectively blocks most of drugs to pass into the central nervous system and impedes the treatment of diseases. Therefore, effective ways of drug transport to the central nervous system are highly required.

Polymeric nanoparticles are drug delivery vectors that have high specificity to their targeted sites and increasingly enhance the stability of encapsulated drugs. Poly(amidoamines) are a promising family of synthetic polymers that can be used in nanoparticles synthesis. Nanoparticles synthesized from linear poly(amidoamines) show very good biocompatibility levels and specific targeting properties. Nevertheless, those nanoparticles are mainly synthesized by self-assembly and usually lack long-term stability.

In this study we developed innovative poly(amidoamine) nanoparticles synthesized by ultraviolet light assisted photo-crosslinking. In order to give those nanoparticles central nervous system targeting properties, the synthesis method was systematically optimized. The final synthesis formulation yielded stable, sub-150 nm sized nanoparticles that had very good biocompatibility. The synthesis method had an advantage of being simple, did not require toxic organic solvents and was shown to be easily scaled-up. Moreover, poly(amidoamine) nanoparticles were coated by Polysorbate 80 surfactant, which not only increased the nanoparticles stability but also gave them central nervous system targeting properties. Poly(amidoamine) nanoparticles were able to successfully encapsulate model therapeutic

compounds and release them in a slow and controlled manner. Furthermore, the nanoparticles showed high permeability levels across an *in vitro* blood brain barrier model.

The developed poly(amidoamine) nanoparticles show great potential to be used as delivery vectors to the central nervous system.

1. INTRODUCTION

1.1 Blood Brain Barrier: Overview and challenges

The central nervous system (CNS) consists of the brain and spinal cord and has a crucial role in controlling many vital functions. CNS is affected by various diseases and many of them so far do not have adequate cure [1]. Many of those diseases, such as Alzheimer's disease, Parkinson's disease, gliomas, stroke and so on, are age related. With the increasingly aging population of the world, CNS diseases are becoming major challenges for healthcare systems. However, the CNS has several unique properties and many drug delivery methods that are very useful for the rest of human body, are not effective for the CNS [2,3]

One of the biggest hurdles for drug delivery to the CNS is the blood brain barrier (BBB). It is a specialized endothelial formation that separates the brain from circulating blood. Except the endothelial cells that are connected by tight junctions, the BBB is formed together with other brain cells such as pericytes, astrocytes and microglia. The BBB maintains the chemical stability of neural tissue, which is required for proper functioning of the brainvoi. The total surface area of human BBB is very large (20 m^2) and its breakdown can significantly compromise brain functionality, making it vulnerable to various diseases [4]. Figure 1.1 illustrates simplified BBB structure compared to capillary structures in the rest of the body.

Although the BBB plays a very important role in blocking hazardous molecules and complexes from entering the CNS, it is also impermeable for many drugs. Indeed, many therapeutic compounds that show big promises in their site of action have been discarded from clinical trials due to their failure to cross the BBB. Therefore, efficient ways of crossing the BBB is highly required in order to deliver drugs and genes to the CNS [5].

The BBB permeability is highly regulated and it depends on several physiological and pathological conditions of various origins. Usually there are specific molecular mediators in each case and those compounds are considered as means for drug delivery to the CNS [6]. It has been shown that some CNS diseases, such as stroke, multiple sclerosis and meningoencephalitis enhance the BBB permeability by loosening its tight junctions through specific molecular receptors. Nonetheless, the usage of pathological mechanisms is not the optimal choice for drug delivery to the CNS, because this process is not well controlled and poses significant risks to the patients' health [7].

Another approach to enhance the BBB permeability by temporary opening its tight junctions is the use of magnetic resonance. For this purpose nanosized contrast agents were introduced externally to the rats CNS. This method is successful in increasing drug delivery across the BBB and allows determination of the BBB opening and closure rates. Nevertheless, it also damages the delicate structure of the BBB and makes the CNS vulnerable to various toxins and pathogens [8].

Accordingly, effective delivery tools that can successfully deliver therapeutic compounds to the CNS across the BBB without damaging it, are highly required.

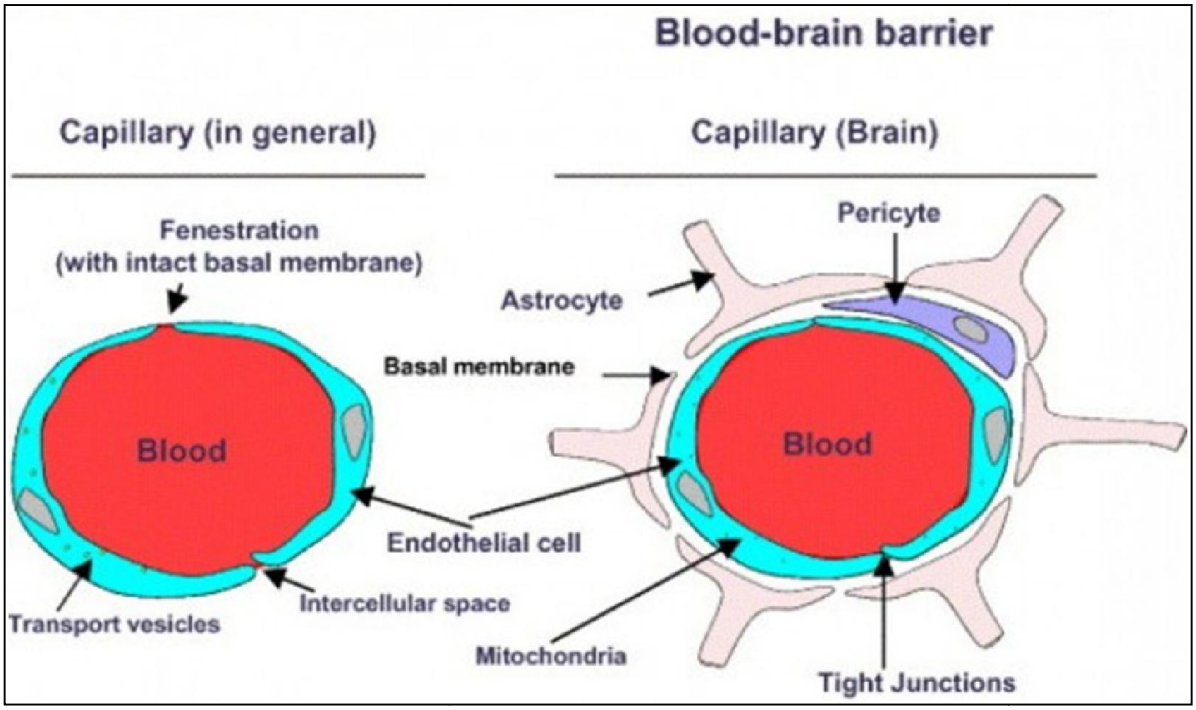

Figure 1.1 Capillary systems in the brain compared to the rest of the body. Adapted from http://web.stanford.edu/group/hopes/cgi-bin/hopes_test/cerebrovascular-and-blood-brain-barrier-impairments-in-huntingtons-disease-potential-implications-for-its-pathophysiology/ (03.10.2015).

1.2 Polymeric nanoparticles: general overview

Polymeric materials have been extensively used in biotechnology and medicine already for several decades. One of their applications is the synthesis of multifunctional polymeric nanoparticles (NPs) for targeted and controlled drug delivery. Polymeric NPs can widely facilitate drug formulation and delivery and offer great protection both on shelves and inside organisms [9]. Some of the most extensively used polymers are poly(lactic-co-glycolic acid) (PLGA) [10], polylactic acid (PLA) [11], chitosan [12], gelatin [13], and polybutylcyanoacrylate (PBCA) [14]. Those polymers can have either positive or negative charge, be of synthetic or biological origin, and have molecular weights (MW) in a very wide range. NPs can

encapsulate drugs in different ways according to their structure (Figure 1.2). Furthermore, the variability of polymeric NPs makes them advantageous compared to other delivery vectors because the NPs can be designed to be used in diverse specific applications [15]. NPs synthesized via self-assembly of electrolytes and amphiphilic block copolymers show particular promise thanks to their capability of creating multifunctional hybrid nanostructures and supramolecular structures [16].

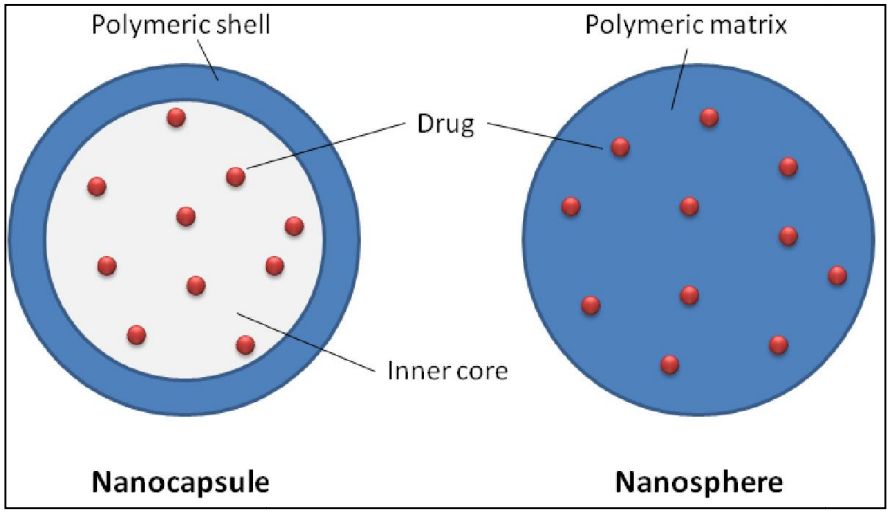

Figure 1.2 Different structures of polymeric NPs for drug encapsulation.

Polymeric NPs have been able to revolutionize drug delivery approaches by making possible spatially and temporary controllable drug release. However, many NPs do not possess stealth properties in the bloodstream; therefore they are easily recognized by mononuclear phagocytic system (MPS), which quickly removes non-stealth drug delivery vectors long before they are able to deliver their cargo to the target sites. This problem is more prominent for NPs synthesized from hydrophobic polymers [17]. In order to increase the stealth properties of NPs, many approaches have been employed, mainly based on increasing the NPs hydrophilicity. One of the most preferred methods is NPs coating by poly(ethylene glycol) (PEG). PEG coating significantly enhances NPs stealth properties, which in its turn

gives a huge boost in NPs circulation time in the bloodstream [18]. Various *in vivo* studies have shown that stealth NPs are able to circulate in blood for a prolonged time and deliver drugs to their target sites thanks to the enhanced permeability and retention (EPR) effect, which is a passive way of targeting [19]. In order to have enhanced specificity, active targeting approaches are used. The stealth NPs surface functionalization by specific targeting molecules, such as proteins (antibodies, antibody fragments, transferrin) [20], polysaccharides (chitosan, hyaluronic acid, etc.) [21], peptides (RGD, octetride, etc.) [22], aptamers or small biomolecules (such as folic acid or biotin) [23] further increases the NPs accumulation in their target sites and enhances the drug delivery efficiency. The choice of ligands is very important, because every particular targeting site requires NPs surface functionalization by its own specific moieties. This functionalization decreases systemic side effects of the drugs and enables the NPs to be used in therapeutic niches never exploited before [24].

The very small size of NPs, which is often comparable to virus size, has a major role in determination of their properties. Indeed, the very high surface-to-volume ratio of NPs makes many of their properties considerably different from macroscopic materials properties, which must be considered when the NPs behavior inside biological systems is assessed [25]. Additionally, NPs can be designed to be sensitive to environmental changes. For example, it has been shown that pH or temperature sensitive NPs are able to release their payload in a highly controllable manner at their specific delivery sites [26,27].

Polymeric NPs are designed to deliver drugs in *in vivo* environment, where there are complex environmental conditions. To this aim, the NPs' targeting specificity, drug loading amounts and tissue exposure kinetics are deliberately planned. The use of multifunctional NPs opens

new perspectives in enhancing both drug safety and efficacy [28]. It is noteworthy that the properties of drugs encapsulated into polymeric NPs are vastly different from the drugs alone. The drug's solubility, target tissue accumulation, metabolism rates, plasma binding, biodistribution and other important parameters change considerably due to the different physicochemical properties of the NP. In this case, it is reasonable to argue that drugs together with the NPs where they are encapsulated are new types of therapeutics. The combinations of appropriate drugs with optimally designed NPs give potential to have much better clinical outcomes [29]. NPs are also commonly used for vaccine development. Slow release, alternative administration and specific targeting are advantages of nanovaccines [30].

Novel multifunctional NPs can be used in different fields combining applications in imaging, sensing, diagnostics, and controlled drug delivery. Because the NPs research is a multidisciplinary, joint efforts from physicists, chemists and biologists are required to better understand the complex nature and applications of NPs. In spite of all these advancements, we still need to have a better understanding of NPs' intrinsic properties and find better polymeric compounds for NPs synthesis [31]. Although NPs have been extensively investigated, many aspects on their use require more thorough attention. For instance, there is little data about NPs environmental effects or their long term toxicity effects [32].

NPs characterization, functionalization and drug release kinetics are described in many reviews; but a deeper understanding of NPs long term influence on biological systems is still required [33]. Many aspects of NPs behavior in complex biological media are still topic of intense research from various researches from all over the world. The topics include: NPs

transmembrane permeability, multicompartmentalization inside tissues, biomolecules loading dynamics etc. [16].

1.3 Polymeric NPs targeted to the CNS

The unique properties of polymeric NPs open new perspectives for CNS diseases treatment by using innovative drug delivery systems based on NPs. Remarkably, many CNS drugs have poor stability and are not able to cross the BBB. By encapsulating those molecules inside NPs, they receive protection form harsh environmental conditions, acquire increased targeting to the brain and obtain enhanced permeability across the BBB [34]. Several targeting motifs, such as transferrin, insulin or OX26 antibody can specifically target drug loaded NPs to the brain. PEG coating also significantly enhances NPs stealth properties for brain targeting [35].

Many brain diseases, such as Parkinson's disease do not have a precise treatment and require a combination of different approaches to create new ways of their treatment. In this case the use of NPs is especially promising. Thanks to their small size, NPs have high permeability in biological systems. Polymeric NPs can simultaneously encapsulate multiple drugs and be effective treatment tools for diseases with complex origin [36]. NPs allow the delivery of various types of therapeutic compounds to the CNS starting from peptides and low molecular weight drugs up to big enzymes and nucleic acids. Each type of therapeutic compound requires NPs to be specifically designed in order to adapt to the drug's specific physico-chemical properties. However, there are some very important features that are necessary for all types of NPs for brain delivery [37]. Particularly, NPs should be completely biocompatible to avoid any toxic side effects in the CNS; NPs should have controlled

biodegradability (usually a few days) in order to release their drugs at their target sites; and also the NPs should be able to effectively cross the BBB. The NPs delivery of drugs is promising also because of its non-invasive nature, thanks to the potential of delivering non BBB-permeable drugs by using simple intravenous administration [38].

For instance, Lockman and others demonstrated that thiamine-coated NPs had significantly higher BBB permeability than non-coated NPs. They showed that the most important step of drug delivery to the brain is the crossing of the BBB barrier. After this, the NPs degradation in brain parenchyma was even favorable. Moreover, the authors showed that in case of specific coating, the NPs pass across the BBB through active cellular transport. They discovered that NPs size of around 100 nm is optimal for brain targeting [39].

As previously highlighted, the BBB is the major obstacle for NPs delivery to the CNS. In order to test NPs permeability through the BBB *in vivo* animal models are mostly employed. Nevertheless, these approaches are costly, time and labor consuming and often raise ethical questions. To address this issue, in recent years efficient *in vitro* BBB models have been proposed. Particularly, mouse or rat brain endothelial cell cultures have been found to successfully mimic the BBB due to the tight junctions formed between those cells, forming a structure very similar to the BBB. By incubating those cells into transwell inserts (Figure 1.3), the permeability of model drugs through the BBB model can be analyzed [40].

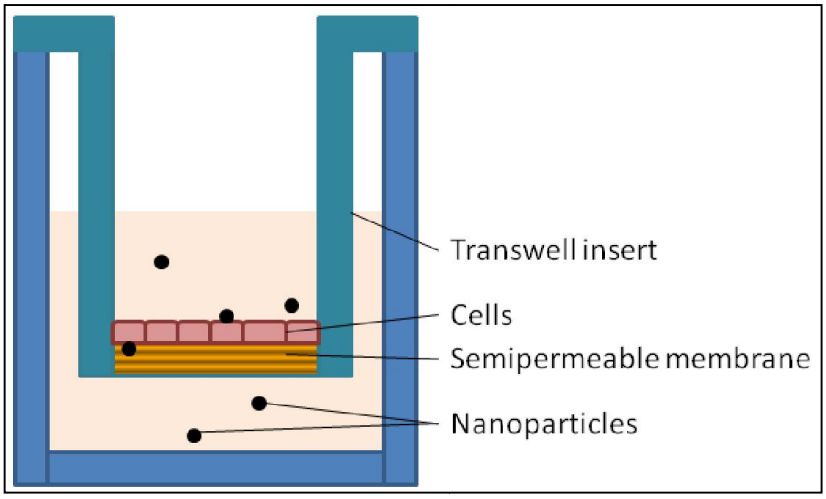

Figure 1.3 *In vitro* blood brain barrier model based on transwell inserts.

Polymeric NPs are also widely investigated for the treatment of brain tumors. Finding innovative brain tumor treatments based on NPs is very important because traditional methods have only moderate success. Lim and others developed NPs made from curcumin drug, which were quite efficient in suppressing *in vitro* brain tumor models. It is noteworthy that curcumin in its free form had significantly lower anticancer effect than the NPs [41].

There are many mechanisms by which NPs can pass through the BBB, nonetheless the most broadly available mechanism is receptor mediated endocytosis. To induce it, NPs are usually functionalized on their surface with proper ligands. Many functional moieties that are used to enable NPs with BBB crossing properties have chemical structure recognizable for transferrin or insulin receptors. Another class of ligands is represented by compounds recognizable by lipoprotein receptor-related protein, which is a member of low-density lipoprotein receptor family. This protein is exceedingly expressed in the BBB and is linked with the transcytosis of many active compounds across the BBB.

For example, Angiopep is a peptide recognizable by lipoprotein receptors and NPs surface functionalization by this peptide has proved to vastly improve the NPs delivery to the CNS [42].

An alternative approach to make the NPs recognizable by specific receptors and pass the BBB is NPs surface coating with specific CNS targeting surfactants. Particularly, NPs coating with Polysorbate 80 (P80) surfactant has shown big promises in this regard [43].

1.4 NPs coating by Polysorbate 80

In order to provide NPs with stealth and specific targeting properties, they can be coated by various surfactants. One of the most promising of them is Polysorbate 80 (P80). It has amphiphilic and non-ionic chemical structure composed of fatty acid esters of polyoxyethylene sorbitan (Figure 1.4). P80 has found many applications in food industry, pharmaceutics and biotechnology, including its use as a dispersing agent in broth preparation for microbiological studies. [44].

P80 is broadly used in pharmacology to coat and protect drugs from unfolding, precipitation and aggregation during their storage and shipping [45]. Similarly, P80 coating plays an important role in protein formulations by increasingly enhancing their stability. P80 coating also greatly stabilizes NPs formulations. It has been demonstrated that P80 coating of NP surface gives them negative charge [46]. This is crucial because the negative charge prevents NPs from aggregation with blood plasma proteins due to their electrostatic repulsions. Moreover, negatively charged NPs have been found to be less toxic than positively charged

ones [47]. The injection of P80 coated NPs to blood has no hemolytic activity or platelet aggregation and those NPs are successfully accumulated in inflamed tissues [48].

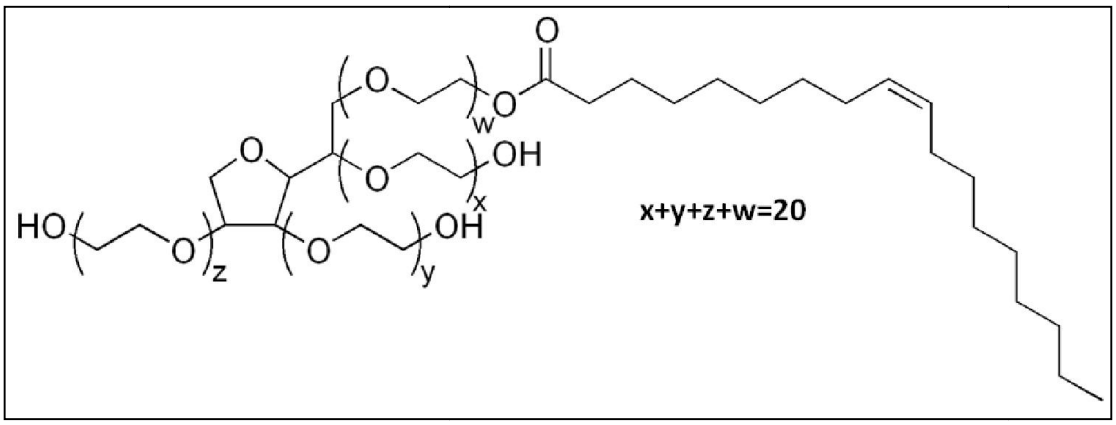

Figure 1.4 The chemical structure of Polysorbate 80.

P80 coating functionalizes a wide range of nanocarriers including solid lipid nanoparticles (SLNs) prepared by a solvent-diffusion method. The P80-emulsified SLNs demonstrated improved intestinal absorption, lymphatic uptake and relatively high oral bioavailability of anticancer drug docetaxel compared with an intravenous docetaxel formulation. Additionally, the SLNs had higher intestinal absorption and lymphatic uptake in rats [49].

There are many studies showing that P80 coating of NPs significantly enhances NPs permeability across the BBB. P80 coating is used for the delivery of many types of drugs including anticancer and anti-neurodegenerative drugs. For instance, Wilson and others demonstrated that PBCA NPs coated with 1% P80 showed much higher delivery of an anti-Alzheimer's drug tacrine to the brain compared to uncoated ones. When the NPs were coated with the surfactant, the drug's accumulation in the liver and spleen was considerably reduced [50].

In another study, the influence of P80 coating on anticancer drug doxorubicin delivery via PBCA NPs was investigated on rat models. The P80 coating significantly increased the NPs concentration in the brain and decreased the NPs concentration in the hearts of the animals. Moreover, the brain concentrations of all controls were always significantly lower (below the detection limit of high-performance liquid chromatography), indicating that P80-coated NPs pass through the BBB intact and there was an active transport mechanism mediated by P80 [51]. Furthermore, P80 coated PBCA NPs can be used to regulate the BBB integrity in vitro as it has been shown that those NPs induce reversible disruption of BBB integrity for three to four hours after administration. During that time the permeability of BBB is increase for NPs is increased. The integrity can be measured by using transendothelial electrical resistance (TEER). The observed loss of BBB integrity is not due to inflammation but due to cell morphology change and moderate and reversible disruption of tight junctions. The initial integrity of the BBB is fully recovered after six to ten hours of NPs administration [52].

It has been shown that the NPs size play important role in their permeability across biological barriers [25]. In order to see if NPs size is critical for BBB permeability too, P80 coated PBCA NPs having sizes ranging from 70 nm to 345 nm were investigated for their accumulation in cerebrospinal fluids and brain tissue of rats after intravenous injection. The study showed that the lower is the NPs size, the higher is their permeability. This was especially evident for the NPs with sizes less than 150 nm. Nonetheless, the most determining factor of NPs permeability was not the size but the P80 coating. Indeed, not-coated NPs had significantly lower permeability compared with the coated ones, regardless their size [53]. On the other hand, Voigt and others used blood-retina barrier as a BBB model and concluded in their study that the most important factor determining NPs' ability to pass through the BBB is their

surface chemistry, and particularly surfactant coating. According to the authors, NPs' size or surface charge (Zeta potential) are not determining the passage efficacy [54]. Nevertheless, blood-retina barrier is cannot be considered as an exhaustive analog of the BBB.

Thus, P80 coating does not increase NPs toxicity and helps to enhance NPs permeability across the BBB not because of cells damaging but rather specific interactions with receptors expressed in the BBB [55].

1.5 Poly(amidoamine) based nanocarriers

Poly(amidoamines) (PAAs) are a family of synthetic polymers, which are very promising for pharmaceutical applications. PAAs are obtained by stepwise polyaddition of prim-or sec-amines to bisacrylamides. Almost all possible bisacrylamides and prim- or sec-amines can be employed as monomers, providing PAAs with unique structural versatility among other stepwise polyaddition polymers. PAAs are degradable in aqueous media including physiological fluids [56]. Though they are cationic, their many types show remarkable biocompatibility. The carbonyl groups, which are situated in β-position to the amine groups, significantly lower the PAAs toxicity. PAAs can be highly functionalized and by using proper synthetic parameters there are countless possibilities of acquiring different PAA variations. This allows tailoring PAAs design depending on their applications in different fields. [57]. It was found that PAA nanocarriers with 200-300 nm size were effective only *in vitro* but they failed to be used *in vivo*. The maximum size of NPs to be used for drug delivery in vivo has been found to be 150 nm [58].

The polyaddition of 4-aminobutylguanidine (Agmatine) to 2,2-bisacrylamidoacetic acid can result to a new novel class of PAAs which can be successfully used as complexing agents for negatively charged bioactive compounds, such as proteins and nucleic acids [59]. It has been demonstrated that Agmatine successfully interacts with the arginin–glycin–aspartic acid (RGD)-binding αVβ3 integrins, which are expressed by many cell types and it is specifically recognized by proteins involved in cell adhesion, such as vitronectin, fibronectin and laminin. Although, immobilization of RGD peptide into NPs surface has been shown to greatly enhance several NPs bioavailability, it is costly to manufacture and Agmatine represents a cheap and effective alternative to it [60].

Another approach for the use of Agmatine-functionalized PAAs is preparation of biodegradable hydrogels. The degradation rate of the polymer was found to be accurately controllable by adjusting the molecular weight of PAA oligomers and acrylic co-monomer concentration in the initial reaction mixture. Cell adhesion and proliferation tests on kidney epithelial cells demonstrated that PAA hydrogels enhanced cell adhesion up to two times compared to the controls [61].

Agmatine containing linear PAA NPs were also used to deliver anti-malarial drugs to plasmodium infected red blood cells. The experiments showed that used PAAs NPs were able to specifically recognize plasmodium-infected red blood cells and even to recognize the parasite itself. The NPs had high loading capacity for primaquine and chloroquine anti-malarial drugs. In addition, the studies showed that the NPs did not exhibit cytotoxic effects against normal red blood cells and had in general very good biocompatibility [62].

So far PAAs are mostly used for the synthesis of dendrimers, which are synthetic, highly branched supramolecular structures. The synthesis generations of PAA dendrimers

determines their structure. The higher is the dendrimer generation, the more branched is the dendrimer itself (Figure 1.5). Several types of multifunctional dendrimer-based nanocarriers have been developed for anticancer therapy [63]. These dendrimers are highly functional and permit incorporation of different types of drugs into their branched structure. The versatility of dendrimers and also the simple methods of preparation have found increased interest from researchers. Dendrimer-drug conjugate formations can be controlled, which leads to tailoring of multifunctional, PAA-based dendritic systems [64]. Cationic PAA dendrimers have shown to form stable complexes with proteins via electrostatic interactions. Particularly, PAA dendrimer complexes with human serum albumin (HSA) are demonstrated to be very stable, because of both electrostatic interactions and physical entrapment of the protein inside the dendrimer branches [65]. PAA dendrimers were also used to prepare PEG-PAA core-shell NPs. The produced NPs had much better biocompatibility compared to PAA dendrimers alone. Those novel nanostructured carriers for drug delivery had excellent structural flexibility and thermoresponsive properties [66].

In spite of all their advantages, PAA dendrimers are toxic due to their polycationic nature [67]. Therefore; new methods of PAA NPs preparation are needed in order to synthesize multifunctional and stable delivery vectors that are also more biocompatible.

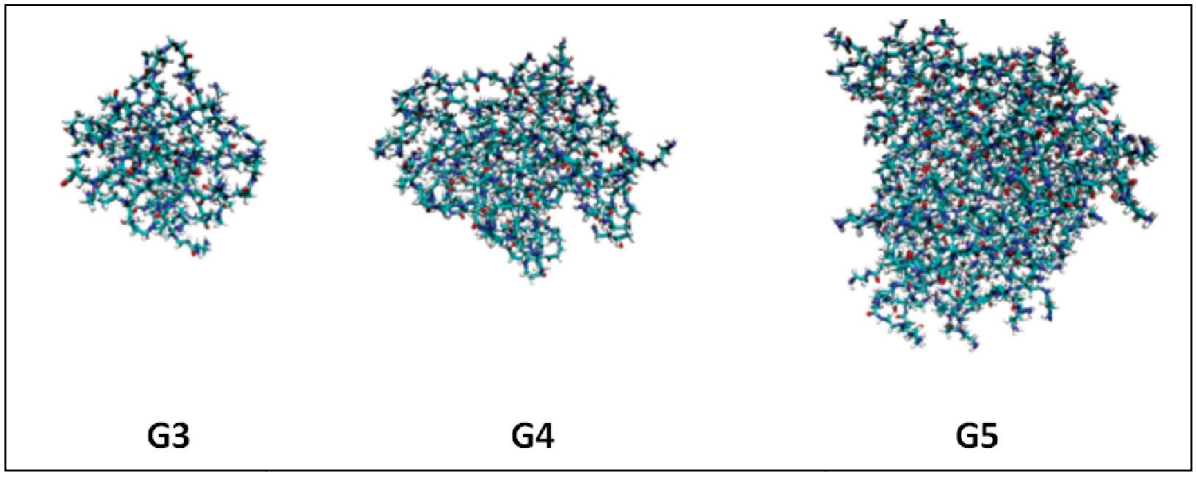

Figure 1.5 3D structure of PAA dendrimers. G3, G4 and G5 are third, fourth and fifth generations of dendrimers. Modified from [68].

1.6 Self-assembled PAAs NPs: state of the art and challenges

Functionalized linear PAAs can form self-assembled cationic complexes with negatively charged compounds. The self-assembly method has advantages over traditional NPs synthesis methods (such as double emulsion solvent evaporation method, DESE) that it does not require toxic organic solvents in the synthesis. By using diverse types of monomers, different types of hydrophilic PAA polymers can be synthesized for various types of complex formations [69]. It has been shown that the properties of those complexes vary considerably depending on the PAA polymer structure. However, in all cases PAA polymers were able to successfully encapsulate proteins (such as β-Galactosidase enzyme) and form nanosized assemblies. The NPs were successfully internalized into cells and showed high levels of enzyme delivery. [70].

The electrostatic interactions between positively charged PAAs and negatively charged proteins ensure that a wide variety of complexes can be formed in this way (Figure 1.6). This

opens many perspectives for PAAs to deliver proteins for therapeutic purposes. Self-assembled PAA NPs were also used for insulin delivery. Nevertheless, the NPs had relatively high surface charge (25–35 mV), which limited their application to non-intravenous conditions (*e.g.* nasal administration) where aggregation with serum proteins does not play an important role [71].

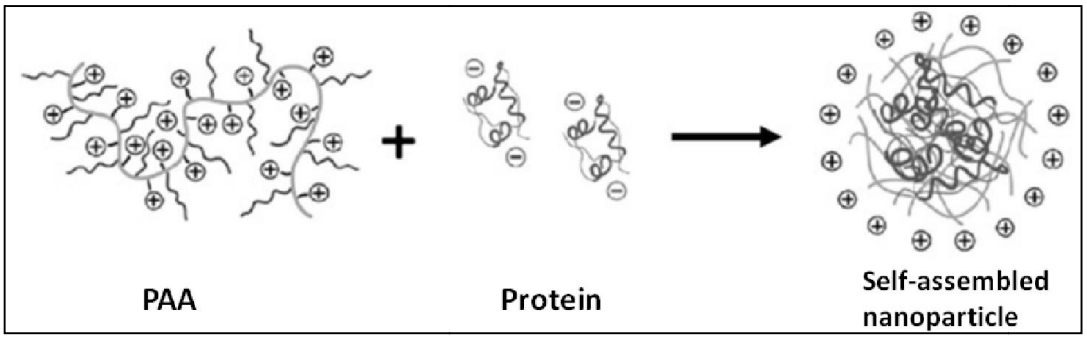

Figure 1.6 Self-assembly of a PAA NP. Modified from [72].

PAAs complexes with proteins can be done in two steps as well. In the first steps PAAs complexes with HSA are made, which enables to have stable nanoparticles with a well characterized properties. In the second step, the self-assembled complexes can be used for encapsulation of various types of drugs that interact with both PAA polymers and HSA [72].

Additionally, the big structural variability of PAA polymers makes it possible to synthesize them with disulfide linkages, which are dissolved in highly acidic environments, such as inside liposomes. The self-assembled NPs made from bioreducable PAA complexes with proteins, can successfully penetrate cell membranes and degrade in liposomes, releasing their cargo inside the cells [73].

Synthetic PAAs can also be used for the preparation of layer-by-layer assembled NPs to be used as potential carriers. The NPs size, internal structure and surface charges can be

controlled by monitoring the PAA polymer's composition. In this way relatively stable NPs are achieved, which notwithstanding their positive charge, have tolerable toxicity levels thanks to their linear structure and relatively lower positive charge compared to PAA dendrimers [74].

As already mentioned, Agmatine functionalization substantially increases the biocompatibility of PAAs. The extraordinary biocompatibility of PAAs polymers can be explained taking into account that repeating units of PAAs are often designed to be reminiscent of peptides. Those polymers are also used for self-assembled NPs preparation. It has been demonstrated that Agmatine-functionalized PAAs have strong antiviral properties by binding on the cell surface heparin sulfate proteoglycans. This inhibits the cell binding of several types of viruses, such as human papillomavirus-16. The Agmatine functionalized self-assembled PAA NPs carrying anitiviral drugs can be effectively used as multifunctional therapeutics against many sexually transmitted viral infections [75]. The NPs suppress the herpes simplex virus and human cytomegalovirus by inhibiting them due to their polycationic nature and their side guanidine groups. These antiviral properties are so prominent that, the NPs had enter preclinical phase of investigations [76].

Self-assembled PAA NPs have shown good biocompatibility and low cytotoxicity both *in vitro* and *in vivo.* PAA internalize into the cell via permeabilization of endocytic vesicular membranes [77]. Amphiphilic PAA-cholesterol conjugates have been found to be stable in blood but cleavable inside the cells. Its easiness of preparation allows synthesis of series of conjugates in order to find the best formulations for drug delivery. These nanocomposites had low cytotoxicity and show good potential in biotechnological applications [78].

In spite of all their advantages, self-assembled NPs lack long term stability both on shelves and during *in vivo* administrations. The other challenge is the difficulty to synthesize NPs with optimal biophysicochemical properties while using vigorous industrial scale up and manufacturing processes. The self-assembled NPs usually show batch to batch variability due to the lack of precise control in their preparation process [79]. Because self-assembly is essentially a molecular process, this way of NPs preparation requires substantial extension of interactive connections. The bottom-up approach of this type of NPs construction requires much more sophisticated approaches to solve all the stability concerns. One of the approaches can be the fusion of self-assembly method with top–down nanofabrication methods in order to yield highly functional NPs with all necessary properties for scientific applications [80]. Thus, effective ways of self-assembled NPs stabilization while maintaining all their intrinsic advantages is decidedly needed.

1.7 Photo-crosslinked NPs

Many NPs synthesis methods, including self-assembly, are very mild and resulted NPs usually have low stability and release drugs prematurely. One of the best ways to enhance NPs' stability is crosslinking [81]. Crosslinked NPs show superior structural stability compared to non-crosslinked ones. The crosslinking also enhances permeability of NPs and their retention time in tissues. This is a very effective way of preventing premature release of drugs and deliver them at sustainably higher concentrations to their target tissues [82]. Crosslinked NPs show significantly higher efficacy and reduced toxicity compared to their direct competitors [83]. Moreover, crosslinking can help to prepare NPs that respond to different environmental factors, such as temperature, pH and ionic strength [84]. One of the crosslinking approaches is chemical crosslinking. Epichlorohydrin is widely used for this purpose [85]. Another approach is ultraviolet (UV) light induced photo-crosslinking that has gained wide popularity in recent years.

Yang and others used UV initiated crosslinking to synthesize gold NPs capped by photo-crosslinkable carboxybetaine-terminated thiols. Those NPs were exceedingly resistant to protein adsorption from undiluted human blood serum, were stable at low pH and high temperature and had good cell uptake [86]. Zou and others demonstrated that crosslinked NPs have enhanced tumor accumulation, much better tumor inhibition rates but lower cytotoxicity against healthy cells. Furthermore, histological studies showed that the photo-crosslinked NPs made less damage to livers and kidneys of mice [87]. In another study, exposure of photo-crosslinkable core containing micelles to UV light greatly stabilized them and enhanced their degradation time [88].

The photo-crosslinking degree of NP can be easily tuned as a function of UV exposure [89]. Dickerson and others made photo-inducible self-assembled nanoassemblies from block copolymers and used UV crosslinking to further stabilize the NPs. Photo-crosslinking did not change doxorubicin drug's release at pH 7.4 but did at pH 6.0, which resembles the low pH of endosomal environment. The UV exposure time was correlated with the NPs crosslinking level that in its turn determined the NPs degradation rate (and subsequent drug release) at pH 6 [90]. Additionally, photo-crosslinking improved hyaluronic acid NPs' stability for tumor-targeted drug delivery [91].

1.8 Aim of the study and brief description of the results

The aim of this study was to develop stable and efficient PAA NPs for drug delivery to the CNS. The NPs were synthesized by UV assisted photo-crosslinking of Agmatine-functionalized PAAs with electrostatic stabilization of HSA. PAA NPs synthesis was optimized to give them all necessary properties for CNS targeting. The NPs were P80 coated, had less than 150 nm size and had very high biocompatibility levels. The P80 coating not only stabilized the NPs, but also gave them CNS targeting properties. The unique photo-crosslinking synthesis method resulted in NPs more stable than other NPs synthesized from linear PAAs. The NPs were shown to successfully encapsulate and release model drugs and pass across *in vitro* BBB models.

2. MATERIALS and METHODS

2.1 Materials

Lithium hydroxide, 4-aminobutylguanidine (Agmatine), hydrochloric acid (37%), 4-(2-hydroxyethyl)-1-piperazineethanesulfonic acid (HEPES), human serum albumin (HSA), chitosan, 2-Hydroxy-4'-(2-hydroxyethoxy)-2-methylpropiophenone (Irgacure 2959), dulbecco's phosphate buffered saline (DPBS), polyoxyethylenesorbitan monooleate (Polysorbate 80), fluorescein isothiocyanate isomer I (FITC), methacrylic anhydride, β-Galactosidase from *Escherichia coli*, isopropanol, acetone, dimethyl sulfoxide (DMSO), Medium 199 (M-199) and in MCDB-131 cell culture media, foetal bovine serum (FBS), heparin, penicillin-streptomycin, L-glutamine and endothelial cell growth factor (ECGF) were purchased from Sigma-Aldrich in the highest purity available and used without further purification. Cyanine® 3 labeled Goat Anti-Mouse IgG (H+L) antibody (IgG-Cy3) was purchased from Jackson ImmunoResearch. ProLong® Gold antifade mountant and Streptavidin-Alexa Fluor® 647 conjugate (STR647) were purchased from ThermoFisher Scientific. In all experiments ultrapure water was used obtained from a Milli-Q® water purification system (Millipore).

2.2 PAA nanoparticles synthesis by UV crosslinking

2.2.1 Synthesis of PAA oligomers

PAA oligomers (OPAAs) with three different MW (2, 4 and 8 kDa) were synthesized in Advanced Biomaterials platform, Filarete Foundation (Milan, Italy) as already described in the literature [61,92].

Briefly, 2,2-bis(acrylamido)acetic acid (BAC) was prepared as previously reported and its purity (99.9%) was determined both by acid–base titration and by nuclear magnetic resonance spectroscopy [93]. BAC (200 mg, 1.0 mM), water (333 µL), lithium hydroxide (48.8 mg) and Agmatine (for 2 kDa OPAA: 168.8 mg; for 4 kDa OPAA: 199.4 mg; for 8 kDa OPAA: 236.2 mg) were mixed in a 2 mL glass tube. The mixture had pH 9.0 and was stirred at 35^{o}C for seven days under inert atmosphere and in the absence of light. The mixture then was diluted at 1:50 ratio with Milli-Q® water and its pH was adjusted to 4.0 by adding 37 % hydrochloric acid. The unreacted BAC was purified from the solution by using ultrafiltration on a membrane with a cut-off of 1 kDa (OPAA-2 kDa) or 3 kDa (OPAA-4 kDA and OPAA-8 kDa) and consequently freeze-dried (Telstar Cryodos 50).

2.2.2 UV-assisted crosslinking

All reagents were dissolved in 10 mM HEPES buffer (pH 7.4) if not specified otherwise. Initially, 150 µL of the OPAAs solution (1.0 mg/mL) was mixed with 37.5 µL of HSA solution (2.0 mg/mL) to induce electrostatic interactions between those oppositely charged molecules. Then, 25 µL of FITC solution (0.4 mg/mL, in water) and 3.75 µL of Irgacure 2959 (1100 mg/mL, in DMSO) photoinitiator were added to the mixture. After each addition, the

mixture was gently shaken for 10 seconds. Then, the mixture was diluted by adding 1150 µL HEPES (10 mM, pH 7.4) buffer. The final mixture (with 1366 µL total volume) was exposed to ultraviolet (UV) irradiation (UVP, Black-Ray B100AP lamp, 365 nm wavelength at 10 mW/cm^{-2} power). Total UV exposure was 10 minutes. Flat bottomed, transparent glass vials with volume of 8 mL were used as containers. The vials were put on an aluminum foil covered support, perpendicular to the UV rays at 10 cm distance (Figure 2.1). All synthetic procedures were performed in an ice bath except for the UV irradiation, which was performed at room temperature (RT).

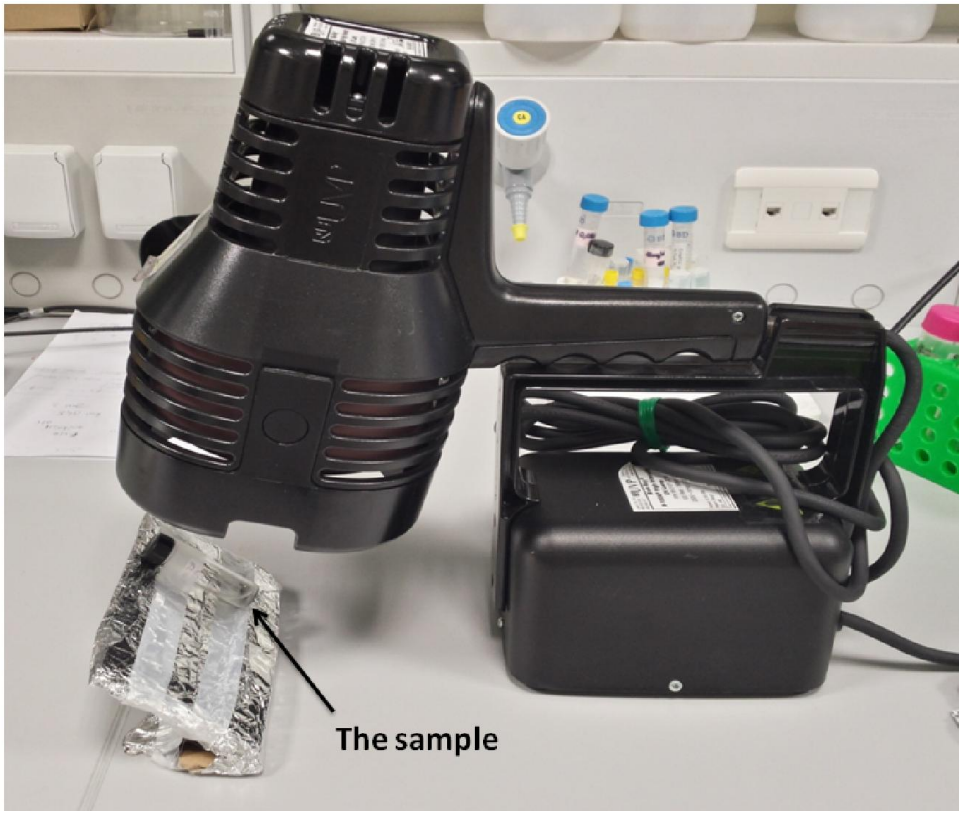

Figure 2.1 The UV lamp and reaction mixture in an 8 mL glass vial for PAA NPs preparation.

2.2.3 Optimization of synthetic parameters and samples naming

During experiments, several parameters were systematically changed and investigated. These parameters are represented in the following list:

1) *Molecular weight (MW) of OPAA*. Polymer chains with an average MW of 2 kDa, 4 kDa and 8 kDa were tested.

2) *HSA/PAA ratio*. HSA was used in 37.5 µL, 75 µL and 150 µL amounts thus the weight ratios between the OPAA and HSA were 2/1, 1/1 or 1/2 correspondingly.

3) *Presence or absence of FITC*.

4) *Irgacure 2959 concentration*. Four different concentrations of Irgacure 2959 (1100 mg/mL, 550 mg/mL, 220 mg/mL and 110 mg/mL) were tested. The final reaction solution volume (1.366 mL) was always kept constant by changing the amount of HEPES buffer added at the end.

The NPs samples were named based on their synthesis formulations (Table 2.1). For example, OHFI-2k sample was synthesized from 2kD MW OPAA, HSA, and FITC in the presence of Irgacure 2959. The number before any initial means increase of the reagent's concentration compared to the initial formulation. A dot (".") and number after any initial means reduction of the reagent's concentration compared to the initial one. For example, O-2HFI.5-2k sample naming means that HSA (H) concentration was increased twice and Irgacure 2959 (I) concentration was reduced five times compared to OHFI-2k sample.

Naming initials	Compound
O	OPAA
H	HSA
F	FITC
I	Irgacure 2959
Ig	IgG-Cy3
S	Streptavidin-Alexa647
B	β-Galactosidase
C	Methacrylated chitosan
T	Polysorbate 80 (Tween® 80)
2k/ 4k /8k	MW of OPAA - 2/4/8 kDa

Table 2.1 PAA NPs samples naming initials based on the reagents used in the synthesis.

2.2.4 Polymeric coating

2.2.4.1 Methacrylated chitosan (MC): Synthesis and coating

PAA NPs were further functionalized by using MC. To this aim, MC was synthesized adapting the method described by Tocchio and others to prepare methacrylated gelatine [94]. Briefly, chitosan was solubilized into DPBS at 10% (w/v) concentration at 60^{o}C. Methacrylic anhydride was added to the chitosan solution at a rate of 0.5 mL/min under constant stirring at 50^{o}C until the concentration of methacrylic anhydride was up to 20% v/v. The mixture was allowed to react for 1 hour (h) and then supplementary DPBS was added to stop the reaction. To remove salts and methacrylic acid, the mixture was dialyzed against distilled water using 12-14 kDa MW cut-off dialysis tubing for 1 week at 40^{o}C. After lyophilization for one week, white porous foam was collected and stored at -20^{o}C.

For PAA NPs synthesis, MC was diluted in 10 mM HEPES buffer at 1.0 mg/mL concentration. During the synthesis MC was added after the addition of Irgacure 2959 at 13 µL (-C), 26 µL (-

2C), 65 µL (-5C) and 130 µL (-10C) amounts. After it, the sample's total volume was adjusted to the standard 1.366 mL and the UV irradiation was applied.

2.2.4.2 Polysorbate 80 (P80)

P80 (known also as Tween® 80) was added in the reaction mixture in order to coat PAA NPs. 15 µL of P80 (20 mg/mL, in HEPES 10 mM buffer, pH 7.4) was added to the PAA NPs mixture immediately after the UV exposure. The sample was gently shaken and left for incubation at +4^{o}C for 3 h. The NPs were methodically characterized both before and after the addition of P80.

2.2.5 Scale-up experiment

In order to have bigger amounts of PAA NPs, a scale-up experiment was designed, where ten times more reagent amounts were used. O-2HI.2-(T8)-2k formulation was used to this aim. The experiment was carried out in a 50 mL glass beaker. 1.5 mL of OPAA solution (1.0 mg/mL, in 10 mM HEPES buffer, pH 7.4) was mixed with 0.75 mL of HSA solution (2.0 mg/mL, in 10 mM HEPES buffer, pH 7.4), then 0.01875 mL of Irgacure 2959 (1100 mg/mL, in DMSO) was added. Afterwards, 11.3 mL of the HEPES buffer was added into the beaker for further dilution. The mixture was exposed to UV light under constant and mild stirring (Figure 2.2). The magnetic stirrer was covered with aluminum foil in order to increase the UV irradiation of the sample. Every fifth minute of irradiation a sample was taken for characterization. Total exposure time was 15 minutes. After the UV irradiation, 0.15 mL of P80 (20 mg/mL, in 10 mM HEPES buffer, pH 7.4) was added and stirred at RT for 10 minutes. The sample then was

incubated at +4^{o}C for 18 h and further characterized. Moreover, an aliquot of the reaction mixture was taken for characterizations before the UV exposure as a control to monitor the NPs formation. This experiment was repeated three times and the results were always consistent.

Figure 2.2 The scale-up experiment for PAA NPs synthesis. 1 – Aluminum covered magnetic stirrer, 2 – beaker with the sample.

2.3 Nanoparticle purification

2.3.1 Centrifugation

NPs sedimentation by centrifugation is widely used for their purification. Usually, multiple rounds of centrifugation and subsequent washing are required to remove byproducts as well as unreacted reagents. This process is usually done by using centrifuges where the rapid rotation of its rotor applies a centrifugal force to the samples and phase separation occurs based on particles size [95,96].

"Eppendorf" 5415 centrifuge was used in order to precipitate and purify PAA NPs. Various centrifugation settings were applied. Namely, following parameters were changed: The rotation speed (5000 G, 10000 G and 15000 G), centrifugation time (10 min, 20 min and 30 min) and temperature (at 4^{o}C or 25^{o}C).

2.3.2 Dialysis

Dialysis is a process used to separate molecules with different MW from each other by using a semipermeable membrane. This technique has many applications in various fields of medicine and biochemistry. It uses the fact that in aqueous solutions all molecules are in Brownian motion and tend to disperse evenly as the time goes on. However, if the sample is inside a dialysis tubing, only small molecules can pass through it and the big molecules and supramolecular assemblies (such as NPs) stay inside the tubing. Usually the dialysis buffer volume should be no less than 100 times bigger than the sample volume. The small molecules move from high concentration to smaller concentration until equilibrium is established. After this, the dialysis buffer is removed and new dialysis buffer is added. The remaining small molecules inside the dialysis tubing start to diffuse again to the fresh buffer

until a new equilibrium is established. Repetition of this cycle for several times virtually removes all the small molecules inside the dialysed sample (Figure 2.3). Dialysis is commonly used for NPs purification since unreacted reagents and solvents can pass through the dialysis membrane keeping the NPs inside the tubing [97].

In order to remove all unreacted reagents from the suspension, PAA NPs were purified by using dialysis membrane (Spectrapor, cellulose ester, 100 kDa MW cut-off) against deionised water for 4 h at RT. The dialysis buffer was replaced once per hour.

Dialysis membranes are usually fully permeable for molecules having sizes 75-80% the size of dialysis membrane pore. This sets the limit for 100 kDa cut off membrane to up to 80 kDa molecules. Yet, some proteins used in PAA NPs synthesis had MW higher than 80 kDa. Accordingly, for their purification another method was used described in the next sections.

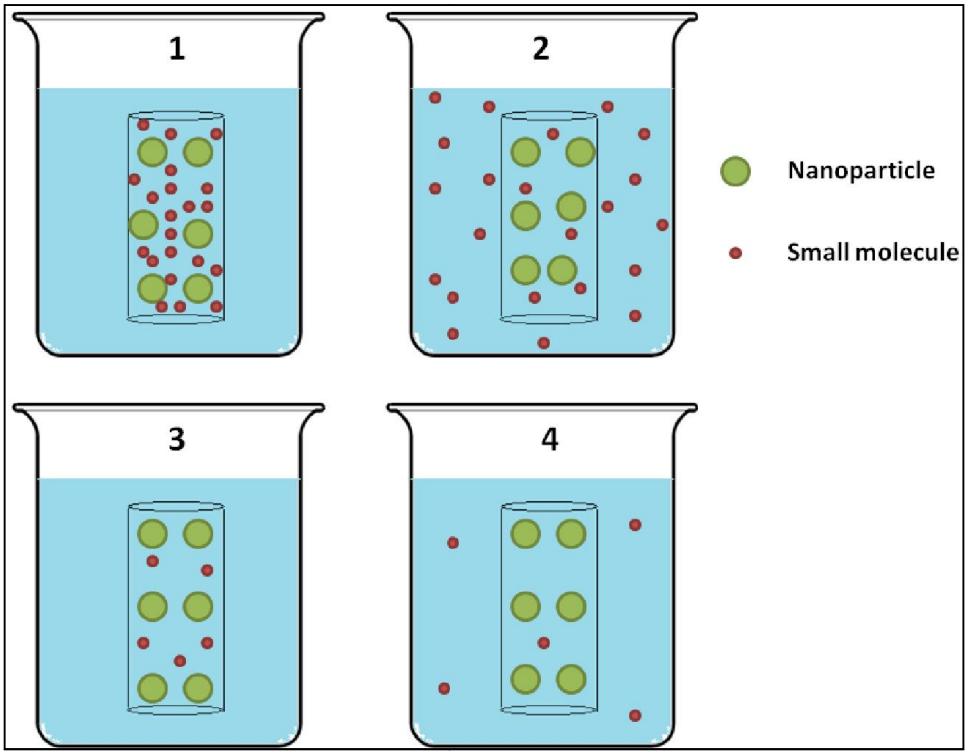

Figure 2.3 Dialysis purification scheme of NPs. 1) Start of the dialysis. 2) Equilibrium is established for small molecules. 3) Removal of old dialysis buffer and addition of a new one. 4) New equilibrium is established.

2.3.3 Size exclusion chromatography

Size exclusion chromatography (SEC) was applied in order to purify PAA NPs from aggregates and molecules having MW more than 80 kDa. It is a chromatographic technique used to separate molecules and particles based on their size and MW. SEC has an advantage of compatibility with a wide range of buffers, because environmental conditions do not affect SEC purification process. That is the reason that SEC is a very good purification method for biomolecules that are sensitive to pH or ionic strength changes. SEC columns consist of a porous matrix composed of spherically shaped, chemically inert and tightly packed particles. This matrix is filled with a preservation buffer. When a mixture of differently sized particles is added on top of a SEC buffer, fractional separation occurs due to the universal gravitational

pull and entrapment of particles within the matrix pores. The bigger is the particle, the faster it elutes through a SEC column [98].

Illustra NAP-25 columns (GE healthcare) were used for PAA NPs purification. After removing the preservation buffer from the columns, they were washed by 25.0 mL of 10 mM HEPES buffer (pH 7.4). The NPs suspension (total reaction volume: 1.366 mL) and 8.0 mL HEPES 10 mM (as eluting buffer) were subsequently added. After this the eluted buffer was collected and methodically characterized to find out when the NPs get eluted. The data showed that most PAA NPs eluted in the range between 3.0-4.5 mL. This experiment was repeated four times for differently sized NPs and the above-mentioned data was always consistent.

2.4 NPs characterization

2.4.1 Dynamic light scattering and zeta (ζ) potential

2.4.1.1 Determination of NPs size, polydispersity and count rate

Dynamic light scattering (DLS, also known as Photon Correlation Spectroscopy) is a technique used to assess the size, polydispersity and relative concentration of NPs and small microparticles. DLS measures the Brownian motion of colloidal particles dispersed in liquid phase and relates this motion to the particles size. The smaller is a particle the faster its Brownian motion is. Moreover, it is related to the viscosity of the liquid phase and the viscosity in its turn is correlated to the temperature. Particles motion velocity is characterized by a property known as translational diffusion coefficient. Therefore, the exact knowledge of the temperature is needed for precise size calculations. The particles are illuminated by a monochromatic laser and the light scattered from the particles is collected by photo-

detectors [99]. Two light scattering theories are used for DLS technique, depending on particles size. For particles having sizes considerably smaller than the illuminating wave length, Rayleigh approximation is used and for particles having sizes roughly equivalent to the illuminated light, Mie theory is used. The particle size is calculated by using the Stokes-Einstein equation:

$$d(H) = \frac{kT}{3\pi\eta D}$$

Where

d(H) = hydrodynamic diameter

D= translational diffusion coefficient

k = Boltzmann's constant

T= absolute temperature

η= viscosity

The diameter measured by DLS is the hydrodynamic diameter of the particle, consisting of both NPs and adsorbed water molecules on the NPs surface. It is equal to the diameter of a spherical hypothetical particle which would have the same translational diffusion coefficient as the measured particle. For this reason the particles surface modifications play an important role in the determination of their sizes. Particularly, particles with not smooth surfaces or having polymer chains protruded from their surfaces will show larger hydrodynamic diameters. DLS measurements also depend on the ionic strength of the medium; low conductivity media usually form conductive double layers around particles, which in its turn increase their size.

Malvern Zetasizer Nano ZS90 instrument (with 633 nm laser wavelength) was used to determine the NPs mean size, polydispersity index (PdI), relative concentration (derived

count rate, DCR) and surface charge distribution (Zeta-potential). PdI can have values from 0 to 1. Samples having PdI value of 0 are ideally monodisperse samples. On the other hand, PdI value of 1 indicates about a very polydisperse sample. Usually, PdI values less than 0.2 are considered to be good, and between 0.2-0.4: as acceptable.

The Zetasizer Nano ZS90 instrument uses different attenuator values for different samples to obtain relatively constant detection signal; this means that average count rate among various samples cannot be compared. To have an absolute count rate number for various samples, a DCR is calculated, which is a theoretical value of a count rate if there was no attenuation and the laser power was always 100%. The DCR allows signal strength comparison between different samples. Furthermore, if the DCR of one sample decreases throughout incubation, this is a good indication that the sample is degrading and hence its signal is dropping [100].

The samples were prepared by diluting reaction mixture ten times in MilliQ water. The measurements were carried out in poly(methylmethacrylate) cuvettes and performed at least in triplicates. The means and standard deviations were calculated. Few samples, which had very high PdI and very low DCR (hence indicating that they did not contain any NPs) were analyzed by only one DLS measurement.

2.4.1.2 Determination of NPs zeta potential

Particles in suspensions continuously collide due to their Brownian motions. To prevent them from aggregation, either electrostatic or steric repulsion forces are necessary. In particular, repulsive forces of particles should dominate their attractive forces to ensure suspensions' stability. Colloidal particles are charged intrinsically and in aqueous solutions they become surrounded by ions, which form ionic layers around the particles. These layers are composed

of two sub-layers: the inner part (Stern layer) that is tightly attached to the particles and the second, outer sub-layer that is less firmly attached (Figure 2.4). There is a boundary within the diffuse sub-layer (slipping plane) where the net charge of the particle and ions remain constant. The potential of this boundary is zeta potential. The zeta potentials of negatively charged particles are always higher than their intrinsic surface charges, due to the positive ionic double layer which compensates some part of the surface charge. The same is true for positively charged particles: their zeta potentials are always lower than their surface charges [101].

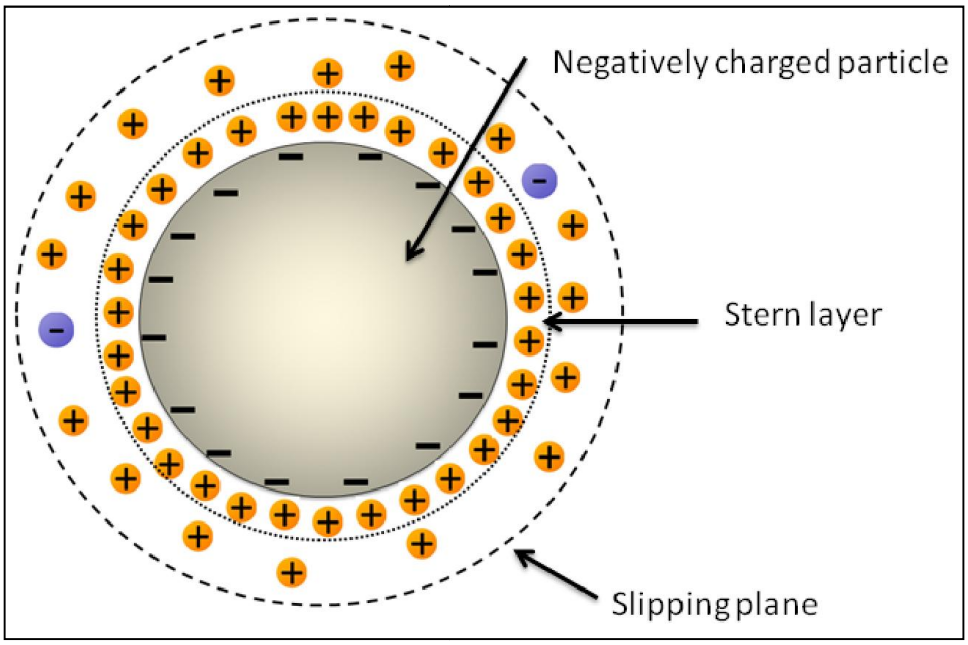

Figure 2.4 Schematic representation of ionic double layers of a charged particle in an aqueous medium. The electric potential of slipping plane is zeta potential.

The zeta potential value is important for the determination of colloidal systems stability. Particles with very positive (more than +20 mV) or very negative zeta-potentials (less than -20 mV) will effectively repel each other, ensuring the suspension's stability. Conversely, the

repulsion between the particles with low zeta potential values is not enough to avoid particles aggregation.

In aqueous media many factors affect on zeta potential. Particularly, the pH of the medium plays a crucial role in this regard. The higher is the pH, the more positive is the zeta potential and vice versa. The ionic strength and temperature of the media are also important factors in determination of zeta potentials.

Zetasizer Nano ZS90 instrument uses micro-electrophoresis system in a disposable folded capillary cell to determine particles' zeta potential. When an electric field is applied in the cell, the charged particles start to move and the instrument's laser beam, which passes through the cell, starts to fluctuate. The detector measures the frequency of these fluctuations (which is proportional to the particle's speed) and the particles' zeta potential is calculated based on these measurements [102].

2.4.2 Confocal laser scanning microscopy

Confocal laser scanning microscopy (CLSM) has been widely used for different scientific imaging applications including NPs visualization. It has distinct advantages over conventional fluorescent microscopes by scanning the samples line by line and collecting the light in a single focal plane. CLSM eliminates out-of-focus background, which vastly improves the image quality [103]. CLSM can be used for imaging of relatively thick samples (up to 0.1 mm). The use of photo-multipliers helps to collect light signal from near-UV range to near-infrared and to increase the signal significantly. A wide range of naturally occurring or synthetic fluorophores can be used for CLSM imaging, enabling to capture very small details in

biological systems up to a single molecule. By using different fluorescent molecules in the same specimen, it is possible to spot several target molecules simultaneously [104].

Leica TCS SP5 confocal laser scanning microscope was used to visualize fluorescently labeled NPs. Samples were prepared on round glass supports, which were washed and cleaned first with isopropanol and then with acetone to completely remove dirt and dust (especially from the centre of the coverslip). After carefully examining that there was no impurities remaining, 4 mL NPs suspension (in a dilution suitable for DLS measurements) was added in the middle of the glass support. Then it was half-covered, and left to dry overnight. The images were captured by using a 63x Immersion oil objective (Leica) with numerical aperture of 1.4. The images were captured at resolution of 1024x1024. The excitation wavelength of FITC was at 495 nm and the emission signal was collected at 519 nm wavelength. The excitation wavelength of Cyanine® 3 was at 550 nm and the emission signal was collected at 570 nm wavelength.

2.4.3 Stimulated emission depletion microscopy

Stimulated emission depletion (STED) is one of the most popular super-resolution microscopy techniques that has resolution superior to the diffraction barrier of visible light. It is based on CLSM and uses its advantages. STED uses a high power laser, which produces a doughnut-shaped focal spot to superimpose the samples emission wavelength. STED wavelength is usually set a little longer than the emission peak in order to avoid excitation by itself. The doughnut-shaped STED laser induces stimulated emission in the sample's fluorophore, which results to depleted emission, allowing to obtain only the fluorescence signal in the middle of the exposed fluorophore, where there is no STED (Figure 2.5). In this way superior resolutions are achieved compared to the ordinary CLSM. STED requires special sets of

fluorophores that can resist photobleaching [105]. It also requires the samples to be strictly fixed, because even slight disturbances in the location of the sample components greatly affect the STED image quality.

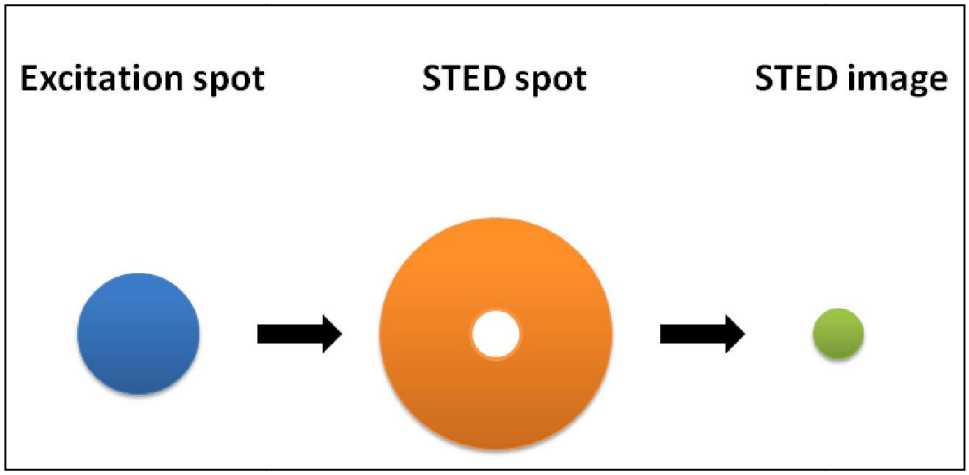

Figure 2.5 Scheme of STED focal spots of the excitation light, STED spot and the resulted STED image.

Leica TCS SP8 microscope equipped with a gated-STED module and an HCX PL APO 100x/1.4 OIL STED ORANGE objective, a white light laser source, and a 592 nm depletion laser was employed. The STED images were acquired using the hybrid detectors with a pixel size of 25 nm. To prepare STED samples, PAA NPs were purified from exceeding FITC molecules using SEC columns (Sephadex, GE Healthcare) and eluted with HEPES buffer (10 mM, pH 7.4). The PAA NPs were deposited onto a glass coverslip and left to dry for 1 h, then one drop of ProLong®Gold was added, another glass coverslip was placed above and cured in the dark for 24 h.

2.4.4 Scanning Electron Microscopy

Scanning electron microscopy (SEM) is a type of electron microscope that allows topological characterization of samples at much higher magnifications than visible light microscopes.

This is based on the fact that the wavelength of electrons is about 100000 times shorter than the wavelength of visible light photons, resulting to the higher resolution of electron microscopes. SEM uses a concentrated beam of electrons to scan the surfaces of investigated samples. Electrons in the beam interact with sample's atoms and induce several types of secondary signals from the sample, which are captured by SEM detectors [106]. There are different types of signals that SEM samples can emit, such as back-scattered electrons, secondary electrons and specific X-rays. SEM samples should be electrically conductive and grounded in order to avoid electric charge accumulations and subsequent image distortions. Those samples that are composed of non-conductive materials (such as polymeric samples and biological samples) should be coated by a thin layer of a coating material, which is usually sputtered in vacuum. Although SEM resolution is lower than that of transmission electron microscopy (TEM), it is still very high, reaching up to 0.4 nm in the most advanced instruments. Compared to TEM, SEM has a larger field of view and capability of bulk materials characterization. Field Emission Scanning Electron Microscope (FE-SEM) has a superior resolution over traditional SEM, thank to the fact that FE-SEM uses field emission electron guns instead of thermionic emitters used in traditional SEM. [107].

Zeiss-Sigma FE-SEM was used to take images of PAA NPs. SEM samples were prepared according to the following procedure. Silicon dioxide supports were cleaned carefully with isopropanol and acetone and left to dry at RT. NPs dilute suspension with the volume of 2 µL was added to the support, spread carefully and left to dry at RT. Subsequently, the dry NPs were gold sputtered in argon atmosphere (Polaron e5100) and used for imaging. Images were acquired using an acceleration voltage of 1 kV.

2.4.5 Determination of NPs composition by bicinchoninic acid assay

Bicinchoninic acid (BCA) assay is a biochemical colorimetric assay, which is used to determine protein concentration in solutions. This method uses BCA as a detection agent for Cu^{+} ions that are formed when proteins reduce Cu^{2+} ions in an alkaline environment. Then two BCA molecules chelate to one Cu^{+} ion and the resulting complex has purple color and strong absorbance in 562 nm wavelength. This absorbance increases linearly in correlation to protein concentration increase [108].

Micro BCA™ Protein Assay Kit (ThermoFisher Scientific) was used to evaluate HSA content in PAA NPs. Diluted bovine serum albumin (BSA) solutions at concentrations of 0, 2, 5, 10, 15 and 20 μg/mL were prepared as calibration standards. The BCA working reagent was prepared by mixing solutions “A” “B” and “C” at the ratios 25:24:1 respectively. Then 1 mL of investigated sample was mixed with 1 mL of working reagent and incubated for 1 h in water bath (Grant GLS 400) at 60^{o}C. After incubation, the samples were quickly cooled to RT to stop the reaction. The samples were analyzed by Agilent, Cary 100 UV-Vis spectrophotometer for their absorption at 562 nm wavelength. A standard calibration curve was constructed based on BSA standards and, consequently, protein concentrations of analyzed samples were calculated based on the curve.

2.4.6 Spectroscopy detection techniques

2.4.6.1 UV-Vis spectrophotometry

Ultraviolet-visible (UV-Vis) absorption spectroscopy is one of most extensively used techniques in chemistry. The main principle of this technique focuses on the fact that most

molecules have the ability to absorb electromagnetic light in ultraviolet or visible spectrum. This absorption corresponds to the excitation of an outer electron in the tested molecules from the highest occupied molecular orbital to the lowest unoccupied molecular orbital [109].

The instrument used to determine the absorbance spectra was Agilent, Cary 100 UV-Vis spectrophotometer. It consists of three core elements: UV-light source, a monochromator and a detector. The monochromator works as a diffraction grating to dispense the beam of light into the various wavelengths, while the detector function is to record the intensity of the transmitted light.

2.4.6.2 Fluorescence spectroscopy

Some molecules known as fluorochromes absorb light by transferring the energy of the photons to their electrons, which occupy higher energy levels. Some of the energy is released after a few nanoseconds as a lower energy (and therefore longer wavelength) photon than the initial photon. This phenomenon is called fluorescence. The remaining energy is released within 10-15 seconds as thermal energy when the electron returns to the lowest vibrational energy state. The wavelengths that induce a molecule to fluoresce are known as the *excitation spectrum*, and the wavelengths of emitted fluorescent light the *emission spectrum* [110].

The fluorescence spectra of tested molecules were recorded with Horiba, Fluoromax-4 spectrofluorometer.

2.5 Encapsulation of model drugs

2.5.1 Encapsulation of Immunoglobulin G - Cyanine® 3

Goat anti-mouse Immunoglobulin G labeled with Cyanine® 3 fluorescent marker (IgG-Cy3) was used as a model compound for encapsulation. PAA NPs encapsulated by IgG-Cy3 (OIg-2HI.2-(T8)-2k formulation) were prepared as follows. All reagents were dissolved in 10 mM HEPES buffer (pH 7.4) if not specified otherwise. 150 µL of the OPAAs solution (1.0 mg/mL, 2kDa) was mixed with 3.75 µL IgG-Cy3 (12.5 mg/mL) and then 75.0 µL of HSA solution (2.0 mg/mL). After that, 3.75 µL of Irgacure 2959 (550 mg/mL, in DMSO) photoinitiator was added to the mixture. After each addition, the mixture was gently shaken for 10 seconds. The sample was diluted by adding 1119 µL HEPES buffer (10 mM, pH 7.4). The mixture was exposed to UV irradiation for 10 min and then 15 µL of P80 (20 mg/mL) was added to it and left to incubate at +4^{o}C for 3 h. After that the samples were purified by SEC (Illustra MicroSpin G-25 Columns).

To evaluate the release of IgG-Cy3 (OSHI.2-(T8)-2k) five NPs samples (0.88 mL each) were incubated at 37^{o}C under constant 100RPM stirring (Heidolph Incubator 1000, Unimax 1010). At certain time points (0 h, 6 h, 24 h, 48 h and 72 h) one sample was taken, purified by SEC and analyzed by DLS (to evaluate the stability) and then by spectrofluorometer (Horiba, Fluoromax-4) for detection the fluorescent signal of IgG-Cy3. The excitation wavelength was set at 530 nm and the emission signal was collected at 565 nm. A standard calibration curve was constructed by spectrofluorometry analysis of IgG-Cy3 solutions in HEPES buffer (10 mM, pH 7.4) at 1, 2, 4, 8, 16 and 32 µg/mL concentrations. The protein encapsulation and subsequent release was calculated based on the calibration curve.

2.5.2 Encapsulation of Streptavidin-Alexa 647

Alexa Fluor® 647 fluorescent dye conjugated Streptavidin (STR647) was used for the encapsulation into PAA NPs (OSHI.2-(T8)-2k formulation).

All reagents were dissolved in 10 mM HEPES buffer (pH 7.4) if not specified otherwise. 150 µL of the OPAAs solution (1.0 mg/mL, 2kDa) was mixed with 3.75 µL STR647 (20.0 mg/mL) and then with 37.5 µL of HSA solution (2.0 mg/mL). After that, 3.75 µL of Irgacure 2959 (550 mg/mL, in DMSO) photoinitiator was added to the mixture. After each addition, the mixture was gently shaken for 10 seconds. The sample was diluted by adding 1119 µL HEPES buffer (10 mM, pH 7.4). The mixture was exposed to UV irradiation for 10 min and then 15 µL of P80 (20 mg/mL) was added to it and left to incubate at +4^{o}C for 3 h. After that the samples were purified by SEC (illustra MicroSpin G-25 Columns).

2.5.3 Encapusulation of β-Galactosidase

β-Galactosidase was encapsulated into two formulations: OBHFI-8k and OB-2HI.2-(T8)-2k. OBHFI-8k formulation was prepared as follows. Initially, 150 µL of the OPAAs solution (1.0 mg/mL, 8kDa) was mixed with 10 µL of β-Galactosidase (1 mg/mL) and then with 37.5 µL of HSA solution (2.0 mg/mL). After that, 25 µL of FITC solution (0.4 mg/mL, in MilliQ water) and 3.75 µL of Irgacure 2959 (1100 mg/mL, in DMSO) photoinitiator were added to the mixture. After each addition, the mixture was gently shaken for 10 seconds. The sample was diluted by adding 1140 µL HEPES buffer (10 mM, pH 7.4). The mixture was exposed to UV irradiation for 10 min.

OB-2HI.2-(T8)-2k formulation was prepared as follows. 150 µL of the OPAAs solution (1.0 mg/mL, 2kDa) was mixed with 10 µL of β-Galactosidase (1.0 mg/mL) and then with 75 µL of HSA solution (2.0 mg/mL). After that, 3.75 µL of Irgacure 2959 (550 mg/mL, in DMSO) photoinitiator was added to the mixture. After each addition, the mixture was gently shaken for 10 seconds. The sample was diluted by adding 1112 µL HEPES buffer (10 mM, pH 7.4). The mixture was exposed to UV irradiation for 10 min and then 15 µL of P80 (20 mg/mL) was added to the mixture and left to incubate at room temperature for 2h. Both samples were purified by SEC (illustra MicroSpin G-25 Columns).

2.6 Stability studies

PAA NPs stability was assessed by incubating them in different media, namely: 1) HEPES buffer (10 mM, pH 7.4); 2) HEPES buffer (10 mM, pH 7.4) supplemented with 20 % FBS; 3) HEPES buffer (10 mM, pH 4.5) supplemented with 20% FBS (the pH was brought to 4.5 value by adding 5 M hydrochloric acid); and 4) 100 % FBS.

Then the NPs were characterized by DLS at certain time points. The evaluation of the NPs degradation rate was performed by evaluating the NPs mean size, PdI and DCR change dynamics.

Following incubation parameters were used: 1) 25^{o}C, static condition; 2) 37^{o}C, static condition; 3) 37^{o}C, stirring at 100 RPM. Heidolph Incubator 1000 with Unimax 1010 stirrer was used for this purpose.

2.7 Assessment of PAA NPs influence on cell viability

2.7.1 Study of NPs behavior in the tested biological medium

Before biological experiments, PAA NPs were incubated in cell culture medium to assess their stability in a complex biological medium and to be sure that there is no any premature degradation. OHFI-10C-8k formulation was synthesized, then dialyzed and subsequently sterilized using short wave UV-C rays (265 nm) exposure for 5 min. The stability of the following samples was tested for 48 h (the cell viability test duration). The tested samples were: the NPs after synthesis (sample 1), the NPs after dialysis (sample 2) and the NPs after sterilization (sample 3) were incubated in HEPES buffer (10 mM, pH 7.4). In addition, sterilized PAA NPs were diluted in HUVEC medium at 1/5 ratio (sample 4), 1/10 ratio (sample 5) and 1/20 ratio (sample 6). As a control only HUVEC medium was incubated as well. The stability was checked at 0 h, 24 h and 48 h time points by DLS.

2.7.2. MTT assay

The tetrazolium dye MTT (3-(4, 5-dimethylthiazolyl-2)-2,5-diphenyltetrazolium bromide) assay is a colorimetric assay that allows detection of cell viability. Metabolically active live cells reduce yellow MTT to insoluble purple formazan that can be later solubilized and detected by high-throughput spectrometry. This reduction occurs only in the presence of living cells because they secret dehydrogenase enzymes that produce equivalents of NADH and NADPH, which in their turn reduce the MTT [111].

Cell Proliferation Kit I (MTT, Roche Diagnostics) was used to investigate the influence of PAA NPs on human umbilical vein endothelial cells (HUVEC, ATCC, passages 15-20) viability. The

cells were cultured in M-199 medium supplemented with 20% FBS, 100 unit/mL penicillin, 0.1 mg/mL streptomycin, 0.1 mg/mL heparin and 50 ng/mL ECGF.

The experiment was performed as follows: HUVEC with the density of 10^5 cell per well were seeded in a 96-well multiwell plate and were incubated for 24 h at 37^{o}C in humidified air containing 5% CO_2. Then, the medium of each well was changed with medium containing NPs at different dilutions (1/5, 1/10 and 1/20 times) and left to incubate for another 24 h. Next day, 10 µL MTT solutions were added to each well and incubated for 4 h and afterwards 100 µL formazan diluting solution was added to each well. Following an overnight incubation, the plates were read by Tecan, Sunrise ELISA plate reader. Each sample was tested in five separate wells. Standard deviations were calculated for each measurement.

2.8 Permeability studies across *in vitro* BBB model

IgG-Cy3-loaded PAA NPs (OIg-2HI.2-(T8)-2k) permeability across an *in vitro* BBB model was assessed by using transwell inserts. Transwell permeability supports (0.4 µL polycarbonate membrane, 0.33 cm^2 surface area) were purchased from Corning Incorporated. bEnd5 immortalized mouse brain endothelioma cell line was kindly donated by prof. Elisabetta Dejana (IFOM, Milan, Italy) with the permission of prof. Britta Engelhardt (Theodor Kocher Institute, Bern, Switzerland).

The cells were cultured in MCDB-131 medium supplemented with 20% FBS, 100 unit/mL penicillin, 0.1 mg/mL streptomycin, 0.1 mg/mL heparin and 50 ng/mL ECGF. The lower chambers of transwell inserts were filled with 0.6 mL complete medium, and the upper chambers – with 0.1 mL medium. The cells were cultured on transwell inserts at 50000

cells/cm^2 density and incubated at 37°C in humidified air with 5% CO_2. After three days of incubation, bEnd5 cells reached confluence. Then, the transwell's upper chamber medium was replaced with fresh medium containing NPs or controls. Following samples were used for the permeability tests: NPs encapsulated with IgG-Cy3 (OIg-2HI.2-(T8)-2k), NPs without IgG-Cy3 (O-2HI.2-(T8)-2k), HEPES buffer, IgG-Cy3 alone at the concentration of 34.3 µg/mL (equal to the concentration of IgG-Cy3 in the NPs), and cells grown in a complete medium. The first three samples were used at 1/10 dilutions in cell culture medium. After 6 h and 24 h of incubation, the media in the lower chambers of transwells were taken for analysis and replaced by fresh media. The samples were analyzed by spectrofluorometry (Horiba, Fluoromax-4) to check the amount of fluorescent IgG-Cy3 passed across bEnd5 cells monolayer and the semipermeable membrane of transwells. All measurements were performed in triplicates and standard deviations were calculated.

To check if the NPs had toxic effect on the cells, confluent bEnd5 cells were exposed to the investigated samples and checked visually for the presence of dead cells and evaluation of structural integrity. The images of the cells were captured by Leica DMC4500 microscope camera with 5-Megapixel CCD Sensor.

3. RESULTS and DISCUSSION

3.1 Synthesis of PAA NPs

3.1.1 Development of PAA NPs synthesis method

Due to the presence of tertiary amines in the polymeric backbone, PAA oligomers (OPAAs) in aqueous solutions behave like polyelectrolytes. Accordingly, at pH values lower than 7.4, OPAAs are present as polycations as a result of partial protonation of agmatine groups in their polymer chain [112]. This property play a crucial role in the PAA NPs synthesis. Indeed, so far PAA NPs have been synthesized by self-assembly of positively charged OPAAs with negatively charged proteins or nucleic acids, using ionic interactions [113]. This synthetic approach is very easy, the only difficulty being to optimize experimental conditions for inducing polymer condensation in nanosized particles. However, self-assembled NPs usually suffer from intrinsic instability; further, they may disassemble in the presence of more affine proteins/molecules. This is not desirable, because it leads to premature drug release and subsequent failure of the NPs therapeutic aim [79]. Therefore, an effective method of PAA NPs stabilization is highly required.

In order to get more stable PAA NPs, a novel synthesis method was developed by using UV-assisted photo-crosslinking. To this aim, photo-polymerizable acrylate end-groups were introduced into the OPAA for crosslinking reaction. The diacrylamide-terminated OPAAs (Figure 3.1) were mixed with different types of proteins including BSA, gelatin and insulin. Nevertheless, nanosized stable complexes were only obtained by mixing the OPAA chains with HSA solution. All the syntheses were done in 10 mM HEPES buffer at pH 7.4. This buffer

is broadly used in NPs syntheses such as for gold NPs [114]. Moreover, Coué and others used 10 mM HEPES buffer as a medium for self-assembled PAA NPs synthesis [115].

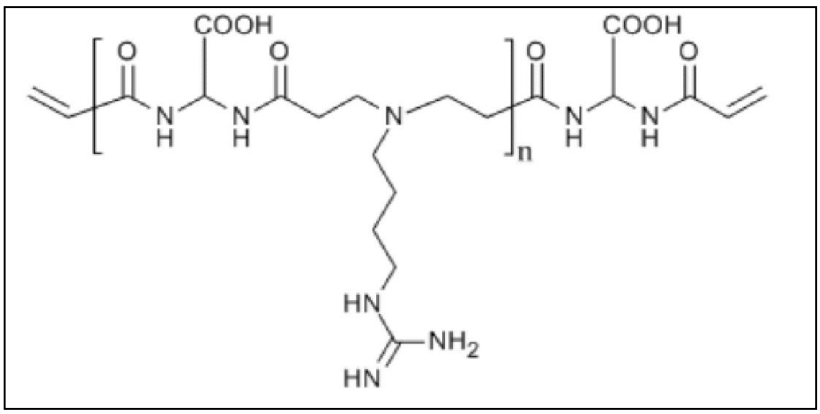

Figure 3.1 Chemical structure of PAA oligomers.

The synthesis was started by mixing the 8 kDa MW OPAAs with HSA solution and left them to interact. At the tested pH value (7.4), OPAAs were positively charged (zeta potential: +17.2 ± 0.7 mV), whereas the HSA was negatively charged (zeta potential: -21.7 ± 3.1 mV). Even though no NPs were formed under these conditions (as suggested by the DLS results), it is reasonable to assume that electrostatic interactions were established between the negatively charged proteins and the positively charged OPAAs.

To achieve well-stabilized NPs, further UV-treatment was performed. UVP, Black-Ray B100AP lamp, which produces 365 nm UV light at 10 mW/cm^{-2}power, was used for UV irradiation. This lamp is a mercury-vapor lamp that uses electric arc through mercury vapor to produce light by gas discharge. The produced UV light is in UV-A range which is the longest wavelength UV and accordingly the safest one [116]. B100AP lamp is widely used for many scientific applications, including NPs synthesis [117].

The general scheme of the synthesis is represented in Figure 3.2. The double bonds on both edges of OPAAs reacted under UV irradiation to form covalent bonds. Thanks to those bonds, OPAAs were crosslinked to each other and HSA molecules became entrapped among those newly formed chains. Moreover, FITC molecules, which were used for the NPs fluorescent labeling, were entrapped as well. The formation of PAA NPs was monitored by DLS analysis.

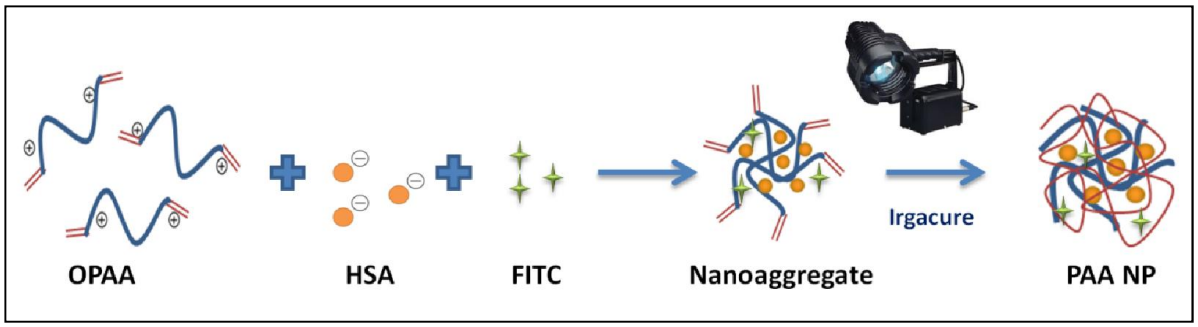

Figure 3.2 Synthesis procedure of PAA NPs. The electrostatic interactions between OPAAs and HSA resulted nanoaggregates where FITC became entrapped. UV irradiation of the nanoaggregates produced HSA and FITC containing PAA NPs.

3.1.2 Control experiments

To assess the role of each constituent in the formation of PAA NPs, control experiments were performed. The samples were analyzed by DLS both before and after UV treatment, as shown in Table 3.1. The OPAAs alone (O-8k formulation) did not form any NPs under UV irradiation. Even when OPAAs were in the presence of Irgacure 2959 photoinitiator (OI-8k), only large and unstable NPs were detected after UV treatment. In fact, they formed micron sized aggregates within 3 h. This sharp instability was ascribed to low zeta potential value and subsequent particle aggregation. The important role of the UV initiator was demonstrated by OH-8k (OPAA and HSA), OF-8k (OPAA, HSA and FITC) and OHF-8k (OPAA, HSA and FITC) formulations; since in all cases polydisperse and unstable aggregates were obtained, meaning that almost no NPs were synthesized under these conditions. The OFI-8k

sample resulted in very unstable NPs, highlighting the principal importance of HSA in PAA NPs synthesis. Accordingly, it was clear that OPAAs, combined with HSA, were able to photo-crosslink in the presence of a photoinitiator and form NPs. Finally, FITC enabled achieving more stable NPs, because the OHI-8k formulation (OPAA, HSA and Irgacure 2959) aggregated within 30 min. The zeta potential of the HEPES buffer was also calculated in order to evaluate its influence on the previous zeta potentials. As expected, it had a negative value, which did not change considerably after UV irradiation. Since all measurements were done in HEPES buffer, this should be considered when evaluating samples' real charges. Particularly, the "O" sample, which was simply OPAAs in HEPES buffer, had higher zeta potential (-6.6 mV after UV exposure) than the buffer alone (-12.4 mV after UV exposure). This made it evident that OPAAs in pure water would have a positive charge, which was in fact confirmed (+17.2 ± 0.7 mV in water).

Formulation	UV	Size (nm)	PdI	DCR (kcps)	Zeta-pot.(mV)
O-8k	before	1740 ± 226	1 ± 0.01	1.5 ± 0.5	-4.6 ± 2.9
	after	1738 ± 302	1 ± 0.02	1.6 ± 0.7	-6.6 ± 1.8
OI-8k	before	288 ± 48	0.32 ± 0.15	29 ± 1	-2.8 ± 1.8
	after	959 ± 53	0.29 ± 0.06	922 ± 62	-1.0 ± 0.4
OH-8k	before	688 ± 122	0.48 ± 0.12	59 ± 8	-11.5 ± 0.5
	after	526 ± 27	0.41 ± 0.1	65 ± 3	-12.4 ± 1.0
OF-8k	before	272 ± 36	0.46 ± 0.9	7 ± 2	-10.5 ± 1.1
	after	420 ± 59	0.55 ± 1.8	12 ± 5	-3 ± 1.5
OFI-8k	before	414 ± 78	0.61 ± 0.11	17± 6	-5.1 ± 0.84
	after	670 ± 76	0.52 ± 0.08	127 ± 15	-9.3 ± 1.9
OHF-8k	before	309 ± 6	0.29 ± 0.08	54 ± 8	-13.2 ± 0.5
	after	280 ± 3	0.19 ± 0.07	158 ± 9	-15.7 ± 0.3
OHI-8k	before	450 ± 61	0.43 ± 0.1	31 ± 11	-12.0 ± 0.3
	after	287 ± 6	0.18 ± 0.01	571 ± 12	-17.1 ± 0.2
OHFI-8k	before	386 ± 108	0.51 ±0.24	61 ± 19	-12.3 ± 1.8
	after	401 ± 1	0.16 ± 0.04	1772 ± 8	-17.0 ± 1.1
HEPES 10 mM	before				-10.4 ± 3
	after				-12.4 ± 3.5

Table 3.1 Control experiments of PAA NPs synthesis. PdI: polydispersity index, DCR (kcps): derived count rate (kilo counts per second). The zeta potential values of HEPES buffer was measured as a control. All measurements were done at least in triplicates and the means and standard deviations are presented.

3.1.3 Synthesis of NPs with methacrylated chitosan

Chitosan is a positively charged, hydrophilic polymer that is usually used in NPs synthesis and coating. Due to its cationic nature, it can effectively coat negatively charged NPs, providing them with mucoadhesive properties and enhancing NPs biocompatibility and stealth properties in biological fluids. Chitosan coating has been applied for both metallic and polymeric NPs [118,119]. To enhance its effective properties, chitosan can be functionalized by various structural groups. One of the approaches is chitosan functionalization by methacrylic groups. Methacrylated chitosan (MC) has double bonds in its methacrylate groups (Figure 3.3) and can crosslink under UV irradiation, like OPAAs. It is shown in the

literature that MC was used for photo-polymerization reactions [120]. MC has been also used in photo-curable hydrogel preparation where it proved to be a very promising material, thanks to its biocompatibility and controllability [121].

As MC was also photo-crosslinkable, the role of OPAAs in the NPs formation was assessed, by designing control experiments where NPs were prepared in the absence of OPAAs and with MC instead.

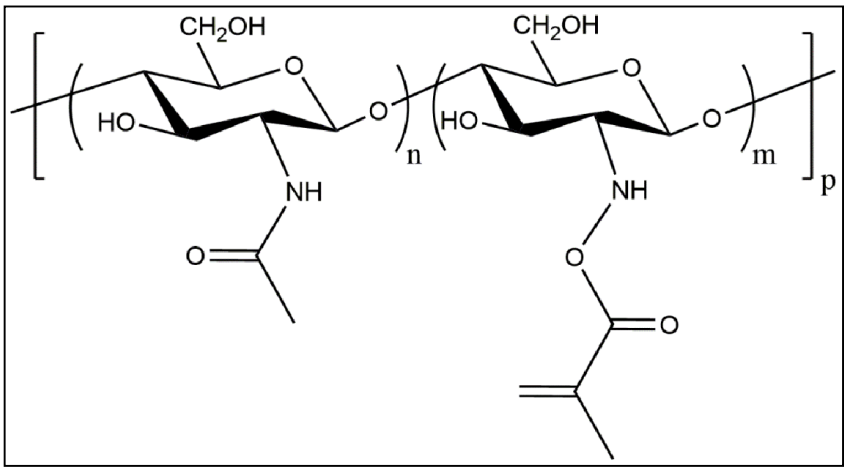

Figure 3.3 Chemical structure of methacrylated chitosan.

Two types of formulations were tested, namely HFI (HSA mixed with FITC and Irgacure 2959) and HI (HSA mixed with only FITC). MC at the concentration of 19.3 µg/mL (2C), 4.76 µg/mL (5C) and 95 µg/mL (10C) was added to both HFI and HI reaction mixture. The DLS measurements of the NPs size, PdI and DCR showed that in the absence of OPAAs, none of the tested formulations produced NPs; neither by just electrostatic interactions (before UV), nor by UV assisted photo-crosslinking (Table 3.2).

Formulation	UV	Size (nm)	PdI	DCR (Kcps)
HFI-2C	Before	558	0.52	18.7
	After	1764	0.9	31.1
HFI-5C	Before	238	0.45	13.7
	After	238	0.33	25.6
HFI-10C	Before	241	0.37	19.3
	After	238	0.26	32.4
HI-2C	Before	290	0.62	3.9
	After	258	0.56	21.1
HI-5C	Before	316	0.59	3.7
	After	567	0.84	6
HI-10C	Before	457	0.73	2.9
	After	304	0.55	3.3

Table 3.2 Controls experiments for NP preparation in the absence of OPAAs. The size, PdI and DCR of reaction mixtures were analyzed by DLS.

After determining the crucial role of OPAAs in photo-crosslinkable NPs synthesis, the influence of MC on the formation process and stability of PAA NPs was investigated.

The OHFI formulation after UV treatment yielded spherical particles with a mean size of 320 nm and negative surface charge (-17 mV). Although it showed good stability with respect to the controls, after 24 h it degraded. In order to get more stable NPs, MC was synthesized and used in NPs synthesis. The obtained polymer was very positively charged (zeta potential: 37.8 ± 1.9 in water) therefore making it possible to interact with negatively charged PAA NPs. The MC was added in the reaction mixture before the UV treatment, but after inducing the interaction between the OPAAs and HSA. Since the OPAA/HSA assemblies and MC are oppositely charged, it is reasonable to assume that MC was mainly grafted onto PAA NPs surface. Then the UV-assisted synthesis of PAA NPs was run by exploiting the potential crosslinking of the double bonds of MC and OPAAs. Two series of formulations of PAA NPs were synthesized in the presence of MC, using 2 kDa OPAAs (OHFI-2k) and 4 kDa OPAAs

(OHFI-4k). Both formulations were synthesized in the presence of four different MC concentrations: 9.5 µg/mL (OHFI-C), 19.3 µg/mL (OHFI-2C), 47.6 µg/mL (OHFI-5C) and 95 µg/mL (OHFI-10C). The results are presented in Table 3.3. The samples were analyzed both before and after UV irradiation. It is evident from the table that for both formulations with 19.3 µg/mL concentration of MC produced the smallest NPs (OHFI-2C). On the other hand, higher or lower MC concentrations resulted in bigger and more polydisperse NPs. This is probably connected to the fact that there was an optimal concentration of MC which had electrostatic interactions with OPAA/HSA complexes to result smaller and more monodisperse NPs.

Formulation	**MC conc. (µg /mL)**	**Size (nm)**		**PdI (nm)**		**DCR (kcps)**	
		Before UV	After UV	Before UV	After UV	Before UV	After UV
OHFI-2k	0	864	310	0.81	0.29	9.7	153
OHFI-C-2k	9.5	278	441	0.45	0.43	10.1	179
OHFI-2C-2k	19.3	206	223	0.35	0.27	17.7	151
OHFI-5C-2k	47.6	173	244	0.25	0.36	23	132
OHFI-10C-2k	95	225	314	0.11	0.12	89	107
OHFI-4k	0	414	328	0.54	0.24	11.4	173
OHFI-C-4k	9.5	1115	858	0.93	0.66	8.3	116
OHFI-2C-4k	19.3	794	209	0.92	0.19	4.8	176
OHFI-5C-4k	47.6	492	565	0.7	0.79	18.5	115
OHFI-10C-4k	95	509	661	0.52	0.71	25.4	125

Table 3.3 Influence of methacrylated chitosan (MC) concentration on PAA NPs mean size, polydispersity index (PdI) and derived count rate (DCR) before and after UV irradiation. PAA NPs synthesized from 2 kDa and 4 kDa oligomers were synthesized by using four different MC concentrations (OHFI-C, OHFI-2C, OHFI-5C and OHFI-10C) in addition to control NPs synthesized without MC (OHFI). All measurements were performed at least in triplicates and the means are represented.

3.2 NPs Characterization

3.2.1 Scanning Electron Microscopy

Scanning electron microscopy (SEM) is a powerful tool in NPs morphological characterization, since it allows the evaluation of NPs surface structure, shape, size and aggregations. Moreover, by using proper preparation methods NPs images can even be taken inside biological samples, without damaging structural integrities of cells [122]. Those properties make SEM widely used by researchers for characterization of both inorganic [123] and polymeric, self-assembled NPs [124].

SEM of PAA NPs (OHFI-8k formulation) (Figure 3.4) showed that the NPs had well-shaped, spherical structures. As the NPs were gold-sputtered, there was a thin (10 nm) gold layer on NPs surface, which made their sizes around 20 nm larger. Taking this into account, PAA NPs had average sizes around 250-300 nm, which was comparable to the hydrodynamic diameter determined by DLS for the same formulation (310 nm), considering that NPs' hydrodynamic diameters are usually slightly bigger than the sizes determined by SEM (as already shown in the literature [125]). Moreover, SEM images showed that there were not any noticeable aggregations in the sample (Figure 3.4 B).

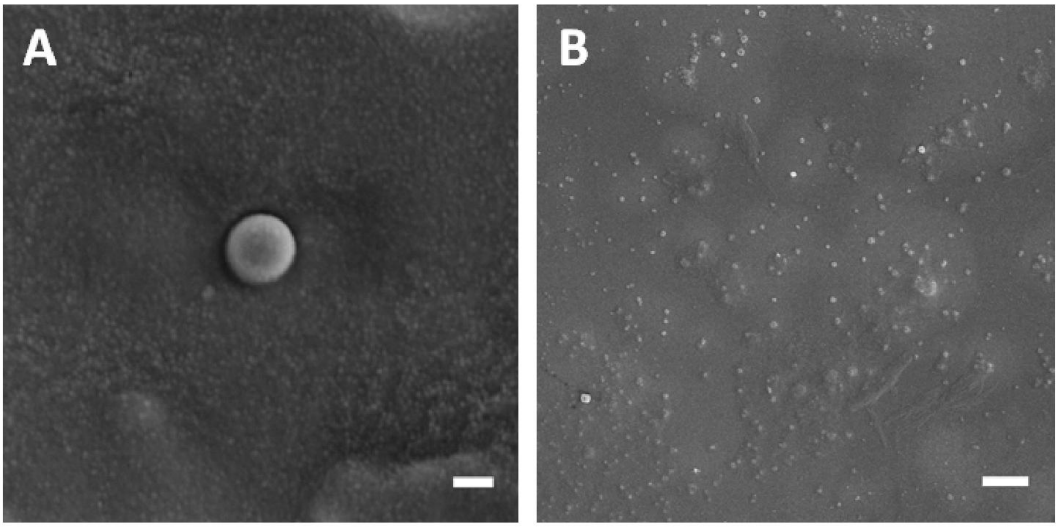

Figure 3.4 Scanning Electron Microscopy (SEM) images of OHFI-8k NPs. A) a single NP (the scale bar is 100nm). B) group of NPs (the scale bar is 2 μm).

3.2.2 Confocal laser scanning microscopy

Confocal laser scanning microscopy (CLSM) has numerous applications in biomedical research. It is extensively used for NPs imaging. Although CLSM does not have as high resolution as electron microscopes, it still can successfully detect encapsulation of fluorescently labeled molecules up to a single molecule and localization of whole NPs [126]. This makes CLSM a very useful tool for the detection of fluorescently labeled compounds encapsulated into NPs [127].

For CLSM analysis, the NPs were synthesized by encapsulating both Cyanine® 3 labeled Immunoglobulin G (IgG-Cy3) and fluorescein isothiocyanate (FITC) (Figure 3.5). In this way the simultaneous encapsulation of a model protein with a large MW (IgG-Cy3, 160 kDa [128]) and a low MW model drug (FITC, 389 Da [129]) was investigated by detecting their signals at different wavelengths. The FITC signal was collected in green channel at 519 nm (Figure 3.5 A) and Cy3 signal - in red channel at 570 nm (Figure 3.5 B). Those two images showed that the fluorescent signal was concentrated into PAA NPs and there was not much background

noise, signifying that tested molecules were actually encapsulated. To see if both IgG-Cy3 and FITC were encapsulated in the same NPs, Figure 3.5 A and Figure 3.5 B were merged. As shown in Figure 3.5 C, many NPs acquired yellow color, indicating the colocalization between the green signal of FITC and the red signal of IgG-Cy3. This clearly suggested that both IgG-Cy3 and FITC had been encapsulated in PAA NPs. It is noteworthy that almost all red signals after the merge became yellow, but many green signals remained unchanged. It means that IgG-Cy3 amount was not enough to be encapsulated in all NPs and FITC, on the other hand, was encapsulated in almost all NPs. This can be explained by taking into consideration that IgG-Cy3 has much higher MW and therefore there were fewer IgG-Cy3 molecules than FITC to be encapsulated into the NPs.

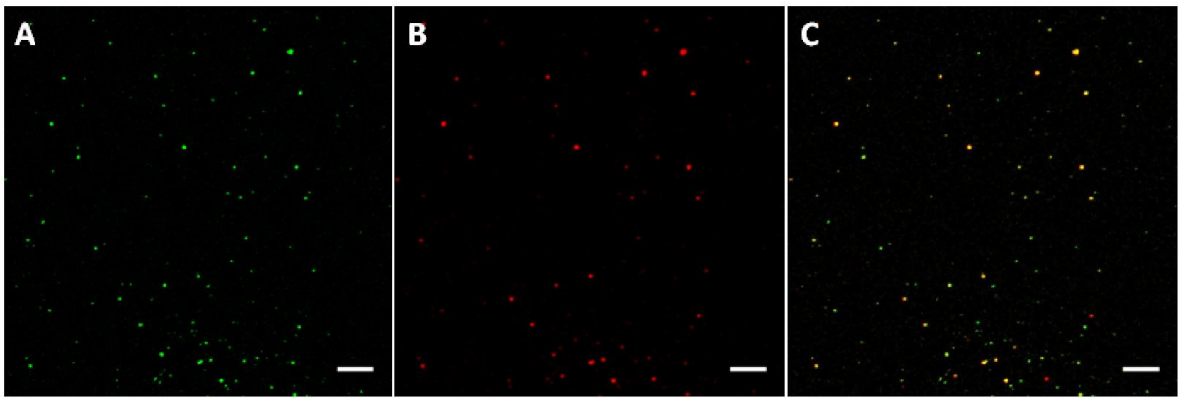

Figure 3.5 CLSM images of PAA NPs encapsulated with IgG-Cy3 and FITC (OIgHFI-8k). A) Fluorescent signal of encapsulated FITC, B) fluorescent signal of encapsulated IgG-Cy3, C) merge of the previous two images. The merge of red and green channels resulted yellow color. Scale bars are set at 2 µm.

3.2.3 Stimulated emission depletion microscopy

CLSM permits detecting the colocalizaton of NPs and the fluorescent signals of encapsulated compounds. However, it has a resolution limit due to the light diffraction. To overcome diffraction limits, in recent years different 'super-resolution' optical microscopy techniques were developed [130]. Stimulated emission depletion (STED) microscopy is one of those

techniques and it is able to push the limits of the optical image resolution to the nanometer scale [131,132].

In order to see FITC localization in the NPs, STED images were acquired for OHFI-8k formulation (Figure 3.6). By comparing CLSM (Figure 3.6 A) and STED images (Figure 3.6 B) of the same observational field, STED images had a better resolution and they showed that FITC was encapsulated predominantly on the surface of PAA NPs, leaving the central zone of the NPs empty. This can be explained considering that during PAA NPs synthesis FITC was added when OPAA/HSA complexes had already been formed and FITC was mainly concentrated on the NPs surface. It is noteworthy to mention that STED microscopy could be used for only special sets of fluorochromes [105] and Cyanine® 3 dyes were not compatible with this technique.

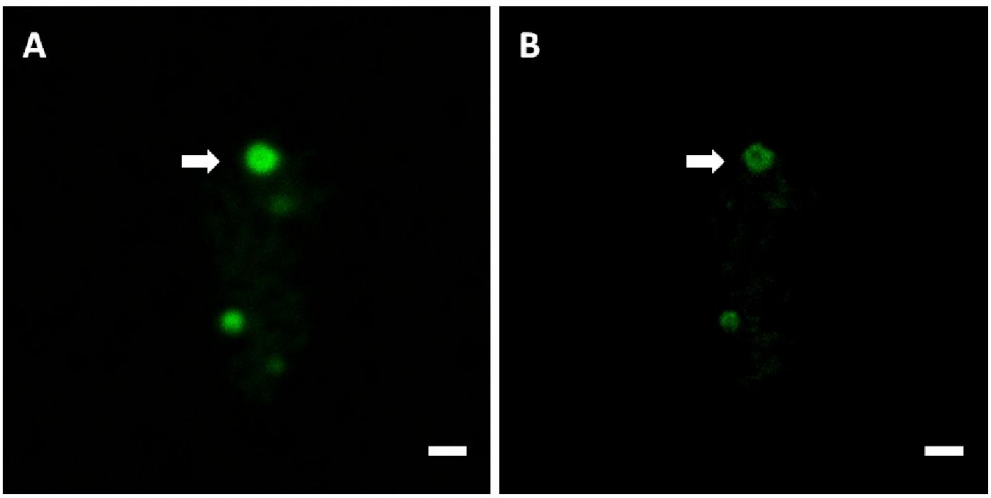

Figure 3.6 CLSM (A) and STED (B) images of OHFI-8k formulation. Scale bars are set at 500 nm.

3.3 PAA NPs synthesis optimization

The photo-crosslinking method initially enabled to synthesize PAA NPs with low polydispersity and sizes of around 300 nm. Yet, those NPs lacked several properties to be considered as good delivery vectors to the CNS. As previously stated, CNS-targeting NPs should optimally have size less than 150 nm, be stable and have special CNS targeting coatings [43,133]. Furthermore, some instability problems have been encountered in PAA NPs formulations, since aggregations were observed after the NPs purification. For this reason, the main synthetic parameters were modified to achieve NPs having the desired properties.

3.3.1 Influence of PAA Oligomers molecular weight

One of the most important parameters to be modified in PAA NPs was the decrease of their size. With regards to Cao and others, who demonstrated that the size and delivery efficacy of polymeric conjugate micelles can be controlled by tuning the MW of polymers [134], it was reckoned that the same effect can be observed also for PAA NPs . As PAA NPs were formed by crosslinking of double bonds at the ends of OPAAs chains, it was assumed that by using smaller OPAAs, smaller NPs could be obtained. In the initial formulation, OPAA with MW of 8 kDa were used. To investigate how the MW of OPAAs affected PAA NPs size, several formulations using OPAAs with 2 kDa, 4 kDa and 8 kDa MW were synthesized. After this, the NPs mean size, PdI and DCR were determined by DLS both before and after UV irradiation (Table 3.4). In case of first formulation (OHFI) no correlation was observed between the NPs size and MW of the oligomers, since the size was around 300 nm in all MWs after UV crosslinking (Table 3.4, samples OHFI-2k, OHFI-4k, and OHFI-8 k). The samples' DCR values were also comparable, showing that for OHFI formulation the PAA oligomers MW did not

affect their main characteristics. For O-2HFI formulation, the samples synthesized from 2 kDa OPAA and 4 kDa OPAAs had similar sizes (257 nm and 265 nm respectively) that was smaller than the size of NPs synthesized from 8 kDa OPAAs (345 nm) (Table 3.4, samples O-2HFI-2k, O-2HFI-4k, and O-2HFI-8k). In case of O-4HFI formulation, the results were similar to that of OHFI formulation. All three samples had similar sizes after the UV irradiation (227 nm, 238 nm and 221 nm respectively). However, when it was tried to see how OPAAs MW affects the encapsulation of the model drug IgG-Cy3 the results were very different. After UV irradiation, 2 kDa OPAAs resulted in much smaller NPs (242 nm) compared to the 8 kDa OPAAs (660 nm) and especially for 4 kDa OPAAs (1446 nm) (Table 3.4, samples OIgHFI-10C-2k, OIgHFI-10C -4k, and OIgHFI-10C -8k). This indicated that for the encapsulation of IgG-Cy3 the 2 kDa OPAA gave the most optimal result and, consequently, 2 kDa MW OPAAs were chosen for further studies.

Formulation	Size (nm)		PdI		DCR (kcps)	
	Before UV	After UV	Before UV	After UV	Before UV	After UV
OHFI-2k	864	310	0.81	0.29	9.7	153
OHFI-4k	414	328	0.54	0.24	11.4	173
OHFI-8k	334	300	0.43	0.19	9	174
O-2HFI-2k	972	257	1	0.43	11	108
O-2HFI-4k	307	265	0.37	0.17	17	168
O-2HFI-8k	238	345	0.24	0.23	33	242
O-4HFI-2k	804	227	0.85	0.39	10	122
O-4HFI-4k	264	238	0.21	0.18	72	222
O-4HFI-8k	240	221	0.51	0.2	26	204
OIgHFI-10C-2k	233	242	0.37	0.39	18.8	82
OIgHFI-10C-4k	342	1466	0.47	0.57	3.9	140
OIgHFI-10C-8k	558	660	0.77	0.45	13	193

Table 3.4 Influence of OPAAs MW on PAA NPs mean size, polysispersity index (PdI) and derived count rate (DCR, in kilo counts per second – kcps) before and after UV irradiation analyzed by DLS. Four formulations (OHFI, O-2HFI, O-4HFI and OIgHFI-10C) were synthesized by using three OPAA MWs (2 kDa, 4 kDa and 8 kDa). All measurements were performed at least in triplicates and the means are represented.

3.3.2 Influence of HSA concentration

HSA is one of the most abundant proteins in blood plasma and it has been generally used in pharmaceutical applications and particularly in drug delivery [135]. HSA has been extensively used in NPs preparation by either covalent attachment on polymeric/metallic NPs or by self-assembly [136].

The electrostatic interactions between HSA and OPAAs played crucial role in the formation of PAA NPs. In fact, in the absence of HSA, no NPs were formed. According to the evidence shown in the literature, the HSA amount in the formation of NPs drastically influences many of NPs properties including their the size [137] which leads to the hypothesis that changing the amount of HSA during PAA NPs synthesis may change their size too. To this aim, three

concentrations were used, namely 54.9 μg/mL (H), 109.8 μg/mL (2H) and 219.6 μg/mL (4H). Three different formulations of PAA NPs were tested, where the only changed parameter was the HSA concentration (Table 3.5). It was evident that HSA amount increase in OHFI-2k formulation decreased the NPs size after UV irradiation from 310 nm to 257 nm when HSA concentration was increased twice (O-2HFI-2k) and, even more prominently, up to 227 nm mean size in case of four times HSA concentration increase (O-4HFI-2k). In case of the second PAA formulation, the OHFI.2-2k and O-2HFI.2-2k samples gave NPs with comparable size. Although the O-4HFI.2-2k sample had much smaller NPs (75 nm), its DCR was significantly lower than the previous two samples, suggesting that PAA NPs synthesis yield was low. In the third formulation (OHI.2-2k), the sample with two times HSA increase (O-2HI.2-2k) had much smaller mean size after UV exposure (122 nm) compared to both the initial sample (385 nm) and the sample with four times HSA increase (O-4HI.2-2k, 514 nm). This suggested that two times increase of HSA amount is the most optimal experimental modification.

It is noteworthy that the DLS data of all three formulations before UV irradiation showed that there were no NPs, confirming the crucial role of photo-crosslinking in PAA NPs formation. The obtained data proved the hypothesis that HSA amount, indeed, was essential in the PAA NPs synthesis by UV photo-crosslinking.

Formulation	Size (nm)		PdI		DCR (kcps)	
	Before UV	After UV	Before UV	After UV	Before UV	After UV
O-HFI-2k	864	310	0.81	0.29	9.7	153
O-2HFI-2K	972	257	1	0.43	11	108
O-4HFI-2k	804	227	0.85	0.39	10	122
O-HI.2-2k	541	385	0.74	0.28	2.2	131
O-2HI.2-2k	319	122	0.59	0.09	1.9	220
O-4HI.2-2k	331	514	0.65	0.41	2.7	364
O-HFI.2-2k	458	180	0.8	0.16	3.1	124
O-2HFI.2-2k	1406	200	1	0.27	7.5	137
O-4HFI.2-2k	42	75	0.45	0.38	1.1	40

Table 3.5 Influence of HSA concentration on PAA NPs mean size, polydispersity index (PdI) and derived count rate (DCR) before and after UV irradiation. Three formulations (OHFI-2k, OHI.2-2k and OHFI.2-2k) were synthesized by using HSA concentrations: 54.9 µg/mL (H), 109.8 µg/mL (2H) and 219.6 µg/mL (4H). All measurements were performed at least in triplicates and the means are represented.

3.3.3 Influence of Irgacure 2959 concentration

Irgacure 2959 is a photoinitiator, widely used in photo-crosslinked and photo-polymerized NPs synthesis [138,139]. Its chemical structure (Figure 3.7) allows its employment in aqueous systems where its active hydroxyl groups under UV light can react with unsaturated double bonds of photo-cured molecules [140].

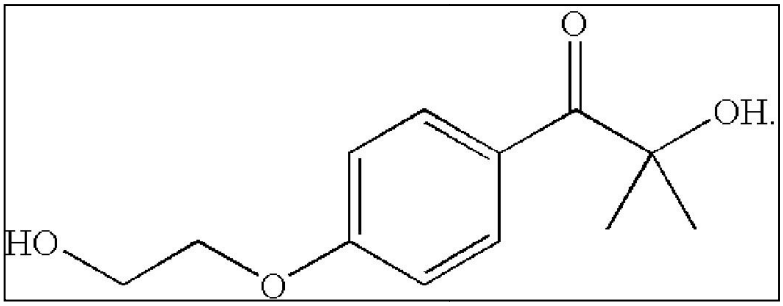

Figure 3.7 Chemical structure of Irgacure 2959.

As already discussed above, after exposing the initial OHFI formulation's reacting solution to the UV light in the absence of Irgacure 2959, no stable NPs were formed. It is noteworthy that the Irgacure 2959 concentration was high in the OHFI formulation's reacting solution (47.4% w/wt of overall reagents), thus it was possible that part of Irgacure 2959 was encapsulated into PAA NPs. Although it is shown that Irgacure 2959 has good biocompatibility [141], its encapsulation was not desired, mainly because it could change the NPs main characteristics including their sizes. With the aim of reducing the Irgacure 2959 amount necessary for obtaining stable PAA NPs with high yied; four concentrations of Irgacure 2959 were tested in two formulations (OHFI-2k and OHFI-8K). In particular, the initial concentration of Irgacure 2959 (3.02 mg/mL) was reduced two times (1.51 mg/mL, OHFI.2-2k and OHFI.2-8k), five times (0.604 mg/mL, OHFI.5-2k and OHFI.5-8k) and ten times (0.301 mg/mL, OHFI.10-2k and OHFI.10-8k). As shown in Table 3.6, in case of OHFI-2k formulation, the reduction of Irgacure 2959 concentration two (OHFI.2-2k) or five times (OHFI.5-2k) considerably decreased the NPs size after UV irradiation, making them from 310 nm to 180 nm and 195 nm respectively. Moreover, OHFI.2-2k and OHFI.5-2k NPs had smaller PdI, hence, were more monodisperse than OHFI-2k. This can be explained by considering that Irgacure 2959 in the initial formulation was excessive and as a result, some part of it could enter PAA NPs composition and/or result too much crosslinking between OPAAs, producing

bigger and more polydisperse NPs. However, ten times reduction of Irgacure 2959 initial concentration (OHFI.10-2k) yielded NPs with bigger sizes (267 nm) than the previous two samples and much higher PdI value (0.52) than even the initial formulation. Evidently in this case the amount of Irgacure 2959 was not enough to catalyze efficiently the photo-crosslinking reaction.

In the OHFI-8k formulation, the above-mentioned dynamics worked, though less prominently. OHFI.2-8k and OHFI.5-8k samples had relatively lower PdI than the OHFI-8k and OHFI.10-8k samples. Noteworthy, for both formulations the samples with ten times less Irgacure 2959 amount had the lowest DCR, indicating that the synthesis yield was not high. Additionally, before UV exposure all the samples had very low DCR and high PdI, demonstrating that no NPs were formed.

Based on the obtained data, Irgacure 2959 concentrations of 1.51 mg/mL (I.2) and 0.604 mg/mL (I.5) were used for next NPs synthesis experiments.

Formulation	Size (nm)		PdI		DCR (kcps)	
	Before UV	After UV	Before UV	After UV	Before UV	After UV
OHFI-2k	864	310	0.81	0.29	9.7	153
OHFI.2-2k	458	180	0.8	0.16	3.1	124
OHFI.5-2k	775	195	1	0.17	5	151
OHFI.10-2k	838	267	0.94	0.52	6.4	119
OHFI-8k	334	300	0.43	0.19	9	174
OHFI.2-8k	373	291	0.49	0.12	5.2	167
OHFI.5-8k	361	266	0.56	0.12	5.1	144
OHFI.10-8k	383	293	0.5	0.2	6.6	128

Table 3.6 Influence of Irgacure 2959 concentration on PAA NPs mean size, polydispersity index (PdI) and derived count rate (DCR) before and after UV irradiation. Two formulations were synthesized by using Irgacure 2959 concentrations: 3.02 mg/mL (OHFI-2k and OHFI-8k), 1.51 mg/mL (OHFI.2-2k and OHFI.2-8k), 0.604 mg/mL (OHFI.5-2k and OHFI.5-8k) and 0.302 mg/mL (OHFI.10-2k and OHFI.10-8k). All measurements were performed at least in triplicates and the means are represented.

3.3.4 Influence of FITC removal

Fluorescent markers are extensively used in NPs synthesis because they enable the detection of NPs in complex biological media (including *in vivo* imaging) as well as visualization of fluorescently labeled biomolecules encapsulation into NPs [142]. FITC is one of the most broadly used fluorescent compounds for NPs labeling. It is derived from fluorescein molecule where one of its hydrogen atoms of the bottom rings is replaced by an isothiocyanate group (Figure 3.8), which is reactive towards nucleophiles including amine and sulfhydryl groups of proteins. FITC is used both for labeling compounds that are encapsulated into NPs [143] and structural polymers used for NPs synthesis [144].

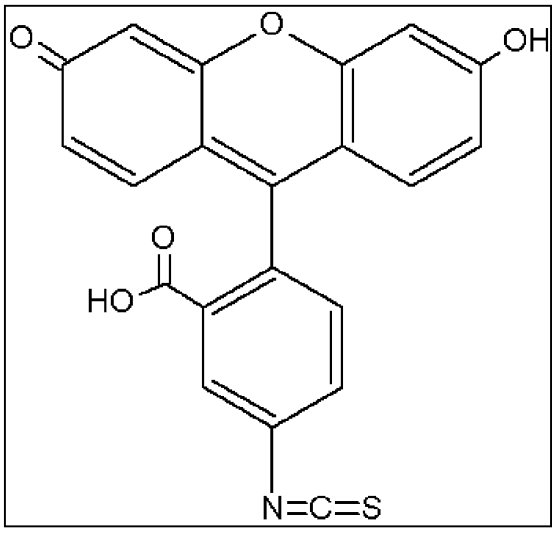

Figure 3.8 Chemical structure of fluorescein isothiocyanate (FITC).

FITC was used in the initial formulation to fluorescently label PAA NPs. Moreover, it was found that FITC encapsulation increased the NPs stability and made them more monodisperse. Yet, FITC needed to be removed to make PAA NPs completely biocompatible, while preserving the reduced size and PdI. The OHFI.2-2k synthesis formulation (which produced the smallest NPs up to that moment) was chosen to be synthesized in the absence of FITC. Nonetheless, the FITC-free formulation (OHI.2-2k) produced NPs with bigger size and higher PdI. To solve the problem, the HSA concentration was doubled and then FITC was removed (Table 3.7), (O-2HI.2-2k). This time the synthesis was successful and the resulted NPs had considerably smaller size (122 nm), which increased their potential to be used for drug delivery applications to the CNS.

Formulation	FITC	Size (nm)	PdI	DCR (kcps)
OHFI.2-2k	+	180 ± 6	0.16 ± 0.05	124 ± 7
OHI.2-2k	-	385 ± 10	0.28 ± 0.13	131 ± 6
O-2HFI.2-2k	+	200 ± 6	0.27 ± 0.02	137 ± 6
O-2HI.2-2k	-	122 ± 3	0.09 ± 0.02	220 ± 2

Table 3.7 Influence of FITC encapsulation on PAA NPs mean size, polysispersity index (PdI) and derived count rate (DCR) after UV irradiation. Two formulations (OHFI.2-2k and O-2HFI.2-2k) were synthesized and compared to their FITC-free variants (OHI.2-2k and O-2HI.2-2k correspondingly). All measurements were performed at least in triplicates and the means and standard deviations are presented.

3.3.5 Polysorbate 80 coating

The O-2HI.2-2k formulation was selected for further studies, since it produced FITC-free NPs having size less than 150 nm. However, a common problem related to PAA NPs was that during dialysis purification they were not stable and tended to aggregate. To enhance PAA NPs stability, Polysorbate 80 (P80, also known as Tween® 80) surfactant was added into the NPs suspension after their synthesis in order to coat the NPs surface. As already discussed in the Introduction section, P80 greatly helps NPs stabilization and also allows them to have CNS targeting properties [38].

In fact, the assumption was correct, and P80 addition significantly stabilized PAA NPs, enabling dialysis purification to be performed without aggregation. To check if NPs were actually coated by P80, DLS measurements were done before and after its addition (Table 3.8). NPs incubated in the presence of P80 showed an increase in mean size by 12 nm, an increase in the DCR (from 220 to 243 kcps) and a slight decrease in the surface charge of the NPs (from -27.6 to-26.1 mV). As the PdI of both samples remained the same, the increase of the mean size was connected to NPs coating by P80 and not aggregation.

Sample name	P80	Size (nm)	PdI	DCR (kcps)	Zeta-pot. (mV)
O-2HI.2-2k	**-**	122 ± 3	0.1 ± 0.02	220 ± 2	-27.6 ± 3.9
O-2HI.2-(T8)-2k	**+**	134 ± 4	0.1 ± 0.02	243 ± 5.8	-26.1 ± 1.5

Table3.8 Influence of Polysorbate 80 (P80) coating of PAA NPs mean size, PdI, DCR and zeta potential. The NPs were analyzed by DLS both before P80 coating (O-2HI.2-2k) and after (O-2HI.2-(T8)-2k). All measurements were performed at least in triplicates and the means and standard deviations are presented.

3.3.6 Summary of PAA NPs synthesis optimization

Table 3.9 summarizes the systematic procedures to reach the optimized formulation. The first step was the synthesis of FITC labeled PAA NPs by UV photo-crosslinking. After this 2 kDa OPAAs were chosen instead of initial 8 kDa MW ones. In the third step, HSA amount was doubled in order to obtain smaller NPs. Next, the amount of photoinitiator Irgacure 2959 was reduced twice, resulting in a further decrease of PAA NPs size. The removal of FITC in the subsequent step not only was necessary to achieve complete NPs biocompatibility but also sensibly reduced their size. Finally, PAA NPs were coated by P80 surfactant, which both increased the NPs stability during dialysis purification and provided a CNS targeting property.

Steps	Formulation	Size (nm)	PdI	DCR (kcps)
1 - The initial fomulation	OHFI-8k	300 ± 17	0.19 ± 0.06	174 ± 8
2 - Use of 2 kDa OPAAs	OHFI-2k	310 ± 16	0.29 ± 0.09	153 ± 9
3 - Increase of HSA amount	O-2HFI-2k	257 ± 16	0.43 ± 0.02	108 ± 8
4 - Reduction of IRG	O-2HFI.2-2k	200 ± 6	0.27 ± 0.02	137 ± 6
5 - Removal of FITC	O-2HI.2-2k	122 ± 3	0.09 ± 0.02	220 ± 2
6 - Addition of P80	O-2HI.2-(T8)-2k	134 ± 4	0.1 ± 0.02	243 ± 6

Table 3.9 Parameters changed for reaching the final PAAs NPs synthesis formulation with NPs mean size, PdI and DCR in each step. Each measurement was performed at least in triplicates and the standard deviations are presented. IRG - Irgacure 2959.

3.4 Scale-up experiment

The increasing applications of NPs in various fields of industry and pharmaceutics have increased the commercial interest for synthesizing NPs in large amounts. Conversely, most NPs synthesis techniques are reproducible only in small scales and researchers fail to reproduce those synthetic methods in larger experimental setups due to the complicated nature of experimental parameters at larger scales. Accordingly scaling-up is of paramount importance for successful industrial large-scale applications of NPs [145,146].

In this study PAA NPs production was scaled up, benefitting from the fact that the synthesis procedure was easy and the experimental parameters that could cause hurdles in larger scales were limited. For this purpose, PAA NPs were prepared with ten times more reagent amounts. To see after how many minutes of UV irradiation the NPs were formed, samples were taken in real-time every five minutes and characterized by DLS (Table 3.10). Total UV exposure was 15 minutes. After five minutes of irradiation, the PdI value was 1 and the DCR (9.3 kcps) of PAA NPs were very low suggesting that no NPs were synthesized yet. After 10 minutes of irradiation, the DCR increased around 18 times (168 kcps) and the PdI was very low (0.079) showing that considerable amount of monodisperse PAA NPs were synthesized with around 126 nm size. Finally, 15 minutes of irradiation resulted in NPs with approximately the same average size and PdI (129 nm and 0.088 respectively) but the DCR increased more (203 kcps), demonstrating that new NPs were formed. After three hours of incubation with P80 at +4^{o}C, PAA NPs size increased around 23 nm (153 nm), while the PdI remained almost same (0.09). This suggested that PAA NPs size increased due to P80 coating and not aggregation. The results showed that the scale-up of the synthesis process was

successfully accomplished and PAA NPs produced with this method had similar sizes and PdI as the NPs synthesized in the smaller scale.

Samples	Size (nm)	PdI	DCR (kcps)
UV 5 min	1161	1	9.3
UV 10 min	126 ± 1.6	0.079 ± 0.027	168 ± 4.4
UV 15 min	129 ± 1.3	0.088 ± 0.03	203 ± 1.6
P80 incubation	153 ± 3.6	0.09 ± 0.02	318 ± 2

Table 3.10 Real time DLS analysis of PAA NPs scale-up synthesis experiment (O-2HI.2-(T8)-2k formulation). Except the first measurement, all other measurements were performed at least in triplicates and the standard deviations are represented.

3.5 NPs HSA content evaluation by BCA assay

The determination of both NPs protein loading and protein adsorption on their surface in biological fluids is very important in evaluating NPs properties biodistribution and drug binding potential. One of the most widely used methods to evaluate NPs protein content is bicinchoninic acid (BCA) assay, which is very sensitive and resistant to impurities [147]. This makes BCA assay very suitable for NPs protein content detection, because inside NPs proteins are usually tightly conjugated with other organic compounds and the purification of proteins inside the NPs is very hard [148].

In this study, the HSA loading in PAA NPs was determined by BCA assay. O-2HI.2-(T8)-2k formulation was chosen for this reason because it produced small, FITC-free and stable NPs and, accordingly, was the best candidate for further optimizations. To have a precise quantitative evaluation, a standard calibration curve was constructed based on bovine serum albumin (BSA) solutions with different concentrations. It is visible in the Figure 3.9 that even at low protein concentrations, the spectrophotometric absorbance levels were linearly

correlated to the protein concentrations. Subsequently, HSA loading in lyophilized PAA NPs was evaluated in four independent measurements. The results were: 15.9 %, 18.3%, 17.1 % and 20.1% w/w. Based on this numbers a mean HSA content with standard deviation was calculated (17.85 ± 1.79 % w/w). This relatively low HSA content could not be explained by only low HSA entrapment during NPs synthesis but also it was an evidence that the NPs were substantially coated by P80, which could make up a considerable part of the NPs weight.

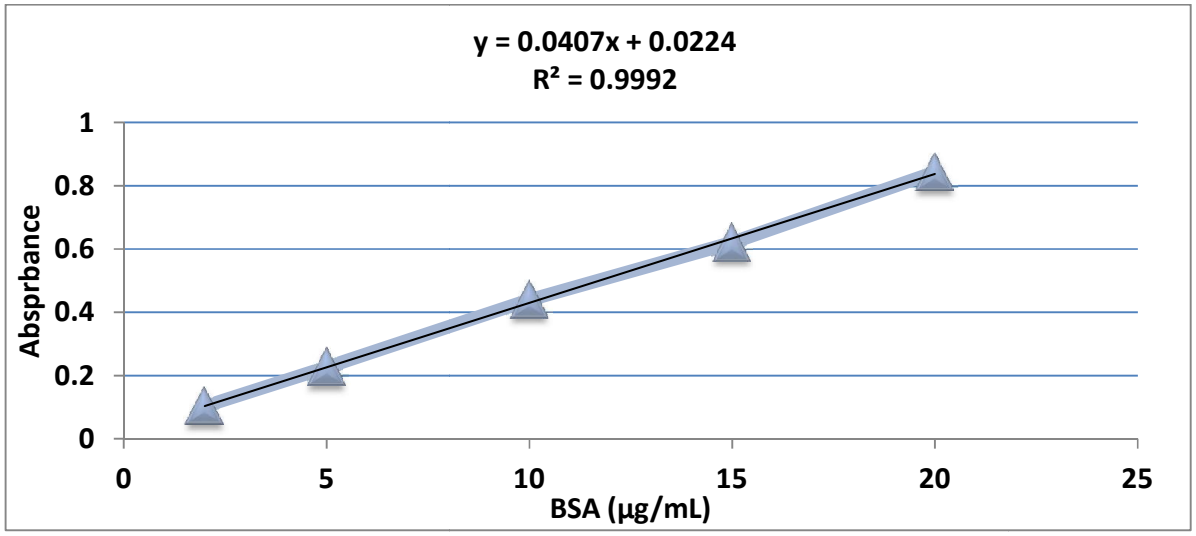

Figure 3.9 Standard calibration curve for BCA assay. All measurements were repeated five times and means are represented.

3.6 Encapsulation of model compounds and their release

3.6.1 IgG-Cy3 encapsulation

Immunoglobulin G (IgG) is broadly used in research as a model drug when investigation of heavy MW proteins incorporation into NPs is required [149]. It is the most common type of antibody in humans and has a complex protein structure with a MW of 140-160 kDa MW

depending on the subtype. Moreover, the conjugation of fluorescent markers to IgG opens new perspectives in drug encapsulation and release detection by highly sensitive spectrofluorometric methods [150].

PAA NPs described in this study were hydrophilic because they were synthesized from hydrophilic compounds in an aqueous medium. Therefore, the NPs could predominantly be used for encapsulation of hydrophilic compounds. To this aim, Cyanine® fluorescent marker conjugated IgG (IgG-Cy3) was used as a model drug to be encapsulated into PAA NPs as a model drug. Four different formulations were chosen to be synthesized in the presence or in the absence (as controls) of IgG-Cy3 (Tabel 3.11). In case of first three samples, the addition of IgG dramatically reduced the NPs size. This can be attributed to the addition of the antibody itself, which being negatively charged, could interact electrostatically with OPAA/HSA complexes and affect the NPs formulation. Additionally, IgG-Cy3 contained BSA in its buffer as a stabilizer and by adding IgG-Cy3 to PAA NPs synthesis solution, considerable amount (roughly equal to the amount of HSA) of BSA was also added. BSA has a structure very similar to HSA [151] and this could have the same effect as increasing HSA concentration twice, which was already observed to decrease the NPs size (paragraph 3.3.2). However, when IgG-Cy3 was added to NPs already synthesized with twice HSA amounts (O-2HI.2-(T8)-2k), the NPs size did not decrease; it even slightly increased. This demonstrated that the overall amount of HSA/BSA decreased PAA NPs size only up to 134 nm and after this no further decrease was observed. IgG-Cy3 decreased NPs size only when they were synthesized with less HSA.

Formulation	IgG-Cy3	Size (nm)	PdI	DCR (kcps)
OHFI-2k	-	310 ± 16.6	0.29 ± 0.09	153 ± 9
OIg-HFI-2k	+	165 ± 5.8	0.22 ± 0.021	105 ± 3
OHFI.2-2k	-	195 ± 4.6	0.17 ± 0.03	124 ± 4
OIg-HFI.2-2k	+	147 ± 0.92	0.11 ± 0.013	81 ± 2
OHFI.5-2k	-	378 ± 9.8	0.27 ± 0.013	151 ± 5
OIg-HFI.5-2k	+	180 ± 6	0.16 ± 0.05	93 ± 2
O-2HI.2-(T8)-2k	-	134 ± 4	0.1 ± 0.02	243 ± 5.8
OIg-2HI.2-(T8)-2k	+	141 ±3	0.11 ± 0.01	195 ± 5

Table 3.11 Influence of IgG-Cy3 on PAA NPs mean size, PdI and DCR. "+" indicate the presence, whereas "-" the absence of IgG-Cy3 in the NPs composition. Each measurement was performed at least in triplicates and the standard deviations are presented.

3.6.1.1 Influence of MC on IgG-Cy3 encapsulation

To see how MC coating influences on the drug encapsulating properties of PAA NPs, IgG-Cy3 was encapsulated into the NPs in both presence (OIgHFI-2C-2k formulation) and absence of MC (OIgHFI-2k formulation). The main DLS characteristics and zeta potential values were measured both before and after UV irradiation (Table 3.12). Before UV irradiation both samples had high PdI and low DCR. Nonetheless, the PAA NPs synthesized with MC had almost four times higher DCR indicating that the electrostatic interactions between OPAA/HSA complexes and MC had occurred before UV irradiation. The zeta potential values were negative and comparable (around -16 mV for both samples). After UV irradiation, significant improvements in DLS characteristics happened for both samples. Particularly, the DCR increased around eight times for OIgHFI-2C-2k formulation and even more impressively 30 times for OIgHFI-2k. The final DCR values were at the same level for both samples (around 200 kcps), indicating that UV-assisted polymerization yielded comparable amounts of NPs for both formulations. Furthermore, the post-UV NPs had considerably lower PdI and size. The zeta-potential values became slightly more negative for both samples (around -19 mV for

both samples). The encapsulation of the model protein (IgG-Cy3) appreciably reduced PAA NPs size in this case too.

Remarkably, the OIgHFI-2C-2k NPs had 10 nm bigger sizes than the OIgHFI-2k NPs. This can be an indication that MC indeed had coated PAA.

Formulation	UV	Size (nm)	PdI	DCR (kcps)	Zeta-pot. (mV)
OIgHFI-2C-2k	before after	694 ± 260 165 ± 5	0.75 ± 0.22 0.16 ± 0.04	24 ± 1 196 ± 1	-16.6 ± 0.6 -19.1 ± 0.9
OIgHFI-2k	before after	446 ± 116 155 ± 4	0.68 ± 0.21 0.13 ± 0.02	7 ± 1 209 ± 1	-16.3 ± 5 -19.5 ± 0.6

Table 3.12 Influence of MC on IgG-Cy3 encapsulation in PAA NPs. Two formulations with MC (OIgHFI-2C-2k) and without MC (OIgHFI-2k) were considered. All measurements were done at least in triplicates and standard deviations are presented.

3.6.1.2 IgG-Cy3 release studies

In order to see how PAA NPs release IgG-Cy3 in *in vivo* conditions mimicking environments, the model protein was encapsulated into OIg-2HI.2-(T8)-2k formulation and incubated in 10 mM HEPES buffer (ph 7.4) at 37^{o}C, under constant stirring. After certain time points, the NPs were purified by SEC and analyzed by both DLS (to see the NPs degradation rate) and spectrofluorometry (to see the fluorescence level of purified NPs). The IgG-Cy3 release was calculated by subtracting the IgG-Cy3 amount of incubated NPs from the initial amount of the encapsulated drug. Afterwards, the IgG-Cy3 release rate was compared to the NPs degradation data measured by DLS (Table 3.13). As it is visible from Figure 3.10, PAA NPs released the model protein in a slow and constant manner, by releasing just 6% of IgG-Cy3 after 6 h of incubation and around 30% after 24 h. Compared to the NPs main DLS parameters presented in Table 3.13, it was evident that the protein release was correlated to PAA NPs degradation. After 24 h and 48 h of incubation, the NPs sizes and PdI increased significantly and on the other hand their DCR decreases in a very rapid rate. This was a clear

indication of the NPs degradation. Furthermore, it can be assumed that most NPs were degraded after 72 h, which was also confirmed by the highest release level of IgG-Cy3.

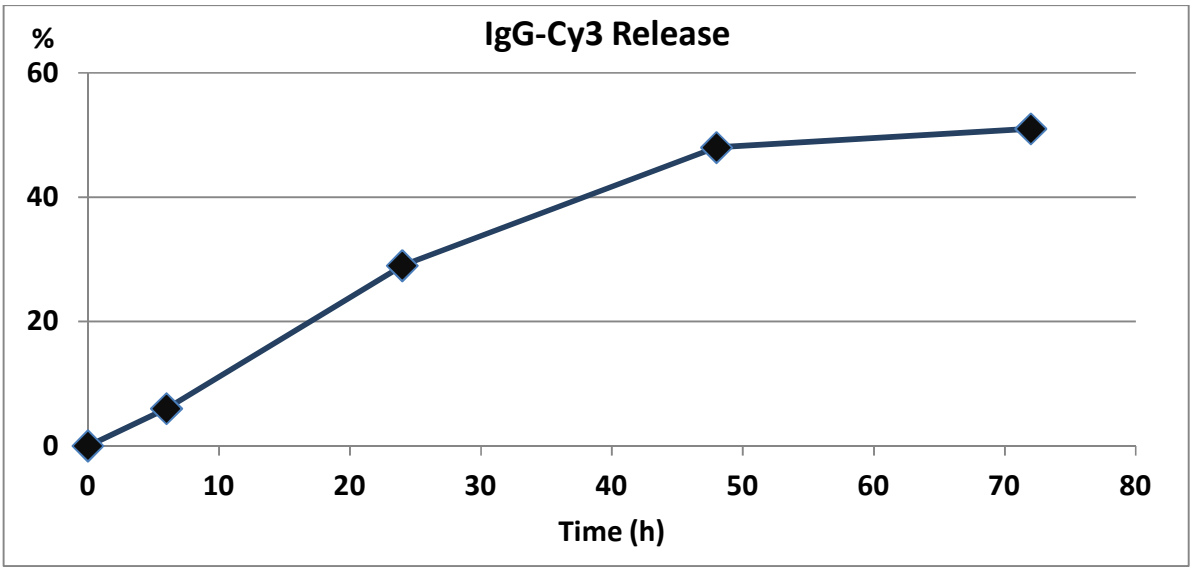

Figure 3.10 The IgG-Cy3 release from PAA NPs. The measurements were repeated five times and the means are represented. Standard deviations are not visible due to their very small values.

Time points	Size (nm)	PdI	DCR (Kcps)
0 h	168 ± 1	0.11 ± 0.01	1211 ± 7
6 h	194 ± 3	0.1 ± 0.02	1328 ± 5
24 h	532 ± 7	0.42 ± 0.02	657 ± 6
48 h	599 ± 38	0.65 ± 0.08	97 ± 3
72 h	1127 ± 149	0.99 ± 0.02	34 ± 2

Table 3.13 The degradation studies of OIg-2HI.2-(T8)-2k formulation. The NPs size, PdI and DCR were measured by DLS. Each measurement was performed at least in triplicates and the standard deviations are presented.

3.6.2 Encapsulation of Streptavidin-Alexa Fluor® 647

Streptavidin is extensively used in molecular biology and nanomedicine research thanks to its resistance against many enzymes, stability under harsh environmental conditions and very

high affinity to biotin. Many researchers use Streptavidin as a model compound for NPs encapsulation [152,153].

To see how PAA NPs encapsulate other model proteins, Streptavidin conjugated with Alexa Fluor® 647 (STR647) was used for this rationale. PAA NPs with O-2HI.2-(T8)-2k formulation were synthesized in the presence of STR647 (Table 3.14). However, the resulted NPs, which had OS-2HI.2-(T8)-2k formulation, were much bigger than the initial formulation. It was hypothesized that the increase of NPs size was due to very large amount of proteins (HSA and STR647) during NPs synthesis, therefore a synthesis was designed where the HSA amount was reduced twice (OSHI.2-(T8)-2k). The obtained NPs showed size (142 nm) drastically lower than the previous one (346 nm) and it was in the same range as the control NPs without STR647 (O-2HI.2-(T8)-2k).

Formulation	Size (nm)	PdI	DCR (kcps)
O-2HI.2-(T8)-2k	134 ± 4	0.1 ± 0.02	243 ± 6
OS-2HI.2-(T8)-2k	346 ± 11	0.22 ± 0.05	240 ± 1
OSHI.2-(T8)-2k	142 ± 3	0.12 ± 0.004	211 ± 4

Table 3.14 Influence of STR647 encapsulation on PAA NPs mean size, PdI and DCR measured by DLS (OSHI.2-(T8)-2k and OS-2HI.2-(T8)-2k samples). A sample without STR647 (O-2HI.2-(T8)-2k) was synthesized as a control. All measurements were done at least in triplicates and standard deviations are presented.

The fluorescent marker allowed measurement of STR647 encapsulation efficiency by using spectrofluorometric analysis and comparing the data with a standard calibration curve. The measurements were done three times and 76%, 62% and 78% encapsulation efficiency was measured. This means that the average encapsulation efficiency of STR647 was 72 ± 8.7%.

3.6.3 Encapsulation of β-Galactosidase

β-Galactosidase is a hydrolytic enzyme that cleaves β-Galactosidic bonds in poly- and oligosaccharides. This enzyme has found many applications in molecular biology and biotechnology thanks to various sensitive colorimetric assays performed by this enzyme. β-Galactosidase is also extensively used in NPs research where it is immobilized in various types of nanostructures as a model drug [154,155].

In this study, β-Galactosidase encapsulation into PAA NPs was investigated. As shown in Table 3.15, two formulations of PAA NPs were synthesized with (OBHFI-2k, OB-2HI.2-2k) and without β-Galactosidase (OBHFI-2k, OB-2HI.2-2k). In both cases the encapsulation did not significantly affect the NPs formation, only slightly increasing their sizes and DCRs.

Formulation	β-Galactosidase	Size (nm)	PdI	DCR (kcps)
OHFI.2-2k	-	195 ± 4.6	0.17 ± 0.03	124 ± 4
OBHFI.2-2k	+	207 ± 1.6	0.16 ± 0.02	146 ± 3
O-2HI.2-2k	-	100 ± 1	0.03 ± 0.01	199 ± 0.3
OB-2HI.2-2k	+	110 ± 2	0.05 ± 0.02	236 ± 1

Table 3.15 Influence of β-Galactosidase encapsulation on PAA NPs mean size, PdI and DCR measured by DLS. All measurements were done at least in triplicates and standard deviations are presented.

3.7 Stability studies

The stability of PAA NPs was assessed by DLS analysis by incubating them in an environment that mimics the conditions in human body (at 37^{o}C in HEPES buffer and under constant stirring) (Figure 3.11). Two types of formulations were chosen for the incubation: OHFI-2k (without P80, Figure 3.11 A) and O-2HI.2-(T8)-2k (with P80, Figure 3.11 B). DLS data showed

that both formulations were relatively stable during the first four days of incubation and then the NPs DCR and sizes started to gradually drop, whereas the PdI increased, signifying that PAA NPs were progressively degrading. After 21 days, the DCRs of both formulations were very low and PdI values were almost 1, confirming that the NPs were completely degraded. These results are very promising because good drug delivery vectors should not degrade very fast in physiological environments in order to avoid premature drug release. On the other hand, NPs slow degradation is required to help releasing their encapsulated cargo and also making them completely biocompatible [156].

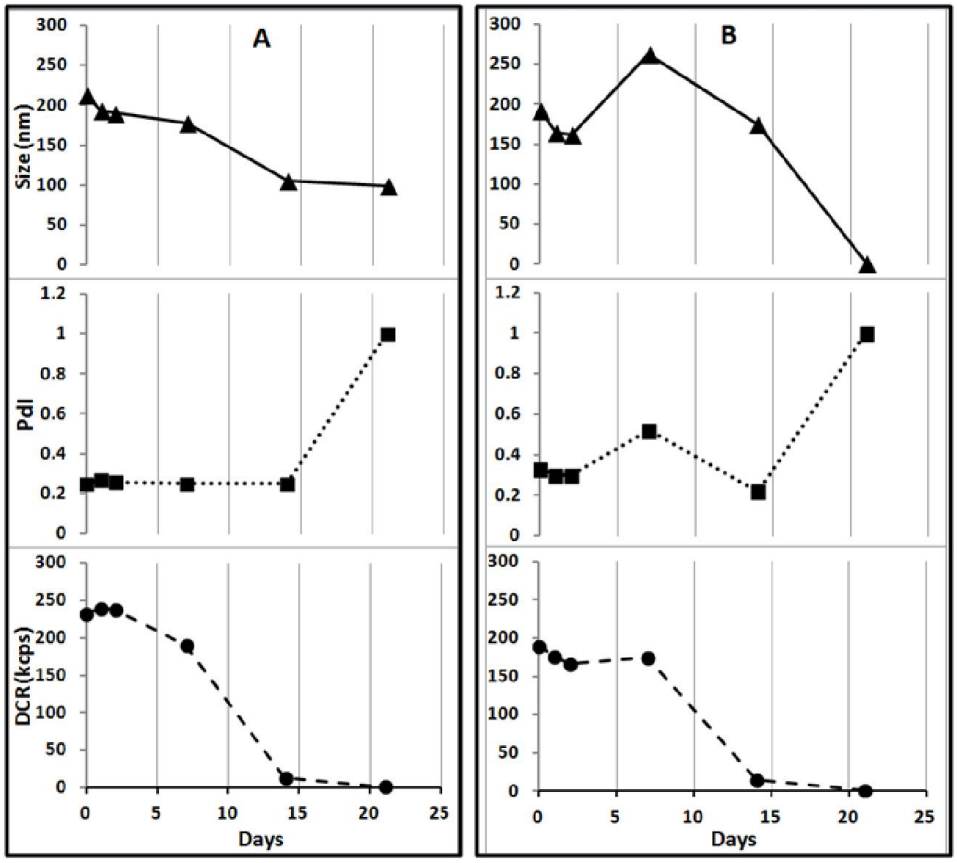

Figure 3.11 DLS data of OHFI-2k (A) and O-2HI.2-(T8)-2k (B) formulations incubation at 37^{o}C in HEPES buffer under constant stirring.

3.8 MTT assay

In order to check whether the optimized PAA NPs had cytotoxic effect or not, MTT cell viability assay was performed on human umbilical vein endothelial cells (HUVEC). Those cells, being a primary cell line, are more sensitive to various environmental stimuli than continuous cell lines, which make them good indicators for even small cytotoxic effects [157,158].

To assess that PAA NPs did not degrade during biological experiments, the NPs stability was monitored in the tested cell culture medium by DLS analysis (Table 3.16). The NPs were

synthesized, dialysed, sterilized by short wave UV-C light and then diluted in three dilutions (1.5, 1/10 and 1/20) in HUVEC culture medium.

An aliquot from each step of NPs preparation was incubated at the same conditions as cells (37^{o}C, humidified air) and their stability was controlled by DLS during 48 h, which corresponds to MTT assay duration. As a control, only HUVEC medium was incubated as well. The results showed that the NPs had good stability in a biological medium and could be used for MTT assay. Additionally, PAA NPs sterilization by short-wave UV light did not change noticeably NPs size, PdI or DCR.

	Time points (h)	**Size (nm)**	**PdI**	**DRC (kcps)**
Synthesis	0	267 ± 7.6	0.24 ± 0.02	246 ± 11
	24	243 ± 2.3	0.21 ± 0.03	229 ± 2.4
	48	235 ± 4	0.23 ± 0.03	197 ± 7
Dialysis	0	274 ± 4.6	0.25 ± 0.05	216 ± 2
	24	247 ± 8	0.23 ± 0.02	243 ± 12
	48	243 ± 3	0.2 ± 0.02	216 ± 1
Sterilization	0	277 ± 15	0.24 ± 0.04	209 ± 7
	24	247 ± 9.6	0.24 ± 0.01	194 ± 7
	48	242 ± 4	0.21 ± 0.02	176 ± 3
1/5 dilution	0	108 ± 39	0.85 ± 0.25	552 ± 13
	24	143 ± 7	0.61 ± 0.09	1280 ± 32
	48	176 ± 17	0.41 ± 0.02	2006 ± 55
1/10 dilution	0	39 ± 0.2	0.93 ± 0.006	304 ± 1.2
	24	150 ± 5	0.44 ± 0.06	1731 ± 37
	48	172 ± 3	0.27 ± 0.001	2914 ± 15
1/20 dilution	0	27 ± 1	0.75 ± 0.02	236 ± 4
	24	145 ± 1.8	0.5 ± 0.05	1694 ± 31
	48	161 ± 2.7	032 ± 0.03	2670 ± 51
Medium (CTRL)	0	25 ± 0.85	0.53 ± 0.12	225 ± 3.4
	24	143 ± 56.6	0.64 ± 0.2	1123 ± 27
	48	153 ± 11	0.53 ± 0.13	1670 ± 25

Table 3.16 The DLS analysis data and zeta potentials for O-2HI.2-(T8)-2k formulation's incubation after its synthesis; dialysis purification; UV sterilization and at three tested dilutions (1/5, 1/10 and 1/20) for MTT assay. As a control (CTRL) only cell culture medium was incubated too. Each sample was analysed at three time points (0h, 24 h and 48 h). Each measurement was performed at least three times and standard deviations are presented.

Two formulations of PAA NPs were used: P80-coated (O-2HI.2-(T8)-2k) and uncoated (O-2HI.2-2k) (Figure 3.12). Furthermore, the NPs were in three different dilutions (1/5, 1/10 and 1/20) and their influence on HUVEC viability was compared to HUVEC grown in a complete medium control (CTRL). Both formulations at the tested dilutions showed remarkable biocompatibility levels, since the HUVEC viability at the presence of PAA NPs was not considerably different from the control. The results demonstrated that HUVEC treated with PAA NPs had high viability (more than 85% of the viability of the control). This confirms the high biocompatibility of linear PAA NPs already shown in the literature [159]. Noteworthy, cells incubated in the presence of uncoated NPs had slightly lower viability (90-95%) compared to the control and P80-coated NPs.

These results showed that PAA NPs had high biocompatibility levels and P80 coating increased it even further.

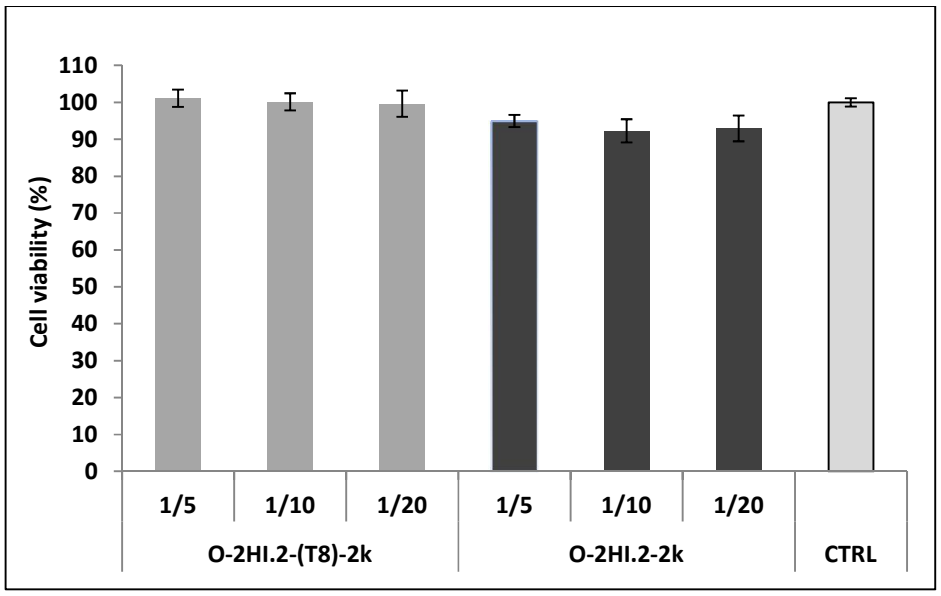

Figure 3.12 Influence of PAA NPs on HUVEC viability. Two formulations of PAA NPs were used in three dilutions (1/5, 1/10 and 1/20), and as a control (CTRL) HUVEC were grown in a complete medium without NPs. The experiment was repeated five times and standard deviations are represented.

3.9 Permeability studies across *in vitro* BBB model

The increased scientific and industrial interest on BBB structure and physiology has led to the development of efficient *in vitro* models that can successfully mimic the BBB conditions *in vivo*. *In vitro* BBB models are mainly based on brain endothelial cells. These cells are able to connect each other via tight junctions and make a barrier that is similar to the real BBB [160]. bEnd5 mouse brain endothelioma cell line has been widely used as an *in vitro* BBB model [161,162]. This cell line has been shown to have high numbers of tight junctions and lower permeability levels compared to other BBB models. Interestingly, bEnd5 cells' permeability levels strongly depend on the type of cell culture medium where they are grown. Studies have revealed that bEnd5 cells grown in MCDB-131 medium have much lower permeability than the cells grown in DMEM medium [163].

Transwell cells have been extensively used for incorporation of *in vitro* cell permeability models. The cells were cultured on the upper chamber of transwells, which is separated from the lower chamber by a semipermeable membrane [164]. Membranes with big pores are suitable for cell transfusion experiments. On the other hand, transwell insert with small pore membranes are good for checking the permeability of drugs or NPs [165]. It has been demonstrated that mouse brain endothelioma cell lines cultured on transwell inserts are very efficient *in vitro* BBB model and the permeability efficiency of NPs across the *in vitro* BBB model was similar to the results acquired *in vivo* [166].

PAA NPs had all necessary properties to be considered as good delivery vectors to the CNS. They had very low cytotoxicity levels, had sizes less than 150 nm, were stable and were able to successfully encapsulate and release model therapeutic compounds. Finally, they had P80 coating, which was shown to facilitate the NPs permeability across the BBB.

PAA NPs capability to transport IgG-Cy3 across an *in vitro* BBB model was analyzed by measuring the NPs' permeability across bEnd5 cell line cultured on transwell inserts. The permeability levels after 6 h and 24 h of incubation were measured by calculating the fluorescence of IgG-Cy3 that crossed the *in vitro* BBB model (Figure 3.13). In addition to the NPs loaded with IgG-Cy3 (sample A) the same formulation of NPs without IgG-Cy3 (sample B), IgG-Cy3 without encapsulation (sample C), 10 mM HEPES buffer (sample D) and complete cell culture medium (sample E) were used as controls.

The results demonstrated that PAA NPs encapsulated with IgG-Cy3 had higher permeability levels (Figure 3.13 A) than the antibody alone (Figure 3.13 C). The autofluorescence levels of empty NPs (Figure 3.13 B), HEPES buffer (Figure 3.13 D) and the cell culture medium were significantly lower than the fluorescence of antibody loaded NPs. Moreover, sample A showed that most of IgG-Cy3 were transported during the first 6 h of incubation, and there was very little increase of overall IgG-Cy3 transport level after 24 h. On the other hand, in case of the non-encapsulated antibody, after 24 h encapsulation the amount of transported antibody almost doubled. The results indicated the PAA NPs greatly increase the permeability of a model compound across *in vitro* BBB models with faster dynamics than the model compound alone.

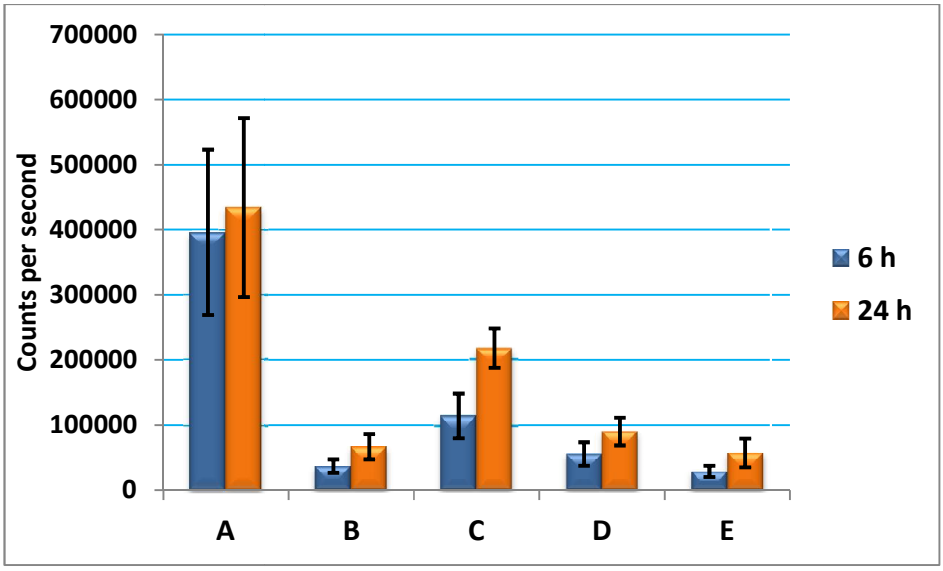

Figure 3.13 The fluorescence level of IgG-Cy3 passed across an *in vitro* BBB model. Transwell cells' upper chambers were added by (A) PAA NPs encapsulated with IgG-Cy3, (B) NPs without IgG-Cy3, (C) not-encapsulated IgG-Cy3, (D) 10 mM HEPES medium (E) and cell culture medium as a final control. The fluorescence of transwell inserts' lower chambers media were measured after 6 h and 24 h of incubation. All measurements were performed in triplicates and standard deviations are presented.

In order to check that PAA NPs did not affect on the structural integrity of cell monolayers by killing the cells, confluent bEnd5 cells were incubated in the presence of the NPs and their controls and visually checked after 24 h of incubation. Figure 3.14 shows that the NPs did not affect on bEnd5 cells viability and the cells monolayer's integrity remained untouched without any visual evidence of dead cells. The cells incubated with PAA NPs encapsulated with IgG-Cy3 (Figure 3.14 A), empty PAA NPs (Figure 3.14 B), 10 mM HEPES mixed with growth medium at 1/10 ratio PAA NPs encapsulated with IgG-Cy3 (Figure 3.14 C) and cells grown in a complete medium. The images revealed that neither PAA NPs nor HEPES buffer did not damage the structural integrity of bEnd5 cells monolayer, and the NPs passed across the BBB not by killing the cells and affecting their integrity but thanks to specific cell permeation mechanisms.

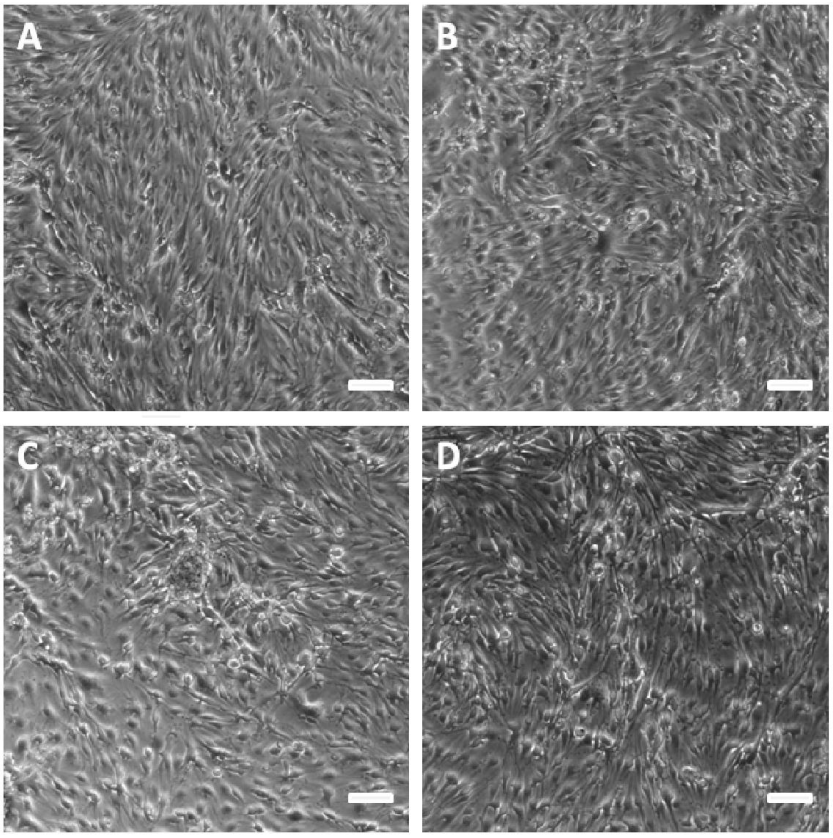

Figure 3.14 Influence of PAA NPs on bEnd5 cells viability. The pictures were taken after 24 h incubation. bEnd5 cells were grown in a medium with the presence of A) 1/10 dilution of PAA NPs encapsulated by IgG-Cy3, B) 1/10 dilution of blank PAA NPs suspension, C) 1/10 dilution of 10 mM HEPES buffer and D) in a complete medium as a control. Scale bars are set at 100 µm.

4. CONCLUSION and PERSPECTIVES

In this research work novel PAA NPs were designed and investigated as efficient vectors for controlled delivery of bioactive molecules to the CNS. Since the PAA oligomers chains had double bonds at both of their ends, they were crosslinked under UV-assisted polymerization in the presence of HSA to form NPs. The proposed synthetic method had an advantage of providing stable NPs (up to three weeks at 37^{o}C) without requiring organic solvents or harsh physical conditions, which are usually employed for preparing NPs by other synthesis techniques and are harmful for many fragile therapeutic compounds. This photo-crosslinking method allowed having high versatility and its easy experimental setup was exploited to effectively scale it up. The scale up experiment was well established and highly reproducible; moreover, the synthesized PAA NPs had similar size and polydispersity to the NPs synthesized at lower scale. PAA NPs were optimized to have less than 150 nm size and were coated by P80. This not only greatly enhanced the NPs stability but also may give them very effective CNS targeting properties. SEM images demonstrated that PAA NPs had well-shaped, spherical structure without aggregations. CLSM imaging showed that the NPs were able to efficiently encapsulate both FITC and IgG-Cy3. Moreover, STED microscopy revealed that FITC was mainly encapsulated onto PAA NPs surface. The optimization of synthetic procedure showed that by controlling the NPs synthesis parameters many important properties, such as NPs size and polydispersity can be changed.

PAA NPs encapsulation of IgG-Cy3 model protein was measured to be reasonably high, and the release studies of the drug showed that PAA NPs released IgG-Cy3 in a slow manner within three days. PAA NPs were shown to successfully encapsulate not only IgG antibody, but also other highly functional proteins, such as fluorescently labeled Streptavidin and β-

Galactosidase. MTT cell viability assay demonstrated that PAA NPs had excellent biocompatibility levels. And finally, IgG-Cy3 containing PAA NPs permeability across an *in vitro* BBB model was assessed to be considerably higher than the permeability of the antibody alone.

In conclusion, PAA NPs meet all the requirements to be used as efficient drug delivery vectors to the CNS: they are small sized and stable, have P80 coating and are able to pass through an *in vitro* BBB model and have very high biocompatibility. Additionally, the synthesis method is simple and straightforward, enabling it to be efficiently scaled up. This opens perspectives for PAA NPs to be used in industrial scales.

In the future studies a better understanding of PAA NPs composition can be achieved by performing thermogravimetric analysis of lyophilized NPs with different formulations to determine the weight ratio of each individual component of the NPs (especially the PAA polymer).

In order to see if the UV irradiation required for PAA NPs synthesis does not damage encapsulated therapeutic compounds, encapsulated β-Galactosidase enzyme's activity can be assessed by using ortho-Nitrophenyl-β-galactoside (ONPG) assay.

Furthermore, transendothelial electrical resistance analysis should be performed in order to measure the integrity of cell monolayers during *in vitro* BBB permeability tests.

The next step should be the encapsulation and release studies of a drug used for the treatment of CNS diseases, namely Remacemide. Subsequently, *in vivo* animal models should be employed to assess PAA NPs efficiency for drug delivery to the CNS.

It is noteworthy to mention that hydrophilic and positively charged PAAs have a great potential to be used for the encapsulation and delivery of hydrophilic and negatively charged nucleic acids. Future studies in this direction can give promising results as well.

5. APPENDIX

Synthesis and characterization of PLGA NPs for siRNA delivery

5.1 Introduction

RNA interference (RNAi) is an inhibition mechanism of specific genes expression by using small interfering RNA (siRNA) molecules. siRNAs are a class of short, double-stranded RNAs which can induce specific post-transcriptional gene silencing by integrating into multi-subunit protein complexes (RISC) and inducing degradation of corresponding messenger RNAs [167]. However, the clinical application of siRNAs has been hampered by their rapid degradation, non-specific distribution, poor cellular uptake and low endosomal escape efficiency [168].

To overcome these limits, several controlled delivery systems have been developed.

To date, viral vectors (including lentiviruses and adeno-associated viruses) and lipid based nanoparticles have been investigated for gene therapy because of their high transfection efficacy [169]. Nevertheless, the use of those vectors has many drawbacks, such as high production cost, technical difficulties in producing the vectors, immune response triggering, and serious safety concerns (such as occurrence of insertional mutagenesis during human gene therapy trials) [170].

Conversely, biodegradable polymeric NPs represent a promising and safe alternative for gene delivery [133]. Their properties include interactions with many biomolecules including proteins and nucleic acids. Indeed, siRNAs encapsulated into polymeric NPs are well

protected up to the target site [171]. By using proper synthetic procedures, several parameters of NPs can be tailored, including size and degradation period. The NPs surface functionalization enables more specific targeting and further enhances their efficacy. Moreover, the adjustable biodegradability of NPs allows slow and controlled release of siRNAs in the targeted cells [172]. Since NPs have to cross biological barriers, their size has to be reduced to less than 200 nm. The smaller is the size, the better pharmacokinetic properties NPs have [173].

Accordingly, the objective of this study was to optimize the synthesis of polymeric NPs for the encapsulation of RNA in gene therapy. To this aim poly (lactic-co-glycolic acid) (PLGA) polymer was investigated.

PLGA polymer is United States Food and Drug Administration (FDA) approved; therefore, it has been commonly used for NP synthesis. This polymer undergoes hydrolysis in the body and releases lactic and glycolic acids, which are by-products of various metabolic pathways in the body. Moreover, prolonged administration of PLGA has shown to be safe even for the CNS [171,174].

5.2 Materials and Methods

5.2.1 Materials

Several types of PLGA polymer were used for the synthesis. They differed by lactic acid and glycolic acid monomer ratio and by molecular weight. PLGA polymers with 50:50 monomer ratio (MW 30000-60000; 7000-17000; 38000-54000) 65:35 monomer ratios (MW 40000-

75000) with 85:15 monomer ratios (MW 190000-240000), polyvinyl alcohol (PVA), dichloromethane, and trehalose were purchased from Sigma Aldrich.

BLOCK-iT™ fluorescein-labelled double stranded (ds) RNA oligomers were purchased from ThermoFisher Scientific.

1X Phosphate-buffered saline (PBS) was prepared by dissolving 137 mM/L NaCl, 2.7 mM/L KCl, 10 mM/L Na_2HPO_4 and 1.8 mM/L KH_2PO_4 in MilliQ® water. The pH was adjusted to 7.4 by using 37% hydrochloric acid.

5.2.2 Synthesis of PLGA NPs

The NPs were synthesized by double emulsion solvent evaporation (DESE) method. Briefly, 500 µL of PLGA polymer dissolved in dichloromethane at 50 mg/mL concentration was mixed with 35 µL of RNA aqueous solution or pure water and sonicated (Vibracell VCX130, 130 watts sonicator, at 30% power) in an ice bath for 1 minute to make water-in-oil emulsions Then 1 mL of 1% PVA stabilizer was mixed with the emulsion and sonicated again for 1 minute using the same conditions described above. After this, the created water-in-oil-in-water emulsions were mixed with 20 mL of 0.3% PVA and stirred at RT for 3 h in order to let toxic dichloromethane evaporate and PLGA NPs form. After 3 h the NPs were filtered by 2.5 µm filter paper and washed three times by centrifuging at +4^{o}C at 18000 g for 20 min. The PLGA NPs pellet was collected and stored at +4^{o}C.

5.2.3 Characterization of nanoparticles

PLGA NPs characterizations by DLS, SEM and CLSM were performed as already described above (Paragraphs 2.4.1, 2.4.2 and 2.4.4)

5.2.4 Lyophilization

PLGA NPs were freezed at -80^{o}C for 24 h and then lyophilized for 48 h by using Teslar Cryodos 50.

5.2.5 Stability studies

PLGA NPs stability was assessed by incubating them at 37^{o}C in either water or 1X phosphate saline buffer (PBS, pH 7.4). At certain time points the NPs were characterized by DLS and their size, PdI and DCR were evaluated. Increasing size and PdI indicated about NPs aggregation and decreased DCR indicated about NPs degradation.

5.2.6 RNA release

PLGA NPs were encapsulated by fluorescein-labelled dsRNA and incubated in 1X PBS (pH 7.4) at 37^{o}C and constantly stirred at 100 RPM (Heidolph incubator 1000 with Unimax 1010 stirrer). At certain time points PLGA NPs were centrifuged and the supernatant's fluorescence was measured by Horiba Fluoromax-4 instrument.

5.3 Results and Discussion

5.3.1 Synthesis of PLGA NPs

Water-in-oil-in-water double emulsion solvent evaporation (DESE) method is commonly used to encapsulate hydrophilic compounds into hydrophobic PLGA NPs. This method has several advantages, such as flexibility of tailoring some important parameters of NPs (size, encapsulation degree, degradability) [175]. Hence this synthetic procedure was optimized to achieve good RNA encapsulation efficiency. Two types of nucleic acids were used for the encapsulation. 1) RNA mixture extracted from Arabidopsis (kindly provided by Plant Models platform, Filarete Foundation) and 2) commercially available dsRNAs designed for using in RNAi analysis. Several series of NPs were synthesized and characterized. The synthesis process was optimized to make monodisperse NPs with high yield.

According to the results, various experimental parameters affected PLGA NP size. The strongest effect on size had the sonication power. The higher was the power, the smaller were PLGA NPs (Figure 5.1). However, it has to be considered that high levels of sonication are a significant physical stresses for NPs and compounds loaded in them. As a matter of fact, samples synthesized at high ultrasound power degraded within few hours.

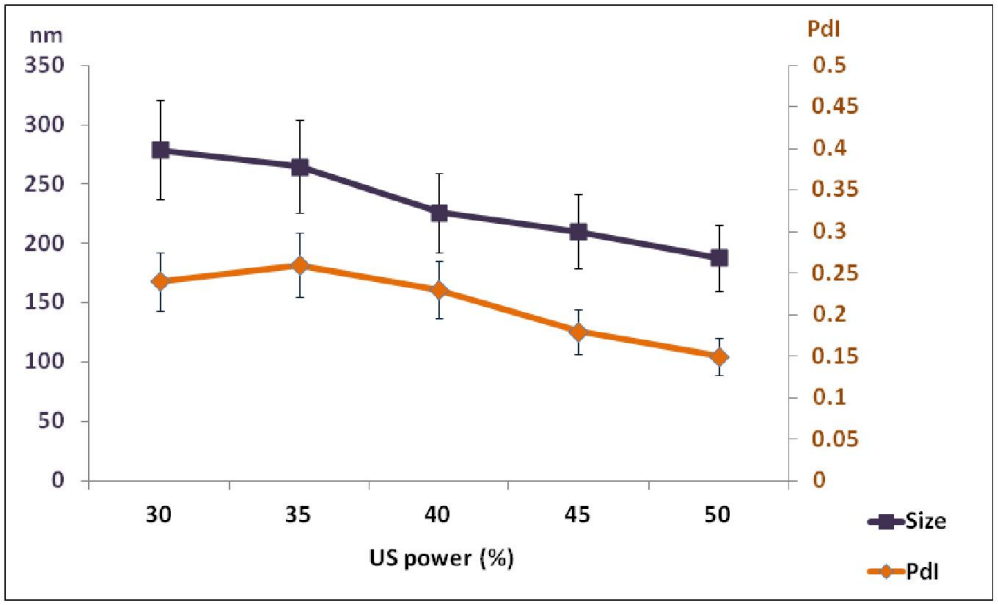

Figure 5.1 Influence of ultrasound (US) power on PLGA NPs size and PdI measured by DLS. All samples were measured at least in triplicates and standard deviations are presented.

5.3.2 Morphological characterization of PLGA NPs

SEM images of PLGA NPs showed the NPs were well-shaped, spherical and had an average size around 250-300 nm. In the Figure 5.2, two NPs from different samples are demonstrated. Figure 5.2A represents a NP with dsRNA inside; Figure 5.2B represents a NP without RNA. Notably, no appreciable morphological differences were observed for the presence or absence of RNA.

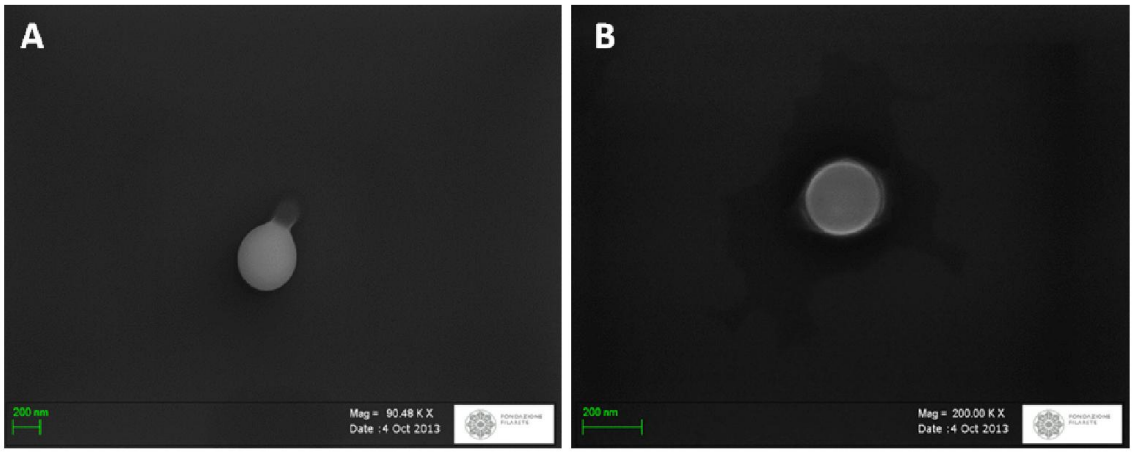

Figure 5.2 SEM images of PLGA NPs. A) a NP with dsRNA inside, B) a NP without RNA.

In order to visualize PLGA NPs by CLSM, fluorescein-labeled dsRNA oligomers were encapsulated into NPs and prepared for imaging. As shown in Figure 5.3, there was colocalization between the fluorescent signal of the dsRNA and the NPs, as well as there were no aggregates.

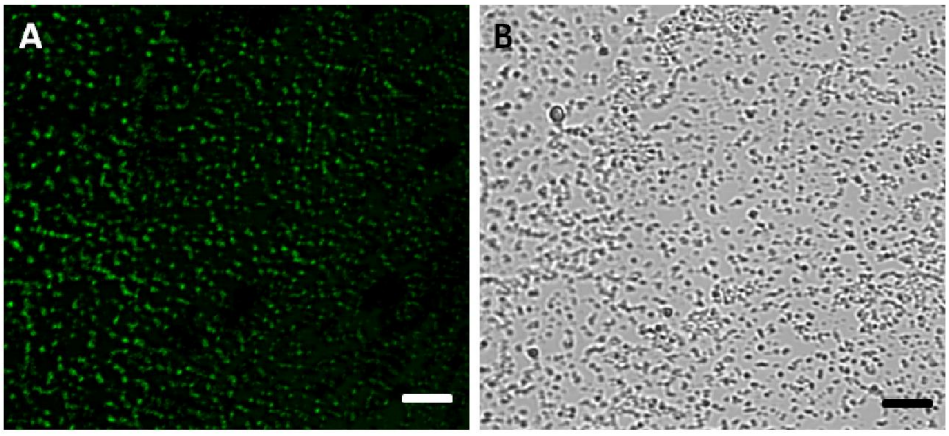

Figure 5.3 CLSM (A) and bright-field (B) images of PLGA NPs encapsulating fluorescein-labeled dsRNA. Scale bars are set at 2 µm.

5.3.3 PLGA NPs stability studies

In order to evaluate synthesized PLGA NPs degradation rate *in vitro*, the NPs were suspended in water or in PBS (pH 7.4) and incubated at 37^{o}C. After certain time points, the samples were measured by DLS instrument to check NPs size, PdI and DCR for 49 days. As shown in Figure 5.4 the DCR of NPs suspension decreased slower in PBS than in water. Furthermore, the the sample's PdI after 30 days incubation increased at slower rate in PBS than in water. These data indicated the possibility that NPs degraded slower in PBS medium. It is noteworthy to mention that PLGA NPs sizes for both formulations did not change throughout 49 days of incubation. The NPs hydrodynamic size was slightly bigger in PBS, which is most probably connected with ionic layers formation around the NPs in PBS.

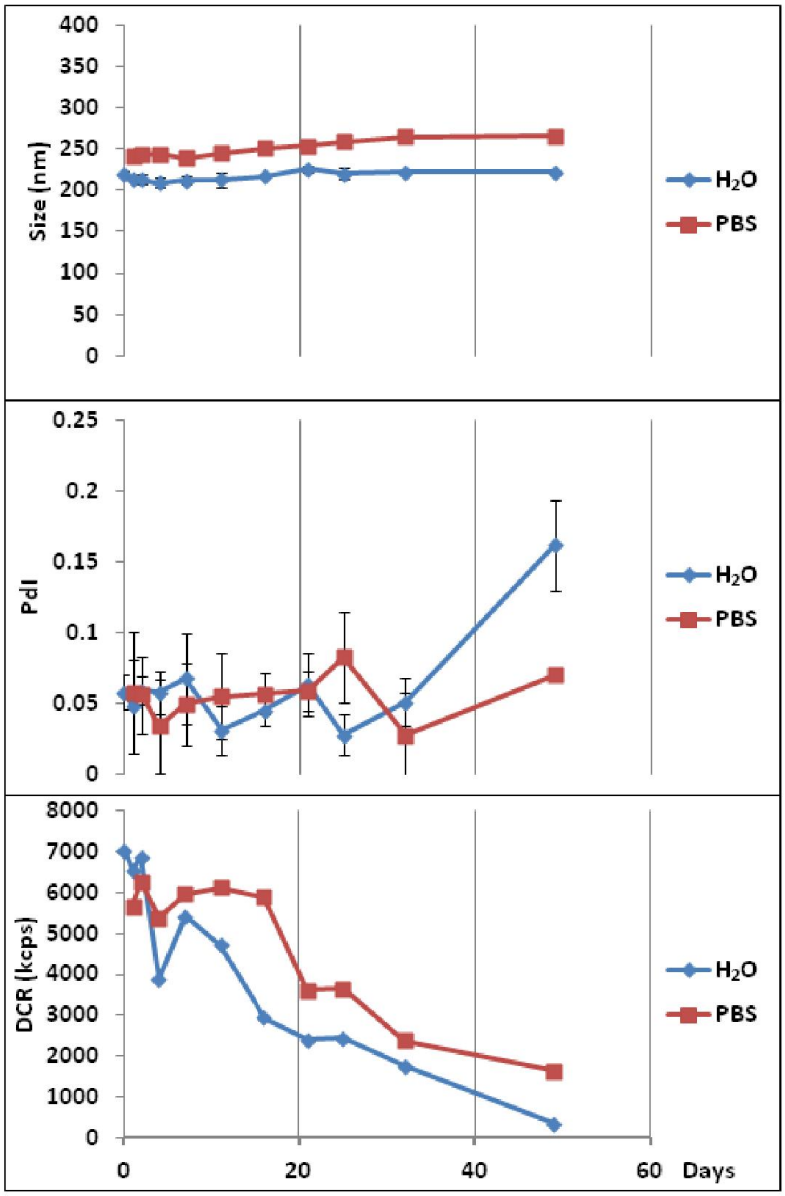

Figure 5.4 PLGA NPs stability studies in water and PBS media. The NPs average size, PdI and DCR were measured by DLS. All samples were measured at least in triplicates and standard deviations are presented. The standard deviations for DCR and size changes are not visible due to their very small values.

PLGA NPs can be collected as wet pellets by using centrifugation. Although freeze-drying (lyophilization) of the NPs is required in order to do precise quantitative measurements and

to achieve long term stability [176], after lyophilization PLGA NPs tended to aggregate and degrade much faster. One of the approaches to let the NPs tolerate harsh conditions of lyophilization is the use of cryoprotectants, which meliorate freezing stress and help NPs to keep their structural integrity intact [177]. Trehalose carbohydrate has been widely investigated for this purpose. It was shown in the literature that trehalose considerably protects several types of NPs during lyophilization [178,179].

Two weight ratios of PLGA NPs/trehalose were used for lyophilization, namely 2/1 and 1/2 (w/w). As a control, the NPs were lyophilized without a cryoprotectant. In order to observe the stability after lyophilization, PLGA NPs were incubated by constantly stirring in PBS (37^{o}C). The samples were analyzed daily by DLS for in total three days. As shown in Figure 5.5, the NPs without a cryoprotectant had big size, very high PdI and very low DCR immediately measured after lyophilization (day 0), which indicates they had been aggregated and irreversibly damaged during freeze-drying. After one day incubation, the PdI reached up to 1 and DCR decreased even lower, which was an indication that the NPs had completely degraded. The sample with NPs/trehalose weight ratio 2/1 had small size, high DCR and low PdI at day 0, but degraded very fast within three days. On the other hand, the sample with NP/trehalose weight ratio 1/2 was more stable compared to the previous two samples. Indeed, PdI and size of this sample did not change significantly within three days and the DCR decreased only moderately during the incubation.

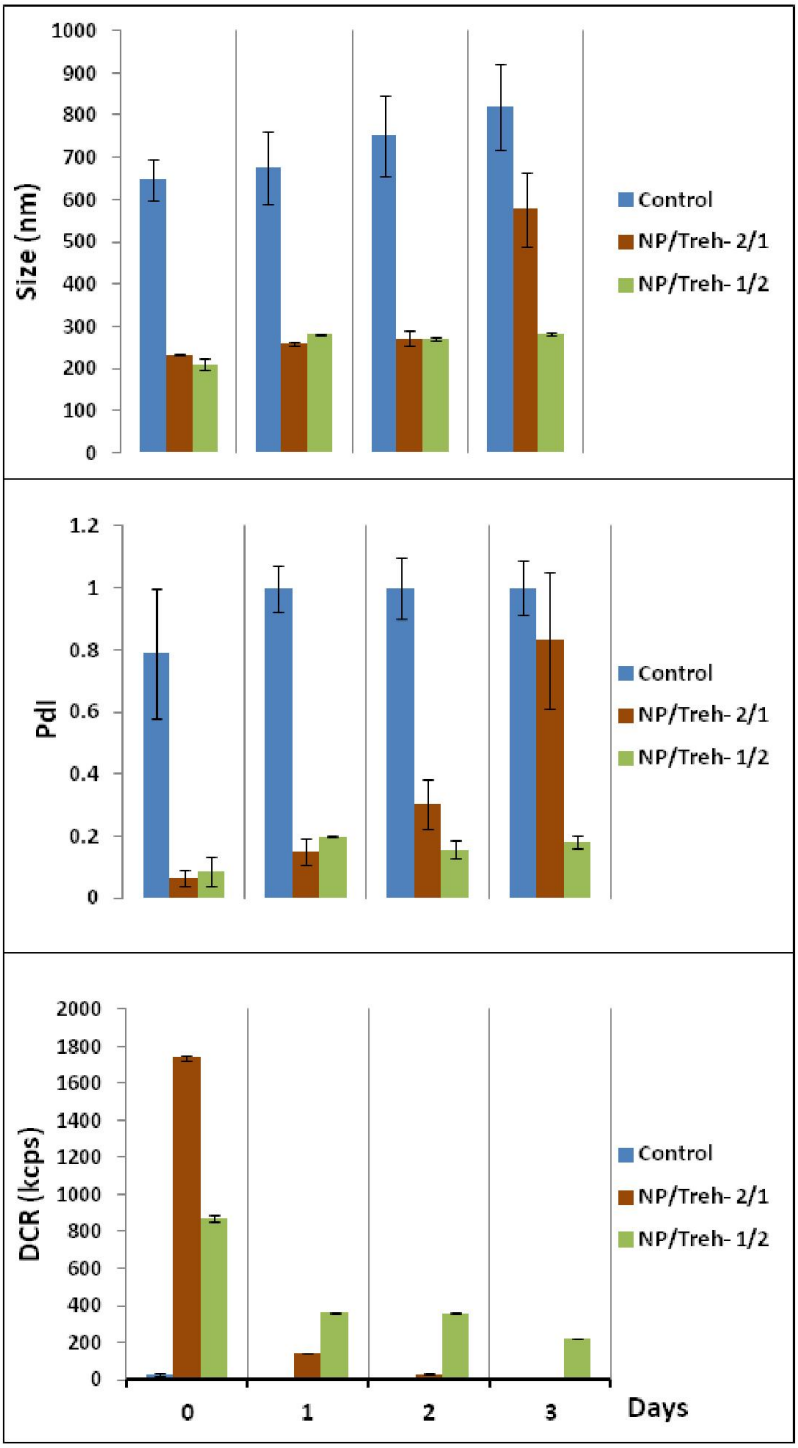

Figure 5.5 PLGA NPs stability after lyophilization by using trehalose cryoprotectant at 1/2 and 2/1 weight ratios with the NPs. PLGA NPs average size, PdI and DCR were measured by DLS. All samples were measured at least in triplicates and standard deviations are presented.

5.3.4 *In vitro* dsRNA release studies

The next step in this project was the encapsulation of dsRNA into NPs and studying *in vitro* release. To this aim, dsRNA molecules were encapsulated into PLGA NPs. Two different samples of PLGA NPs incorporated with dsRNA together with an RNA-free NPs sample (as a control) were suspended in PBS medium (pH 7.4) and incubated at 37^{o}C under constant stirring at 100 RPM. After certain time points the suspension was centrifuged and supernatant's fluorescence was measured by spectrofluorometry. The fluorescence level was measured as counts per seconds (CPS) and the values at the peak 517 nm are represented. Figure 5.6 demonstrates that the encapsulated dsRNAs were rapidly released from both samples during the first 9 h of incubation, and then the release rate was considerably slowed down. This indicated that although PLGA NPs successfully encapsulated dsRNA molecules, they released dsRNA rapidly.

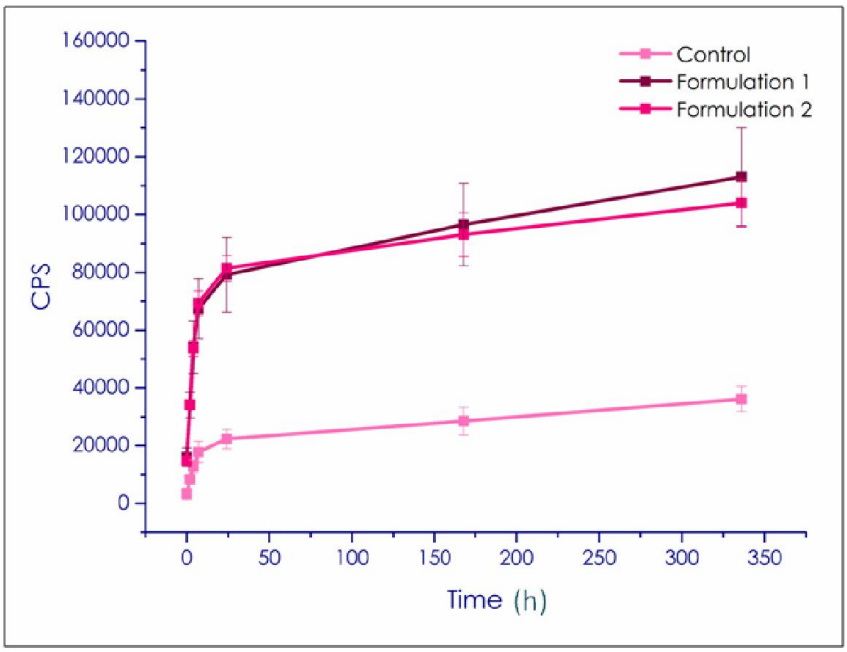

Figure 5.6 Spectrofluorometric measurements of fluorescently labeled dsRNA release from two formulations of PLGA NPs. RNA-free PLGA NPs were used as controls. All measurements were performed five times and standard deviations are presented.

5.4 Conclusion

In this study PLGA NPs were synthesized by double emulsion solvent evaporation method to be used for siRNA delivery. The NPs had average sizes around 250-300 nm, and were monodisperse and remarkably stable in both water and PBS. Moreover, the use of trehalose cryoprotectant drastically improved the NPs stability during lyophilization. The increase of sonication power during PLGA NPs synthesis reduced their size but also decreased their stability. CLSM images confirmed that PLGA NPs successfully encapsulated dsRNA molecules, which were mostly released within 9 h of incubation.

Nevertheless, for subsequent studies PAA was preferred over PLGA. PAA polymer showed remarkable biocompatibility levels thanks to its Agmatine-functionalization. PAA NPs synthesis method was milder, because it did not require use of toxic organic solvents or physical stress caused by sonication. Moreover, PAA NPs synthesis method was able to be scaled up and yielded smaller NPs. Based on those advantages PAA NPs were preferred over PLGA NPs for further studies.

Acknowledgements

I would like to thank my supervisor Prof. Paolo Milani for giving me this opportunity to accomplish PhD project in the field of Medical Nanotechnology and for the support during these four years. Also thanks to my external co-supervisor Prof. Nicola Tirelli and internal co-supervisor Prof. Giuliana Pelicci for their helpful suggestions about my project.

My special acknowledgements to Simona Argentiere, who was following my project throughout these years. Thank you Simona for being always available to help me in all aspects of Science, starting from experimental troubleshooting and finished with scientific writing.

Thanks to Claudia, my fellow PhD candidate in the Nanoparticles lab. We were at the same year of study, so no one could understand me better than you. I had a lot of useful discussions with you about nanoparticles and not only. Thanks to Maria Vittoria Cavanna and Chiara Marotta, my colleges in the Nanoparticles lab. It was a pleasure to work with you.

I would like to thank Eleonora Rossi for helping me in various parts of my project, both in the chemistry part and the biology part. Also, my thanks to Martino Alfredo Cappelluti for helping me accomplish successful results in the biological experiments. Thanks to Laura Morelli for helping me to do the BCA assay and for the useful discussions about the scale-up experiment.

Moreover, thanks to Alexandra Raileanu and Yunsong Yan, my international fellows in Milan. Although we were not working in the same lab, I really enjoyed your company and I am looking forward to new Chinese dinners together.

Furthermore, my acknowledgements to all my former and present colleges in the Advances Biomaterials platform, I enjoyed working with all of you. I will take very nice memories from here.

Many thanks to Mikayel Ginovyan and Andranik Keryan for always supporting me and giving me invaluable advices. You were always there to help me in anything. And also thanks for proofreading my thesis.

Thanks to Julio Aguado for being such a good friend here in Milan. I am sure, no matter where the destiny will take us; we will always be in touch. Remember, I do not forget my friends.

And last but not least, big thanks to my family for being so supportive to me. I never felt that I was far from you. Without your help I could not go so far.

REFERENCES

[1] R. Fu, Q. Shen, P. Xu, J.J. Luo, Phagocytosis of Microglia in the Central Nervous System Diseases, (2014) 1422–1434. doi:10.1007/s12035-013-8620-6.

[2] M. Scarpa, C.M. Bellettato, C. Lampe, D.J. Begley, Neuronopathic lysosomal storage disorders: Approaches to treat the central nervous system, Best Pract. Res. Clin. Endocrinol. Metab. 29 (2015) 159–171. doi:10.1016/j.beem.2014.12.001.

[3] A.K. Ghose, T. Herbertz, R.L. Hudkins, B.D. Dorsey, J.P. Mallamo, Knowledge-based, central nervous system (CNS) lead selection and lead optimization for CNS drug discovery, ACS Chem. Neurosci. 3 (2012) 50–68. doi:10.1021/cn200100h.

[4] B. V. Zlokovic, The Blood-Brain Barrier in Health and Chronic Neurodegenerative Disorders, Neuron. 57 (2008) 178–201. doi:10.1016/j.neuron.2008.01.003.

[5] W.M. Pardridge, Drug and Gene Targeting To the Brain With Molecular Trojan Horses, Nat. Rev. Drug Discov. 1 (2002) 131–139. doi:10.1038/nrd725.

[6] N.J. Abbott, A.A.K. Patabendige, D.E.M. Dolman, S.R. Yusof, D.J. Begley, Structure and function of the blood-brain barrier, Neurobiol. Dis. 37 (2010) 13–25. doi:10.1016/j.nbd.2009.07.030.

[7] M.A. Petty, E.H. Lo, Junctional complexes of the blood-brain barrier: Permeability changes in neuroinflammation, Prog. Neurobiol. 68 (2002) 311–323. doi:10.1016/S0301-0082(02)00128-4.

[8] B. Marty, B. Larrat, M. Van Landeghem, C. Robic, P. Robert, M. Port, et al., Dynamic study of blood–brain barrier closure after its disruption using ultrasound: a quantitative analysis, J. Cereb. Blood Flow Metab. 32 (2012) 1948–1958. doi:10.1038/jcbfm.2012.100.

[9] D. Peer, J.M. Karp, S. Hong, O.C. Farokhzad, R. Margalit, R. Langer, Nanocarriers as an emerging platform for cancer therapy, Nat. Nanotechnol. 2 (2007) 751–760. doi:10.1038/nnano.2007.387.

[10] F. Danhier, E. Ansorena, J.M. Silva, R. Coco, A. Le, V. Préat, PLGA-based nanoparticles: An overview of biomedical applications, J. Control. Release. 161 (2012) 505–522. doi:10.1016/j.jconrel.2012.01.043.

[11] Z. Liang, N. Yang, Y. Jiang, C. Hou, J. Zheng, J. Shi, et al., Targeting docetaxel-PLA nanoparticles simultaneously inhibit tumor growth and liver metastases of small cell lung cancer, Int. J. Pharm. 494 (2015) 337–345. doi:10.1016/j.ijpharm.2015.08.042.

[12] M. Chen, F. Mi, Z. Liao, C. Hsiao, K. Sonaje, M. Chung, et al., Recent advances in chitosan-based nanoparticles for oral delivery of macromolecules, Adv. Drug Deliv. Rev. 65 (2013) 865–879. doi:10.1016/j.addr.2012.10.010.

[13] A.O. Elzoghby, Gelatin-based nanoparticles as drug and gene delivery systems: Reviewing three decades of research, J. Control. Release. 172 (2013) 1075–1091. doi:10.1016/j.jconrel.2013.09.019.

[14] B. Petri, A. Bootz, A. Khalansky, T. Hekmatara, R. Müller, R. Uhl, Chemotherapy of brain tumour using doxorubicin bound to surfactant-coated poly (butyl cyanoacrylate) nanoparticles: Revisiting the role of surfactants, 117 (2007) 51–58. doi:10.1016/j.jconrel.2006.10.015.

[15] A. Kumari, S.K. Yadav, S.C. Yadav, Biodegradable polymeric nanoparticles based drug delivery systems, Colloids Surfaces B Biointerfaces. 75 (2010) 1–18. doi:10.1016/j.colsurfb.2009.09.001.

[16] A. Kowalczuk, R. Trzcinska, B. Trzebicka, A.H.E. Müller, A. Dworak, C.B. Tsvetanov, Loading of polymer nanocarriers: Factors, mechanisms and applications, Prog. Polym. Sci. 39 (2014) 43–86. doi:10.1016/j.progpolymsci.2013.10.004.

[17] A. Albanese, P.S. Tang, W.C.W. Chan, The Effect of Nanoparticle Size, Shape, and Surface Chemistry on Biological Systems, 14 (2012) 1–16. doi:10.1146/annurev-bioeng-071811-150124.

[18] D.E. Owens, N.A. Peppas, Opsonization, biodistribution, and pharmacokinetics of polymeric nanoparticles, Int. J. Pharm. 307 (2006) 93–102. doi:10.1016/j.ijpharm.2005.10.010.

[19] J. Fang, H. Nakamura, H. Maeda, The EPR effect: Unique features of tumor blood vessels for drug delivery, factors involved, and limitations and augmentation of the effect, Adv. Drug Deliv. Rev. 63 (2011) 136–151. doi:10.1016/j.addr.2010.04.009.

[20] A. Salvati, A.S. Pitek, M.P. Monopoli, K. Prapainop, F.B. Bombelli, D.R. Hristov, et al., Transferrin-functionalized nanoparticles lose their targeting capabilities when a biomolecule corona adsorbs on the surface, Nat. Nanotechnol. 8 (2013) 137–43. doi:10.1038/nnano.2012.237.

[21] C. Lemarchand, R. Gref, P. Couvreur, Polysaccharide-decorated nanoparticles, Eur. J. Pharm. Biopharm. 58 (2004) 327–341. doi:10.1016/j.ejpb.2004.02.016.

[22] J. Nicolas, S. Mura, D. Brambilla, N. Mackiewicz, P. Couvreur, Design, functionalization strategies and biomedical applications of targeted biodegradable/biocompatible polymer-based nanocarriers for drug delivery, Chem. Soc. Rev. 42 (2013) 1147–1235. doi:10.1039/C2CS35265F.

[23] Y.B. Patil, U.S. Toti, A. Khdair, L. Ma, J. Panyam, Single-step surface functionalization of polymeric nanoparticles for targeted drug delivery, Biomaterials. 30 (2009) 859–866. doi:10.1016/j.biomaterials.2008.09.056.

[24] Y. Zhong, F. Meng, C. Deng, Z. Zhong, Ligand-directed active tumor-targeting polymeric nanoparticles for cancer chemotherapy, Biomacromolecules. 15 (2014) 1955–1969. doi:10.1021/bm5003009.

[25] S. Prabha, W.Z. Zhou, J. Panyam, V. Labhasetwar, Size-dependency of nanoparticle-mediated gene transfection: Studies with fractionated nanoparticles, Int. J. Pharm. 244 (2002) 105–115. doi:10.1016/S0378-5173(02)00315-0.

[26] D. Ling, W. Park, S.J. Park, Y. Lu, K.S. Kim, M.J. Hackett, et al., Multifunctional tumor pH-sensitive self-assembled nanoparticles for bimodal imaging and treatment of resistant heterogeneous tumors, J. Am. Chem. Soc. 136 (2014) 5647–5655.

doi:10.1021/ja4108287.

[27] Z. Wang, T. Yong, J. Wan, Z. Li, H. Zhao, Y. Zhao, et al., Temperature-Sensitive Fluorescent Organic Nanoparticles with Aggregation-Induced Emission for Long-Term Cellular Tracing, (2015). doi:10.1021/am509161y.

[28] V. Mailänder, K. Landfester, Interaction of nanoparticles with cells, Biomacromolecules. 10 (2009) 2379–2400. doi:10.1021/bm900266r.

[29] N. Kamaly, Z. Xiao, P.M. Valencia, A.F. Radovic-Moreno, O.C. Farokhzad, Targeted polymeric therapeutic nanoparticles: design, development and clinical translation, Chem. Soc. Rev. 41 (2012) 2971. doi:10.1039/c2cs15344k.

[30] L. Zhao, A. Seth, N. Wibowo, C.X. Zhao, N. Mitter, C. Yu, et al., Nanoparticle vaccines, Vaccine. 32 (2014) 327–337. doi:10.1016/j.vaccine.2013.11.069.

[31] S. Onoue, S. Yamada, H.K. Chan, Nanodrugs: Pharmacokinetics and safety, Int. J. Nanomedicine. 9 (2014) 1025–1037. doi:10.2147/IJN.S38378.

[32] S. Nazir, T. Hussain, A. Ayub, U. Rashid, A.J. MacRobert, Nanomaterials in combating cancer: Therapeutic applications and developments, Nanomedicine Nanotechnology, Biol. Med. 10 (2014) 19–34. doi:10.1016/j.nano.2013.07.001.

[33] X. Yuan, S. Naguib, Z. Wu, Recent advances of siRNA delivery by nanoparticles., Expert Opin. Drug Deliv. 8 (2011) 521–536. doi:10.1517/17425247.2011.559223.

[34] J. Li, P. Cai, A. Shalviri, J.T. Henderson, C. He, W.D. Foltz, et al., A multifunctional polymeric nanotheranostic system delivers doxorubicin and imaging agents across the blood-brain barrier targeting brain metastases of breast cancer., ACS Nano. 8 (2014) 9925–40. doi:10.1021/nn501069c.

[35] J. Li, C. Zhang, J. Li, L. Fan, X. Jiang, J. Chen, et al., Brain delivery of NAP with PEG-PLGA nanoparticles modified with phage display peptides, Pharm. Res. 30 (2013) 1813–1823. doi:10.1007/s11095-013-1025-4.

[36] G. Leyva-Gómez, H. Cortés, J.J. Magaña, N. Leyva-García, D. Quintanar-Guerrero, B. Florán, Nanoparticle technology for treatment of Parkinson's disease: the role of surface phenomena in reaching the brain., Drug Discov. Today. 20 (2015) 824–837. doi:10.1016/j.drudis.2015.02.009.

[37] G. Tosi, L. Costantino, B. Ruozi, F. Forni, M.A. Vandelli, Polymeric nanoparticles for the drug delivery to the central nervous system., Expert Opin. Drug Deliv. 5 (2008) 155–174. doi:10.1517/17425247.5.2.155.

[38] J. Kreuter, Drug delivery to the central nervous system by polymeric nanoparticles: What do we know?, Adv. Drug Deliv. Rev. 71 (2014) 2–14. doi:10.1016/j.addr.2013.08.008.

[39] P.R. Lockman, M.O. Oyewumi, J.M. Koziara, K.E. Roder, R.J. Mumper, D.D. Allen, Brain uptake of thiamine-coated nanoparticles, J. Control. Release. 93 (2003) 271–282. doi:10.1016/j.jconrel.2003.08.006.

[40] S. Hanada, K. Fujioka, Y. Inoue, F. Kanaya, Y. Manome, K. Yamamoto, Cell-based in vitro blood-brain barrier model can rapidly evaluate nanoparticles' brain permeability

in association with particle size and surface modification, Int. J. Mol. Sci. 15 (2014) 1812–1825. doi:10.3390/ijms15021812.

[41] K.J. Lim, S. Bisht, E.E. Bar, A. Maitra, C.G. Eberhart, A polymeric nanoparticle formulation of curcumin inhibits growth, clonogenicity and stem-like fraction in malignant brain tumors, Cancer Biol. Ther. 11 (2011) 464–73. doi:10.4161/cbt.11.5.14410.

[42] H. Xin, X. Sha, X. Jiang, L. Chen, K. Law, J. Gu, et al., The brain targeting mechanism of Angiopep-conjugated poly(ethylene glycol)-co-poly(e{open}-caprolactone) nanoparticles, Biomaterials. 33 (2012) 1673–1681. doi:10.1016/j.biomaterials.2011.11.018.

[43] S. Wohlfart, S. Gelperina, J. Kreuter, Transport of drugs across the blood–brain barrier by nanoparticles, J. Control. Release. 161 (2012) 264–273. doi:10.1016/j.jconrel.2011.08.017.

[44] H.S. Sader, P.R. Rhomberg, R.K. Flamm, R.N. Jones, Use of a surfactant (polysorbate 80) to improve MIC susceptibility testing results for polymyxin B and colistin, Diagn. Microbiol. Infect. Dis. 74 (2012) 412–414. doi:10.1016/j.diagmicrobio.2012.08.025.

[45] S.R. Singh, J. Zhang, C. O'Dell, M.-C. Hsieh, J. Goldstein, J. Liu, et al., Effect of Polysorbate 80 Quality on Photostability of a Monoclonal Antibody, AAPS PharmSciTech. 13 (2012) 422–430. doi:10.1208/s12249-012-9759-6.

[46] B. Wilson, M. Kumar, K. Santhi, K. Perumal, S. Kumar, N. Paramakrishnan, et al., Poly (n -butylcyanoacrylate) nanoparticles coated with polysorbate 80 for the targeted delivery of rivastigmine into the brain to treat Alzheimer's disease, 0 (2008) 1–10. doi:10.1016/j.brainres.2008.01.039.

[47] S.-D. Li, L. Huang, Pharmacokinetics and biodistribution of nanoparticles, Mol. Pharm. 5 (2008) 496–504. doi:10.1021/mp800049w.

[48] E.A. Bender, M.D. Adorne, L.M. Colomé, D.S.P. Abdalla, S.S. Guterres, A.R. Pohlmann, Hemocompatibility of poly(ε-caprolactone) lipid-core nanocapsules stabilized with polysorbate 80-lecithin and uncoated or coated with chitosan, Int. J. Pharm. 426 (2012) 271–279. doi:10.1016/j.ijpharm.2012.01.051.

[49] H.J. Cho, J.W. Park, I.S. Yoon, D.D. Kim, Surface-modified solid lipid nanoparticles for oral delivery of docetaxel: Enhanced intestinal absorption and lymphatic uptake, Int. J. Nanomedicine. 9 (2014) 495–504. doi:10.2147/IJN.S56648.

[50] B. Wilson, M.K. Samanta, K. Santhi, K.P.S. Kumar, N. Paramakrishnan, B. Suresh, Targeted delivery of tacrine into the brain with polysorbate 80-coated poly(n-butylcyanoacrylate) nanoparticles, Eur. J. Pharm. Biopharm. 70 (2008) 75–84. doi:10.1016/j.ejpb.2008.03.009.

[51] A. E. Gulyaev; S. E. Gelperina; I. N. Skidan; A. S. Antropov; G. Y. Kivman; J. Kreuter, Significant Transport of Doxorubicin into the Brain with Polysorbate 80-Coated Nanoparticles, (1999) 1564–1569. doi:10.1023/A:1018983904537.

[52] R. Rempe, S. Cramer, R. Qiao, H.-J. Galla, Strategies to overcome the barrier: use of nanoparticles as carriers and modulators of barrier properties, Cell Tissue Res. 355

(2014) 717–26. doi:10.1007/s00441-014-1819-7.

[53] K. Gao, X. Jiang, Influence of particle size on transport of methotrexate across blood brain barrier by polysorbate 80-coated polybutylcyanoacrylate nanoparticles, Int. J. Pharm. 310 (2006) 213–219. doi:10.1016/j.ijpharm.2005.11.040.

[54] N. Voigt, P. Henrich-Noack, S. Kockentiedt, W. Hintz, J. Tomas, B.A. Sabel, Surfactants, not size or zeta-potential influence blood–brain barrier passage of polymeric nanoparticles, Eur. J. Pharm. Biopharm. 87 (2014) 19–29. doi:10.1016/j.ejpb.2014.02.013.

[55] J. Kreuter, P. Ramge, V. Petrov, S. Hamm, S.E. Gelperina, B. Engelhardt, et al., Direct evidence that polysorbate-80-coated poly(butylcyanoacrylate) nanoparticles deliver drugs to the CNS via specific mechanisms requiring prior binding of drug to the nanoparticles, Pharm. Res. 20 (2003) 409–416. doi:10.1023/A:1022604120952.

[56] J.L.N. Dubois, N. Lavignac, Poly(amidoamine)s synthesis, characterisation and interaction with BSA, Polym. Chem. 5 (2013) 1586–1592. doi:10.1039/C3PY01121F.

[57] P. Ferruti, Poly(amidoamine)s: Past, present, and perspectives, J. Polym. Sci. Part A Polym. Chem. 51 (2013) 2319–2353. doi:10.1002/pola.26632.

[58] R. Cavalli, A. Bisazza, R. Sessa, L. Primo, F. Fenili, A. Manfredi, et al., Amphoteric agmatine containing polyamidoamines as carriers for plasmid dna in vitro and in vivo delivery, Biomacromolecules. 11 (2010) 2667–2674. doi:10.1021/bm100685t.

[59] J. Franchini, E. Ranucci, P. Ferruti, M. Rossi, R. Cavalli, Synthesis, physicochemical properties, and preliminary biological characterizations of a novel amphoteric agmatine-based poly(amidoamine) with RGD-like repeating units, Biomacromolecules. 7 (2006) 1215–1222. doi:10.1021/bm060054m.

[60] Z. Zhang, Y. Lai, L. Yu, J. Ding, Effects of immobilizing sites of RGD peptides in amphiphilic block copolymers on efficacy of cell adhesion, Biomaterials. 31 (2010) 7873–7882. doi:10.1016/j.biomaterials.2010.07.014.

[61] F. Martello, A. Tocchio, M. Tamplenizza, I. Gerges, V. Pistis, R. Recenti, et al., Poly(amido-amine)-based hydrogels with tailored mechanical properties and degradation rates for tissue engineering, Acta Biomater. 10 (2014) 1206–1215. doi:10.1016/j.actbio.2013.12.023.

[62] P. Urbán, J.J. Valle-Delgado, N. Mauro, J. Marques, A. Manfredi, M. Rottmann, et al., Use of poly(amidoamine) drug conjugates for the delivery of antimalarials to Plasmodium, J. Control. Release. 177 (2014) 84–95. doi:10.1016/j.jconrel.2013.12.032.

[63] S. Zhu, M. Hong, L. Zhang, G. Tang, Y. Jiang, Y. Pei, PEGylated PAMAM dendrimer-doxorubicin conjugates: In vitro evaluation and in vivo tumor accumulation, Pharm. Res. 27 (2010) 161–174. doi:10.1007/s11095-009-9992-1.

[64] I.J. Majoros, A. Myc, T. Thomas, and Chandan B Mehta, J. James R Baker, PAMAM Dendrimer-Based Multifunctional Conjugate for Cancer Therapy: Synthesis, Characterization, and Functionality, Biomacromolecules. 7 (2006) 572–579. http://pubs.acs.org/doi/abs/10.1021/bm0506142.

[65] J.S. Mandeville, H.A. Tajmir-Riahi, Complexes of dendrimers with bovine serum

albumin, Biomacromolecules. 11 (2010) 465–472. doi:10.1021/bm9011979.

[66] R. Cavalli, A. Bisazza, R. Sessa, L. Primo, F. Fenili, A. Manfredi, et al., Synthesis and characterization of thermoresponsive polyamidoamine-polyethylene glycol-poly(d,l-lactide) core-shell nanoparticles, Acta Biomater. 11 (2010) 465–472. doi:10.1016/j.actbio.2013.12.023.

[67] L. Albertazzi, L. Gherardini, M. Brondi, S. Sulis Sato, A. Bifone, T. Pizzorusso, et al., In vivo distribution and toxicity of PAMAM dendrimers in the central nervous system depend on their surface chemistry, Mol. Pharm. 10 (2013) 249–260. doi:10.1021/mp300391v.

[68] P.K. Maiti, T. Çağin, G. Wang, W.A. Goddard, Structure of PAMAM dendrimers: Generations 1 through 11, Macromolecules. 37 (2004) 6236–6254. doi:10.1021/ma035629b.

[69] G. Coué, I. Hermanns, R.E. Unger, C.J. Kirkpatrick, J.F.J. Engbersen, Development and in vitro evaluation of antigen-loaded poly(amidoamine) nanoparticles for respiratory epithelium applications, ChemMedChem. 8 (2013) 1787–1794. doi:10.1002/cmdc.201300307.

[70] G. Coué, J.F.J. Engbersen, Functionalized linear poly(amidoamine)s are efficient vectors for intracellular protein delivery, J. Control. Release. 152 (2011) 90–98. doi:10.1016/j.jconrel.2011.01.023.

[71] R. Frost, G. Coué, J.F.J. Engbersen, M. Zäch, B. Kasemo, S. Svedhem, Bioreducible insulin-loaded nanoparticles and their interaction with model lipid membranes, J. Colloid Interface Sci. 362 (2011) 575–583. doi:10.1016/j.jcis.2011.05.082.

[72] S. Cohen, G. Coué, D. Beno, R. Korenstein, J.F.J. Engbersen, Bioreducible poly(amidoamine)s as carriers for intracellular protein delivery to intestinal cells, Biomaterials. 33 (2012) 614–623. doi:10.1016/j.biomaterials.2011.09.085.

[73] L.J. van der Aa, P. Vader, G. Storm, R.M. Schiffelers, J.F.J. Engbersen, Intercalating quaternary nicotinamide-based poly(amido amine)s for gene delivery, J. Control. Release. 195 (2014) 11–20. doi:10.1016/j.jconrel.2014.08.005.

[74] P.C. Griffiths, N. Mauro, D.M. Murphy, E. Carter, S.C.W. Richardson, P. Dyer, et al., Self-Assembled PAA-Based Nanoparticles as Potential Gene and Protein Delivery Systems, Macromol. Biosci. 13 (2013) 641–649. doi:10.1002/mabi.201200462.

[75] V. Cagno, M. Donalisio, A. Bugatti, A. Civra, R. Cavalli, E. Ranucci, et al., The Agmatine-Containing Poly(Amidoamine) Polymer AGMA1 Binds Cell Surface Heparan Sulfates and Prevents Attachment of Mucosal Human Papillomaviruses, 59 (2015) 5250–5259. doi:10.1128/AAC.00443-15.

[76] M. Donalisio, E. Ranucci, V. Cagno, A. Civra, A. Manfredi, R. Cavalli, et al., Agmatine-Containing Poly(amidoamine)s as a Novel Class of Antiviral Macromolecules: Structural Properties and In Vitro Evaluation of Infectivity Inhibition, Antimicrob. Agents Chemother. 58 (2014) 6315–6319. doi:10.1128/AAC.03420-14.

[77] S.C.W. Richardson, N.G. Pattrick, N. Lavignac, P. Ferruti, R. Duncan, Intracellular fate of bioresponsive poly(amidoamine)s in vitro and in vivo, J. Control. Release. 142 (2010)

78–88. doi:10.1016/j.jconrel.2009.09.025.

[78] E. Ranucci, M.A. Suardi, R. Annunziata, P. Ferruti, F. Chiellini, C. Bartoli, Poly(amidoamine) conjugates with disulfide-linked cholesterol pendants self-assembling into redox-sensitive nanoparticles, Biomacromolecules. 9 (2008) 2693–2704. doi:10.1021/bm800655s.

[79] J. Shi, Z. Xiao, N. Kamaly, O.C. Farokhzad, Self-assembled targeted nanoparticles: Evolution of technologies and bench to bedside translation, Acc. Chem. Res. 44 (2011) 1123–1134. doi:10.1021/ar200054n.

[80] K. Ariga, J.P. Hill, M. V Lee, A. Vinu, R. Charvet, S. Acharya, Challenges and breakthroughs in recent research on self-assembly, Sci. Technol. Adv. Mater. 9 (2008) 014109. doi:10.1088/1468-6996/9/1/014109.

[81] Y. Li, K. Xiao, W. Zhu, W. Deng, K.S. Lam, Stimuli-responsive cross-linked micelles for on-demand drug delivery against cancers, Adv. Drug Deliv. Rev. 66 (2014) 58–73. doi:10.1016/j.addr.2013.09.008.

[82] A. Al-Nahain, H. Lee, Y.S. Lee, K.D. Lee, S.Y. Park, Development of Disulfide Core-Crosslinked Pluronic Nanoparticles as an Effective Anticancer-Drug-Delivery System, Macromol. Biosci. 11 (2011) 1264–1271. doi:10.1002/mabi.201100083.

[83] R. Shrestha, M. Elsabahy, S. Florez-Malaver, S. Samarajeewa, K.L. Wooley, Endosomal escape and siRNA delivery with cationic shell crosslinked knedel-like nanoparticles with tunable buffering capacities, Biomaterials. 33 (2012) 8557–8568. doi:10.1016/j.biomaterials.2012.07.054.

[84] R. Wang, B. Yu, X. Jiang, J. Yin, Understanding the host-guest interaction between responsive core-crosslinked hybrid nanoparticles of hyperbranched poly(ether amine) and dyes: The selective adsorption and smart separation of dyes in water, Adv. Funct. Mater. 22 (2012) 2606–2616. doi:10.1002/adfm.201102902.

[85] C.Y. Chen, J.C. Chang, A.H. Chen, Competitive biosorption of azo dyes from aqueous solution on the templated crosslinked-chitosan nanoparticles, J. Hazard. Mater. 185 (2011) 430–441. doi:10.1016/j.jhazmat.2010.09.051.

[86] W. Yang, J.R. Ella-Menye, S. Liu, T. Bai, D. Wang, Q. Yu, et al., Cross-linked carboxybetaine SAMs enable nanoparticles with remarkable stability in complex media, Langmuir. 30 (2014) 2522–2529. doi:10.1021/la404941m.

[87] Y. Zou, Y. Song, W. Yang, F. Meng, H. Liu, Z. Zhong, Galactose-installed photo-crosslinked pH-sensitive degradable micelles for active targeting chemotherapy of hepatocellular carcinoma in mice, J. Control. Release. 193 (2014) 154–161. doi:10.1016/j.jconrel.2014.05.016.

[88] D. Roy, B.S. Sumerlin, Let there be light: Photo-cross-linked block copolymer nanoparticles, Macromol. Rapid Commun. 35 (2014) 174–179. doi:10.1002/marc.201300642.

[89] D. Le, L. Lienafa, T.N.T. Phan, D. Deleruyelle, R. Bouchet, D. Bertin, et al., Photo-Cross-Linked Diblock Copolymer Micelles: Quantitative Study of Photochemical Efficiency, Micelles Morphologies and their Thermal Behavior, 47 (2014) 2420–2429.

doi:10.1021/ma5000656.

[90] M. Dickerson, N. Winquist, Y. Bae, Photo-Inducible Crosslinked Nanoassemblies for pH-Controlled Drug Release, Pharm. Res. 31 (2014) 1254–1263. doi:10.1007/s11095-013-1246-6.

[91] H.Y. Yoon, H. Koo, K.Y. Choi, I. Chan Kwon, K. Choi, J.H. Park, et al., Photo-crosslinked hyaluronic acid nanoparticles with improved stability for in vivo tumor-targeted drug delivery, Biomaterials. 34 (2013) 5273–80. doi:10.1016/j.biomaterials.2013.03.050.

[92] A. Tocchio, F. Martello, M. Tamplenizza, E. Rossi, I. Gerges, P. Milani, et al., RGD-mimetic poly(amidoamine) hydrogel for the fabrication of complex cell-laden micro constructs, Acta Biomater. 18 (2015) 144–154. doi:10.1016/j.actbio.2015.02.017.

[93] P. Ferruti, E. Ranucci, F. Trotta, E. Gianasi, E.G. Evagorou, M. Wasil, et al., Synthesis, characterisation and antitumour activity of platinum(II) complexes of novel functionalised poly(amido amine)s, Macromol. Chem. Phys. 200 (1999) 1644–1654. doi:10.1002/(SICI)1521-3935(19990701)200:7<1644::AID-MACP1644>3.3.CO;2-G.

[94] A. Tocchio, M. Tamplenizza, F. Martello, I. Gerges, E. Rossi, S. Argentiere, et al., Versatile fabrication of vascularizable scaffolds for large tissue engineering in bioreactor, Biomaterials. 45 (2015) 124–131. doi:10.1016/j.biomaterials.2014.12.031.

[95] O. Akbulut, C.R. MacE, R. V. Martinez, A.A. Kumar, Z. Nie, M.R. Patton, et al., Separation of nanoparticles in aqueous multiphase systems through centrifugation, Nano Lett. 12 (2012) 4060–4064. doi:10.1021/nl301452x.

[96] D. Steinigeweg, M. Schütz, M. Salehi, S. Schlücker, Fast and cost-effective purification of gold nanoparticles in the 20-250 nm size range by continuous density gradient centrifugation, Small. 7 (2011) 2443–2448. doi:10.1002/smll.201100663.

[97] C. Urata, Y. Aoyama, A. Tonegawa, Y. Yamauchi, K. Kuroda, Dialysis process for the removal of surfactants to form colloidal mesoporous silica nanoparticles, Chem. Commun. (2009) 5094. doi:10.1039/b908625k.

[98] GE Healthcare, Gel Filtration, (2006) 4.

[99] C.M. Hoo, N. Starostin, P. West, M.L. Mecartney, A comparison of atomic force microscopy (AFM) and dynamic light scattering (DLS) methods to characterize nanoparticle size distributions, J. Nanoparticle Res. 10 (2008) 89–96. doi:10.1007/s11051-008-9435-7.

[100] Malvern Instruments, Dynamic Light Scattering: An Introduction in 30 Minutes, Http://Www.Malvern.Com/En/Products/Technology/Dynamic-Light-Scattering/. (2000) 1–8.

[101] S. Patil, A. Sandberg, E. Heckert, W. Self, S. Seal, Protein adsorption and cellular uptake of cerium oxide nanoparticles as a function of zeta potential, Biomaterials. 28 (2007) 4600–4607. doi:10.1016/j.biomaterials.2007.07.029.

[102] Malvern_Instruments, Zeta potential: An Introduction in 30 minutes, Zetasizer Nano Serles Tech. Note. MRK654-01. 2 (2011) 1–6. http://scholar.google.com/scholar?hl=en&btnG=Search&q=intitle:Zeta+Potential+An+Introduction+in+30+Minutes#0.

[103] M. Brissova, Assessment of Human Pancreatic Islet Architecture and Composition by Laser Scanning Confocal Microscopy, J. Histochem. Cytochem. 53 (2005) 1087–1097. doi:10.1369/jhc.5C6684.2005.

[104] N. Claxton, Laser scanning confocal microscopy, Opt. Microsc. 1979 (2006). http://132.248.116.245/_administracion/_unidades_apoyo_inst/microscopia/lecturas/Intro_to_Laser_Scanning_Confocal_Microscopy.pdf.

[105] K. Otomo, T. Hibi, Y. Kozawa, T. Nemoto, STED microscopy—super-resolution bio-imaging utilizing a stimulated emission depletion, Microscopy. 64 (2015) 227–236. doi:10.1093/jmicro/dfv036.

[106] J.-M. Bonard, K. a. Dean, B.F. Coll, C. Klinke, Field Emission of Individual Carbon Nanotubes in the Scanning Electron Microscope, Phys. Rev. Lett. 89 (2002) 197602. doi:10.1103/PhysRevLett.89.197602.

[107] JEOL Ltd., Scanning Electron Microscope A To Z, (2009) 1–32.

[108] A. Bainor, L. Chang, T.J. McQuade, B. Webb, J.E. Gestwicki, Bicinchoninic acid (BCA) assay in low volume, Anal. Biochem. 410 (2011) 310–312. doi:10.1016/j.ab.2010.11.015.

[109] M. Christine, F. Sala, P. Sala, Quantitative determination of hexavalent chromium in aqueous solutions by UV-Vis spectrophotometer, 5 (2007) 1084–1093. doi:10.2478/s11532-007-0038-4.

[110] K. Jores, A. Haberland, S. Wartewig, K. Ma, W. Mehnert, Solid Lipid Nanoparticles (SLN) and Oil-Loaded SLN Studied by Spectrofluorometry and Raman Spectroscopy, 22 (2005). doi:10.1007/s11095-005-7148-5.

[111] Roche, Cell Proliferation Kit I (MTT): Fast Finish for Adherent Cells, (2015) 100.

[112] G. Kali, T.K. Georgiou, B. Iván, C.S. Patrickios, Anionic Amphiphilic End-Linked Conetworks by the Combination of Quasiliving Carbocationic and Group Transfer Polymerizations, J. Polym. Sci. Part a-Polymer Chem. 47 (2009) 4289–4301. doi:10.1002/pola.

[113] G. Coué, I. Hermanns, R.E. Unger, C.J. Kirkpatrick, J.F.J. Engbersen, Development and in vitro evaluation of antigen-loaded poly(amidoamine) nanoparticles for respiratory epithelium applications, ChemMedChem. 8 (2013) 1787–1794. doi:10.1002/cmdc.201300307.

[114] R. Chen, J. Wu, H. Li, G. Cheng, Z. Lu, C.M. Che, Fabrication of gold nanoparticles with different morphologies in HEPES buffer, Rare Met. 29 (2010) 180–186. doi:10.1007/s12598-010-0031-5.

[115] G. Coué, J.F.J. Engbersen, Functionalized linear poly(amidoamine)s are efficient vectors for intracellular protein delivery, J. Control. Release. 152 (2011) 90–98. doi:10.1016/j.jconrel.2011.01.023.

[116] UVP, B-100 Series Ultraviolet Lamps Operating Instructions, (2015) 1–4.

[117] J. Kasanen, M. Suvanto, T.T. Pakkanen, Improved Adhesion of TiO2-Based Multilayer Coating on HDPE and Characterization of Photocatalysis, J. Appl. Polym. Sci. 119 (2011)

2235–2245. doi:10.1002/app.32948.

[118] A. Babu, Q. Wang, R. Muralidharan, M. Shanker, A. Munshi, R. Ramesh, Chitosan coated polylactic acid nanoparticle-mediated combinatorial delivery of cisplatin and siRNA/Plasmid DNA chemosensitizes cisplatin-resistant human ovarian cancer cells, Mol Pharm. 11 (2014) 2720–2733. doi:10.1021/mp500259e.

[119] X. Le Zhang, H.Y. Niu, S.X. Zhang, Y.Q. Cai, Preparation of a chitosan-coated C(18)-functionalized magnetite nanoparticle sorbent for extraction of phthalate ester compounds from environmental water samples., Anal. Bioanal. Chem. 397 (2010) 791–8. doi:10.1007/s00216-010-3592-0.

[120] J. Han, K. Wang, D. Yang, J. Nie, Photopolymerization of methacrylated chitosan/PNIPAAm hybrid dual-sensitive hydrogels as carrier for drug delivery, Int. J. Biol. Macromol. 44 (2009) 229–235. doi:10.1016/j.ijbiomac.2008.12.009.

[121] B.G. Amsden, A. Sukarto, D.K. Knight, S.N. Shapka, Methacrylated glycol chitosan as a photopolymerizable biomaterial, Biomacromolecules. 8 (2007) 3758–3766. doi:10.1021/bm700691e.

[122] M. Havrdova, K. Polakova, J. Skopalik, M. Vujtek, A. Mokdad, M. Homolkova, et al., Field emission scanning electron microscopy (FE-SEM) as an approach for nanoparticle detection inside cells., Micron. 67 (2014) 149–54. doi:10.1016/j.micron.2014.08.001.

[123] I. Sondi, B. Salopek-Sondi, Silver nanoparticles as antimicrobial agent: a case study on E. coli as a model for Gram-negative bacteria, J. Colloid Interface Sci. 275 (2004) 177–182. doi:10.1016/j.jcis.2004.02.012.

[124] W. She, K. Luo, C. Zhang, G. Wang, Y. Geng, L. Li, et al., The potential of self-assembled, pH-responsive nanoparticles of mPEGylated peptide dendron-doxorubicin conjugates for cancer therapy, Biomaterials. 34 (2013) 1613–1623. doi:10.1016/j.biomaterials.2012.11.007.

[125] A. Bootz, V. Vogel, D. Schubert, J. Kreuter, Comparison of scanning electron microscopy, dynamic light scattering and analytical ultracentrifugation for the sizing of poly(butyl cyanoacrylate) nanoparticles, Eur. J. Pharm. Biopharm. 57 (2004) 369–375. doi:10.1016/S0939-6411(03)00193-0.

[126] U. Westedt, L. Barbu-Tudoran, A.K. Schaper, M. Kalinowski, H. Alfke, T. Kissel, Deposition of nanoparticles in the arterial vessel by porous balloon catheters: localization by confocal laser scanning microscopy and transmission electron microscopy, AAPS PharmSci. 4 (2002) E41. doi:10.1208/ps040441.

[127] A.M. Portis, G. Carballo, G.L. Baker, C. Chan, S.P. Walton, Confocal microscopy for the analysis of siRNA delivery by polymeric nanoparticles, Microsc Res Tech. 73 (2010) 878–885. doi:10.1002/jemt.20861.Confocal.

[128] Jackson_ImmunoResearch, Technical information - Affinity-Purified Secondary Antibodies, 2 (2014) 14–16.

[129] Sigma-Aldrich, Fluorescein Isothiocyanate, (2010) 2–4. http://www.sigmaaldrich.com/etc/medialib/docs/Sigma/Product_Information_Sheet/f7250pis.Par.0001.File.tmp/f7250pis.pdf.

[130] S.W. Hell, S.J. Sahl, M. Bates, X. Zhuang, R. Heintzmann, M.J. Booth, et al., The 2015 super-resolution microscopy roadmap, J. Phys. D. Appl. Phys. 48 (2015) 443001. doi:10.1088/0022-3727/48/44/443001.

[131] K. Friedemann, A. Turshatov, K. Landfester, D. Crespy, Characterization via two-color STED microscopy of nanostructured materials synthesized by colloid electrospinning, Langmuir. 27 (2011) 7132–7139. doi:10.1021/la104817r.

[132] K.I. Willig, J. Keller, M. Bossi, S.W. Hell, STED microscopy resolves nanoparticle assemblies, New J. Phys. 8 (2006) 106–106. doi:10.1088/1367-2630/8/6/106.

[133] H.L. Wong, X.Y. Wu, R. Bendayan, Nanotechnological advances for the delivery of CNS therapeutics, Adv. Drug Deliv. Rev. 64 (2012) 686–700. doi:10.1016/j.addr.2011.10.007.

[134] Y. Cao, M. Gao, C. Chen, A. Fan, J. Zhang, D. Kong, et al., Triggered-release polymeric conjugate micelles for on-demand intracellular drug delivery, Nanotechnology. 26 (2015) 115101. doi:10.1088/0957-4484/26/11/115101.

[135] V. Tuan, G. Chuang, U. Kragh-hansen, M. Otagiri, Pharmaceutical Strategies Utilizing Recombinant Human Serum Albumin, 19 (2002). doi:10.1023/A:1015396825274.

[136] K. Langer, M.G. Anhorn, I. Steinhauser, S. Dreis, D. Celebi, N. Schrickel, et al., Human serum albumin (HSA) nanoparticles: Reproducibility of preparation process and kinetics of enzymatic degradation, Int. J. Pharm. 347 (2008) 109–117. doi:10.1016/j.ijpharm.2007.06.028.

[137] A. Bunschoten, T. Buckle, J. Kuil, G.D. Luker, K.E. Luker, O.E. Nieweg, et al., Targeted non-covalent self-assembled nanoparticles based on human serum albumin, Biomaterials. 33 (2012) 867–75. doi:10.1016/j.biomaterials.2011.10.005.

[138] S.J. Buwalda, L.B. Perez, S. Teixeira, L. Calucci, C. Forte, J. Feijen, et al., Self-Assembly and Photo-Cross-Linking of Eight-Armed PEG-PTMC Star Block Copolymers, (2011) 2746–2754. doi:10.1021/bm200515h.

[139] K.L. McGilvray, M.R. Decan, D. Wang, J.C. Scaiano, Facile Photochemical Synthesis of Unprotected Aqueous Gold Nanoparticles, J. Am. Chem. Soc. 128 (2006) 15980–15981. doi:10.1021/ja066522h.

[140] Ciba_Chemicals, Ciba IRGACURE 2959, (2001) 2–4.

[141] C.G. Williams, A.N. Malik, T.K. Kim, P.N. Manson, J.H. Elisseeff, Variable cytocompatibility of six cell lines with photoinitiators used for polymerizing hydrogels and cell encapsulation, Biomaterials. 26 (2005) 1211–1218. doi:10.1016/j.biomaterials.2004.04.024.

[142] A. Vollrath, S. Schubert, U.S. Schubert, Fluorescence imaging of cancer tissue based on metal-free polymeric nanoparticles – a review, J. Mater. Chem. B. 1 (2013) 1994. doi:10.1039/c3tb20089b.

[143] C.S. Hu, C.H. Chiang, P. Da Hong, M.K. Yeh, Influence of charge on FITC-BSA-loaded chondroitin sulfate-chitosan nanoparticles upon cell uptake in human Caco-2 cell monolayers, Int. J. Nanomedicine. 7 (2012) 4861–4872. doi:10.2147/IJN.S34770.

[144] M. Huang, Z. Ma, E. Khor, L.Y. Lim, Uptake of FITC-chitosan nanoparticles by A549 cells, Pharm. Res. 19 (2002) 1488–1494. doi:10.1023/A:1020404615898.

[145] A.P. Ranjan, A. Mukerjee, L. Helson, J.K. Vishwanatha, Scale up, optimization and stability analysis of Curcumin C3 complex-loaded nanoparticles for cancer therapy, J. Nanobiotechnology. 10 (2012) 38. doi:10.1186/1477-3155-10-38.

[146] C.J. Tighe, R.Q. Cabrera, R.I. Gruar, J.A. Darr, Scale up production of nanoparticles: Continuous supercritical water synthesis of Ce-Zn oxides, Ind. Eng. Chem. Res. 52 (2013) 5522–5528. doi:10.1021/ie3025642.

[147] A. Gessner, B.R. Paulke, R.H. Müller, T.M. Göppert, Protein rejecting properties of PEG-grafted nanoparticles: Influence of PEG-chain length and surface density evaluated by two-dimensional electrophoresis and bicinchoninic acid (BCA)-proteinassay, Pharmazie. 61 (2006) 293–297.

[148] A. Gessner, A. Lieske, B. Paulke, R.H. Müller, Functional groups on polystyrene model nanoparticles: influence on protein adsorption., J. Biomed. Mater. Res. A. 65 (2003) 319–326. doi:10.1002/jbm.a.10371.

[149] F.M. Kievit, Z.R. Stephen, O. Veiseh, H. Arami, T. Wang, V.P. Lai, et al., Targeting of primary breast cancers and metastases in a transgenic mouse model using rationally designed multifunctional SPIONs, ACS Nano. 6 (2012) 2591–2601. doi:10.1021/nn205070h.

[150] T. Powell, J.Y. Yoon, Fluorescent biorecognition of gold nanoparticle-IgG conjugates self-assembled on E-beam patterns, in: Biotechnol. Prog., 2006: pp. 106–110. doi:10.1021/bp0501726.

[151] A. Sułkowska, Interaction of drugs with bovine and human serum albumin, J. Mol. Struct. 614 (2002) 227–232. doi:10.1016/S0022-2860(02)00256-9.

[152] G. Lai, J. Wu, H. Ju, F. Yan, Streptavidin-Functionalized Silver-Nanoparticle-Enriched Carbon Nanotube Tag for Ultrasensitive Multiplexed Detection of Tumor Markers, (2011) 2938–2943. doi:10.1002/adfm.201100396.

[153] N. Pedersen, S. Hansen, A. V Heydenreich, H.G. Kristensen, H.S. Poulsen, Solid lipid nanoparticles can effectively bind DNA, streptavidin and biotinylated ligands, Eur. J. Pharm. Biopharm. 62 (2006) 155–162. doi:10.1016/j.ejpb.2005.09.003.

[154] M.P. Klein, M.R. Nunes, R.C. Rodrigues, E. V Benvenutti, T.M.H. Costa, P.F. Hertz, et al., Effect of the support size on the properties of β-galactosidase immobilized on chitosan: Advantages and disadvantages of macro and nanoparticles, Biomacromolecules. 13 (2012) 2456–2464. doi:10.1021/bm3006984.

[155] O.R. Miranda, X. Li, L. Garcia-Gonzalez, Z.J. Zhu, B. Yan, U.H.F. Bunz, et al., Colorimetric bacteria sensing using a supramolecular enzyme-nanoparticle biosensor, J. Am. Chem. Soc. 133 (2011) 9650–9653. doi:10.1021/ja2021729.

[156] P. Szuromi, Rethinking Drug Discovery, Science. 303 (2004) 1795–1795. doi:10.1126/science.303.5665.1795.

[157] R. Bhattacharya, P. Mukherjee, Z. Xiong, A. Atala, S. Soker, D. Mukhopadhyay, Gold nanoparticles inhibit VEGF165-induced proliferation of HUVEC cells, Nano Lett. 4

(2004) 2479–2481. doi:10.1021/nl0483789.

[158] J. Lim, J. Dobson, Improved transfection of HUVEC and MEF cells using DNA complexes with magnetic nanoparticles in an oscillating field, J. Genet. 91 (2012) 223–227. doi:10.1007/s12041-012-0164-4.

[159] G. Coué, C. Freese, R.E. Unger, C. James Kirkpatrick, J.F.J. Engbersen, Bioresponsive poly(amidoamine)s designed for intracellular protein delivery, Acta Biomater. 9 (2013) 6062–6074. doi:10.1016/j.actbio.2012.12.005.

[160] I.A. Wilhelm, I., Fazakas, C., & Krizbai, in Vitro Models of the Blood Brain Barrier, Acta Neurobiol Exp. 71 (2011) 113–128. http://scholar.google.com/scholar?hl=en&btnG=Search&q=intitle:No+Title#0.

[161] O. Steiner, C. Coisne, B. Engelhardt, R. Lyck, Comparison of immortalized bEnd5 and primary mouse brain microvascular endothelial cells as in vitro blood-brain barrier models for the study of T cell extravasation., J. Cereb. Blood Flow Metab. 31 (2011) 315–327. doi:10.1038/jcbfm.2010.96.

[162] M. Yanagita, Y. Kojima, M. Kubota, K. Mori, M. Yamashita, S. Yamada, et al., Cooperative effects of FGF-2 and VEGF-A in periodontal ligament cells, J. Dent. Res. 93 (2014) 89–95. doi:10.1177/0022034513511640.

[163] R. Paolinelli, M. Corada, L. Ferrarini, K. Devraj, C. Artus, C.J. Czupalla, et al., Wnt Activation of Immortalized Brain Endothelial Cells as a Tool for Generating a Standardized Model of the Blood Brain Barrier In Vitro, PLoS One. 8 (2013). doi:10.1371/journal.pone.0070233.

[164] C. Schimpel, B. Teubl, M. Absenger, C. Meindl, E. Fr??hlich, G. Leitinger, et al., Development of an advanced intestinal in vitro triple culture permeability model to study transport of nanoparticles, Mol. Pharm. 11 (2014) 808–818. doi:10.1021/mp400507g.

[165] J.J. Salomon, V.E. Muchitsch, J.C. Gausterer, E. Schwagerus, H. Huwer, N. Daum, et al., The Cell Line NCl-H441 Is a Useful in Vitro Model for Transport Studies of Human Distal Lung Epithelial Barrier, 11 (2014) 995–1006. doi:10.1021/mp4006535.

[166] D. Liu, B. Lin, W. Shao, Z. Zhu, T. Ji, C. Yang, In vitro and in vivo studies on the transport of PEGylated silica nanoparticles across the blood-brain barrier, ACS Appl. Mater. Interfaces. 6 (2014) 2131–2136. doi:10.1021/am405219u.

[167] C.C. Mello, D. Conte, Revealing the world of RNA interference, Nature. 431 (2004) 338–342. doi:10.1038/nature02872.

[168] F.M. Van De Water, O.C. Boerman, A.C. Wouterse, J.G.P. Peters, F.G.M. Russel, R. Masereeuw, Intravenously Administered Short Interfering Rna Accumulates in the Kidney and Selectively Suppresses Gene Function in Renal Proximal Tubules, Pharmacology. 34 (2006) 1393–1397. doi:10.1124/dmd.106.009555.

[169] E. Salvati, F. Re, S. Sesana, I. Cambianica, G. Sancini, M. Masserini, et al., Liposomes functionalized to overcome the blood-brain barrier and to target amyloid-β peptide: The chemical design affects the permeability across an in vitro model, Int. J. Nanomedicine. 8 (2013) 1749–1758. doi:10.2147/IJN.S42783.

[170] K.A. Whitehead, R. Langer, D.G. Anderson, Knocking down barriers: advances in siRNA delivery, Nat. Rev. Drug Discov. 8 (2009) 129–138. doi:10.1038/nrd3182.

[171] N. Vij, T. Min, R. Marasigan, C.N. Belcher, S. Mazur, H. Ding, et al., Development of PEGylated PLGA nanoparticle for controlled and sustained drug delivery in cystic fibrosis, J. Nanobiotechnology. 8 (2010) 22. doi:10.1186/1477-3155-8-22.

[172] G.F. Liang, Y.L. Zhu, B. Sun, F.H. Hu, T. Tian, S.C. Li, et al., PLGA-based gene delivering nanoparticle enhance suppression effect of miRNA in HePG2 cells, Nanoscale Res. Lett. 6 (2011) 447. doi:10.1186/1556-276X-6-447.

[173] D.W. Pack, A.S. Hoffman, S. Pun, P.S. Stayton, Design and development of polymers for gene delivery, Nat. Rev. Drug Discov. 4 (2005) 581–593. doi:10.1038/nrd1775.

[174] M. Andersen, A. Lichawska, A. Arpanaei, S.M. Rask Jensen, H. Kaur, D. Oupicky, et al., Surface functionalisation of PLGA nanoparticles for gene silencing, Biomaterials. 31 (2010) 5671–5677. doi:10.1016/j.biomaterials.2010.03.069.

[175] M. Shin, H.K. Kim, H. Lee, Dopamine-loaded poly(d,l-lactic-co-glycolic acid) microspheres: New strategy for encapsulating small hydrophilic drugs with high efficiency, Biotechnol. Prog. 30 (2014) 215–223. doi:10.1002/btpr.1835.

[176] W. Abdelwahed, G. Degobert, S. Stainmesse, H. Fessi, Freeze-drying of nanoparticles: Formulation, process and storage considerations, Adv. Drug Deliv. Rev. 58 (2006) 1688–1713. doi:10.1016/j.addr.2006.09.017.

[177] K.S. Tang, S.M. Hashmi, E.M. Shapiro, The effect of cryoprotection on the use of PLGA encapsulated iron oxide nanoparticles for magnetic cell labeling, Nanotechnology. 24 (2013) 125101. doi:10.1088/0957-4484/24/12/125101.

[178] C. Vauthier, K. Bouchemal, Methods for the Preparation and Manufacture of Polymeric Nanoparticles, 26 (2009). doi:10.1007/s11095-008-9800-3.

[179] J. Lalani, M. Rathi, M. Lalan, A. Misra, Protein functionalized tramadol-loaded PLGA nanoparticles: preparation, optimization, stability and pharmacodynamic studies, Drug Dev. Ind. Pharm. 39 (2012) 1–11. doi:10.3109/03639045.2012.684390.